CGIAR Research Program on
Climate Change, Agriculture and Food Security (CCAFS)

Climate Change in Indo-Gangetic Agriculture: Recent Trends, Current Projections, Crop-Climate Suitability, and Prospects for Improved Climate Model Information

February 2012

Mark New, Muhammad Rahiz & Jagadishwor Karmacharya

CGIAR

Earth System Science Partnership
DIVERSITAS IGBP IHDP WCRP

UNIVERSITY OF OXFORD

Correct citation:

Mark New, Muhammad Rahiz & Jagadishwor Karmacharya. 2012. Climate Change in Indo-Gangetic Agriculture: Recent Trends, Current Projections, Crop-climate Suitability, and Prospects for Improved Climate Model Information. CGIAR Research Program on Climate Change, Agriculture and Food Security (CCAFS). Copenhagen, Denmark. Available online at: www.ccafs.cgiar.org.

Published by the CGIAR Research Program on Climate Change, Agriculture and Food Security (CCAFS).

CCAFS Coordinating Unit - Department of Agriculture and Ecology, Faculty of Life Sciences, University of Copenhagen, Rolighedsvej 21, DK-1958 Frederiksberg C, Denmark. Tel: +45 35331046; Email: ccafs@cgiar.org

Abstract

The climate of the Indo-Gangetic Plain is investigated and the implications of climate change on agriculture are assessed. The ability of General Circulation Models (GCMs) to reproduce the observed climate was investigated, to establish how reliable future climate and associated crop growth projections might be. Climate in the region is controlled largely by the southwest monsoon. Very few if any climate models capture both monsoon rainfall amount and timing accurately, and the most robust approach to assessing climate change regionally involves using all model projections available. During this century, mean temperature will rise at a rate greater than the global mean. Projections for changes in precipitation are varied, but the ensemble mean changes are generally positive, and more consistently positive over the Ganges than the Indus. Rain-fed agricultural suitability of all crops increases in the future, due to precipitation increases. For irrigated agriculture, maize, wheat and rice are not affected in terms of areas that are suitable for growth, except in the warmest scenarios in the 2090s, especially in the lower Indus valley.

Keywords

General Circulation Model; climate; crop suitability; monsoon; Indus; Ganges.

About the authors

Mark New is Professor of Climate Science at the School of Geography and Environment, Oxford. Since mid-2011 he has held a joint appointment at the University of Cape Town, where he is Director of the African Climate and Development Initiative. His research focuses on climate change detection, processes, scenarios, impacts and adaptation. In his research on climate change monitoring and detection he has worked on the development of global and regional climate datasets which have underpinned climate impacts assessments and integrated modelling, the detection of climate extremes, and issues around uncertainty and accuracy of climate data. **Contact:** mark.new@acdi.uct.ac.za

Jagadishwor Karmacharya is a DPhil candidate at the School of Geography and Environment, Oxford, working with Professor Mark New. His research is on the added-value of high resolution regional climate model simulations in the Himalaya. He has worked as Senior Meteorologist and Chief of Data Section at the Department of Hydrology and Meteorology, an agency mandated by the Government of Nepal to monitor all the hydrological and meteorological activities in Nepal. **Contact:** jagadishwor.karmacharya@ouce.ox.ac.uk

Muhammad Rahiz is a DPhil candidate at Oxford University's School of Geography and the Environment and a researcher affiliated with the ARCC-Water: Water Systems Resilience project under the ARCC Coordination Network. His interests focus on the use of data from climate models for assessment of impacts and uncertainties and to understand the physical mechanisms governing future climate change. He was part of the interdisciplinary team that produced the report "Vulnerability through the eyes of vulnerable: climate change induced uncertainties and Nepal's development predicaments". His current research looks at the nature of 21st century droughts and their implications on water resource systems in the UK. **Contact:** muhammad.rahiz@ouce.ox.ac.uk

Contents

Acronyms

ABC	Atmospheric brown clouds
CDD	Consecutive dry days
CORDEX	Coordinated Regional Downscaling Experiment
CWD	Consecutive wet days
ENSO	El Niño-Southern Oscillation
GCM	General Circulation Model
IGP	Indo-Gangetic Plain
IITM	Indian Institute for Tropical Meteorology
IPCC	Intergovernmental Panel on Climate Change
IOD	Indian Ocean Dipole
MAE	Mean absolute error
RCM	Regional Climate Model
RCP	Representative Concentration Profile
SRES	Special Report on Emissions Scenarios
SST	Sea surface temperature

1. Introduction

The Indo-Gangetic Plain (IGP)—the low-elevation and gently sloping middle and lower reaches of the Indus and Ganges river basins—is critical for agricultural production and food security in the South Asia region. Traditionally fertile, blessed with seasonal monsoon rainfall, dry season river flows and groundwater availability, the region is becoming increasingly stressed as resources are depleted and population increases. Climate change potentially can exacerbate or ameliorate these stresses, depending on the direction and magnitude of changes to climate in variables of relevance to crop growth, and also as a consequence of the impacts of secondary factors such flood and heat-wave damage.

The aim of this report is to provide (i) an initial assessment of recent trends and projected future changes in climate, specifically focused on the IGP, (ii) to assess the potential changes in crop suitability of key crops currently grown in the IGP, and (iii) to summarise the key advances that can be expected in climate model information over the next few years.

The report is laid out as follows. Section 1 provides background on the agriculture and climate of the IGP, with a particularly focus on the monsoon. Section 2 examines recent trends in basic climatic variables—precipitation and temperature—and also trends in several indices of extreme climate events. Section 3 reviews the performance of global climate models over the IGP through a review of the literature, and through original analysis of model performance over the IGP itself. Section 4 examines the projections of temperature and precipitation for the IGP and its sub-regions from the period 1960–2099 including how the monsoon might change in future decades. Section 5 identifies climatic thresholds for key crops in the IGP, and compares the present day and potential future spatial patterns of climatically suitable areas for each crop. Section 6 summarises the main results of the report and discusses the key advances that can be expected from the climate modelling community in the next few years.

1.1 Importance of IGP

Covering parts India, Pakistan, Nepal and almost all of Bangladesh, the IGP is among the most agriculturally productive regions of the world. Characterized by favourable climate, fertile soils and abundant water supply, the IGP is seen as the “bread basket” of South Asia,

providing food and livelihood security for hundreds of millions of its inhabitants (Aggarwal et al. 2004; Erenstein et al. 2007).

The major crops in the IGP are rice, wheat, cotton, pearl millet, maize and sugarcane, grown in the form of dual cropping systems, typically rice-wheat, during the 'rabi' (spring harvest) and 'kharif' (autumn harvest) seasons (Bansal and Koshal 2008). Owing to the seasonal and unpredictable supply of rainfall from the summer monsoon, an indispensable feature of agriculture in the IGP is irrigation in which water is derived from the two contiguous river systems, the Indus and Ganges. However, the effects of climate change over the region have potential for far-reaching consequences on water supply. Already the prospects of extreme weather events such as droughts due to climate change are apparent and are on the rise (Aggarwal et al. 2004; PACS 2008). With climate change, distributions and thresholds of temperature and precipitation are likely to change. While an increase in concentrations of carbon dioxide can be beneficial to crops through aerial fertilization, an associated increase in temperatures and reductions in precipitation would be detrimental to overall food production (Aggarwal, Joshi et al. 2004). In India, for example, studies have illustrated the inverse relationship between climate change and agricultural productivity (Saseendran, Singh et al. 2000; Aggarwal and Mall 2002).

Over-exploitation of land, urbanization, population increase, pests, soil salinity and the growing effects of climate change are seen as threats to the production of food and livelihood security in the region, and to international trade (Mandal and Sharma 2006; Saini 2008; Pal et al. 2009).

1.2 Basic climate

Given the large domain of the IGP (see Appendix 1)—spanning approximately 20° to 32 °N and 60° to 100 °E—it is difficult to generalize the climate of the region. However, four broad seasons are commonly used: winter (December–April), pre-monsoon (April–June), monsoon (June–September) and post-monsoon (October–December). In terms of agriculture, most crops are grown in the rabi (October-March) and kharif (July-October) seasons. The key component that controls the climate of the IGP is the southwest monsoon which abruptly begins and ends in June and September, respectively. The monsoon brings significant rainfall on the west coast of the Indian subcontinent and the northeastern regions, including the zone around 20°N which spans from the northwest to the head of the Bay of Bengal (Gadgil 2003).

Over India alone, the southwest monsoon contributes about 70–90% of the annual rainfall (Rajeevan and McPhaden 2004).

The mountain ranges of the Himalaya-Hindu-Kush and Tibetan Plateau have a strong influence on the evolution of the monsoon (Hahn and Manabe 1975) and the redistribution of monsoon precipitation through the larger rivers draining the region. While many of the details of the monsoon system remain to be unravelled it has traditionally been seen as a large land-sea breeze induced by differential heating between the Indian subcontinent and the Indian Ocean (Webster et al. 1998; Gadgil 2003).

Research on the monsoon attributes its evolution to the reversal of the meridional temperature gradient which is controlled by the Tibetan Plateau (Li and Yanai 1996; Webster et al. 1998; Wu and Zhang 1998). Taking the upper tropospheric seasonal temperature anomaly between 200 hPa and 500 hPa, Li and Yanai (1996) observed that over the Tibetan Plateau the temperature anomaly changes from negative to positive in April and progressively increases until it reaches maximum during summer after which it subsides and returns to negative in October. The change to positive anomaly creates conditions for air at the 500 hPa level to rise to the level of low pressure at 200 hPa. Southwesterly winds at the 500 hPa level travelling at 1 m/s since late January intensify to about 5 m/s from May to September to fill the void of low pressure left behind by the uprising air. The intensification of wind velocity which transports more moisture from the Indian Ocean coincides with the northwards advancement of the rain belt from the equator during winter and spring towards the Himalayas during summer.

However, it has been argued that the hypothesis involving thermal contrast between land and sea is inconsistent with the space-time observations of temperature and rainfall over India (Simpson 1921; Gadgil 1988). Instead, Gadgil (1988) puts forward the notion of the monsoon being the manifestation of the seasonal migration of the inter-tropical convergence zone.

The South Asian monsoon is subject to the influence of a variety of tropical and extra-tropical phenomena and despite its remarkable regularity each year, does exhibit substantial variability at sub-seasonal and interannual time scales (Webster et al. 1998; Annamalai et al. 1999; Meehl 2002). Numerous studies have shown that the warm phase (El Niño) of El Niño-Southern Oscillation (ENSO) is frequently associated with a weakening of the Indian (South Asian) monsoon with an overall reduction in rainfall. Conversely, the cold phase (La Niña) is

associated with the strengthening of the Indian monsoon and enhancement of rainfall (Sikka 1980; Rasmusson and Carpenter 1983; Meehl 2002). During El Niño years, the redistribution of latent heat sources and sinks in the equatorial Pacific determines the rising/descending branches of the anomalous Walker circulation, the most important element in the ENSO–monsoon teleconnection. This is evident in 200 hPa velocity potential anomalies in which changes in the Walker circulation induce large-scale subsidence over India, resulting in weaker monsoons (Annamalai et al. 2007). However, studies have shown that the relationship between monsoon and ENSO, as well as other drivers, is non-stationary. In particular, the ENSO–monsoon relationship during the 1990s was observed to be weaker than in previous decades (Ashok et al. 2001), although there are indications that this relationship has regained strength in recent years (Annamalai et al. 2007). Further, Kumar et al. (2006) have suggested that the location of the warm pool in the Pacific during El Niño events can determine whether there is negative or more neutral effect on the monsoon.

Variability in the Indian Ocean is also known to affect the monsoon. The Indian Ocean Dipole (IOD) is thought to be important (Saji et al. 1999; Webster et al. 1999) but often acting in combination with ENSO. For example, Ashok et al. (2001) show that when the ENSO-monsoon correlation is low, the IOD-monsoon correlation is high, and vice versa. During positive IOD years there is tendency for anomalous convergent flow in the lower troposphere over the Bay of Bengal and South Asia which results in normal or excess monsoon rainfall. In effect, the IOD plays an important role as a modulator of the Indian monsoon rainfall, and influences the correlation between the monsoon rainfall and ENSO.

Many studies have found a statistical relationship between Eurasian snow cover in winter and Indian monsoon rainfall in the following summer (Kripalani et al. 1996). Reduced snowfall in the winter is associated with a stronger than average monsoon in the following summer, while excessive snowfall, on the other hand, is related with a weaker monsoon. As Shukla (1987) noted, an inverse relationship between Eurasian snow cover and the summer rainfall is plausible because larger and persistent winter snow cover over Eurasia can delay and weaken the spring and summer heating of the land masses that is necessary for the establishment of the large scale monsoon flow. Persistence of snow also modulates surface albedo; during the subsequent spring and summer seasons, solar radiation which would otherwise be available to heat the surface is used for melting the snow or evaporating water from the wet soil. Others

(Yang 1996) have suggested that ENSO variability affects Eurasian snow cover, and that snow is therefore only a linking agent between ENSO and the monsoon.

The role of aerosols in precipitation variation in India and the Tibetan Plateau is still uncertain. Lau et al. (2006) have argued that Atmospheric Brown Clouds (ABC) can combine with naturally occurring dust loadings over the Tibetan Plateau to accentuate the elevated heat source during the pre-monsoon, thus enhancing the meridional temperature gradient and contributing to increased rainfall over India during pre-monsoon and monsoon seasons. Ramanathan et al. (2005) showed that ABC aerosols can indeed increase pre-monsoon rainfall, but actually reduce monsoon rainfall, in part due to the effects of ocean coupling and consequent cooler sea surface temperature (SST) in the Northern Indian Ocean. Meehl et al. (2008) found similar results in their model study and suggested that black carbon acts to increase lower-tropospheric heating over South Asia and reduce the amount of solar radiation reaching the surface during the dry season; the increased meridional tropospheric temperature gradient in the pre-monsoon, particularly between the elevated heat source of the Tibetan Plateau and areas to the south, contributes to enhanced precipitation over India in those months. With the onset of the monsoon, black carbon in atmosphere reduces but much of South Asia, including the north Indian Ocean, remains anomalously cool, weakening the latitudinal SST gradient with a consequent decrease in monsoon rainfall. Further, aerosols deposited on the snow surface might also alter the timing of monsoon onset. For example Qian et al. (2010) suggest that darkened snow surfaces polluted by ABC deposition absorb more solar radiation, increasing the surface temperature, which warms the air above through sensible heat flux over the Tibetan Plateau; this, along with effect of warm air due to ABC material in the atmosphere, enhances the upward motion of air and deep convection on the Tibetan Plateau during the pre-monsoon, resulting in a stronger and earlier onset of the monsoon.

2. Observed trends in climate

Table 2.1 shows a list of datasets and their corresponding details used to study trends of climate and extreme events for the common period of the recent past (1960–2001) (see Appendix 2 for trends from 1960 to the end of record for each respective data set). Two of the datasets, CRU and APHRODITE, are based on dense networks of rain gauge and/or

temperature data, that is, gridded datasets interpolated from meteorological station data. The remaining three are quasi-observed 'reanalyses', that is, numerical weather prediction models that assimilate observations to produce 'best guess' spatially complete historical data. As the datasets have varying periods of availability and spatial resolutions, the period of analysis is standardised to 1960–2001, and they are, where necessary, interpolated to a common 0.5 x 0.5 degree resolution in order to work from a single spatial domain over the IGP (see Appendix 1).

Table 2.1: Details of datasets used for trends in climate and extreme events from 1960

Data	Resolution (in degrees)	Period	Variable(s)	Source	Remarks
APHRODITE	0.25 x 0.25	1951-2007	Precipitation	Yatagai et al. 2009	Daily
CRU	0.5 x 0.5	1901-2002	Precipitation Mean temperature Minimum temperature Maximum temperature	Mitchell and Jones 2005	Monthly
ERA-40	1.125 x 1.125	1958-2002	Precipitation Mean temperature	Uppala et al. 2005	Daily
JRA-25	0.5 x 0.5	1948-2007	Precipitation	Hirabayashi et al. 2008	Daily
NCAR/NCEP	1.875 x 1.90	1948-2010	Precipitation Mean temperature Minimum temperature Maximum temperature	Kalnay et al. 1996	Daily

2.1 Trends in annual and seasonal climate

For each dataset in Table 2.1, the trend and significance of trend (p- value) of precipitation and temperatures (mean, maximum and minimum) are calculated for the annual cycle, winter, pre-monsoon, post-monsoon and rabi seasons for the IGP and its associated sub-regions

(Indus, Ganges and Himalaya; refer to Appendix 1). For each dataset, the trend is derived from the value of the slope calculated by fitting a linear regression model to the time series. The Fisher's f-test is then used to calculate the p- value, or statistical significance of the trend; trends with a p- value of less than 0.1 are highlighted in the tables of results (Tables 2.2–2.5).

2.1.1 Precipitation

A rather mixed picture of rainfall trends emerges from the different datasets (Table 2.2). For the larger IGP domain, there is a tendency for most datasets to show an increase, but very few of these trends are statistically significant. This is in agreement with the results from the Intergovernmental Panel on Climate Change (IPCC) 4th Assessment (Working Group 1, Chapter 2), which shows the northern Indian region as an area with no strong positive or negative trend in precipitation. The two observational datasets, CRU and APHRODITE, show opposing trends in the monsoon season, but are consistent in the other seasons (increasing rainfall). In the Indus basin there is a consistent picture of increasing precipitation in all seasons, although few of the trends are statistically significant. Over the Ganges basin, and also the Himalaya, CRU and APHRODITE disagree on annual and monsoon-season trends, and the reanalysis datasets exhibit varying trends as well. For other seasons, there is general agreement in small, generally non-significant, increasing trends. It should be noted that while the trends for the Himalaya sub-region are comparable with that of the IGP region and other sub-regions, the confidence in the underlying data in the Himalaya is not high given the paucity of underlying meteorological observations and the difficulties that reanalysis models have in representing processes in areas of complex terrain.

Table 2.2: Trends in seasonal climate from 1960-2001: Precipitation

	Annual		Winter		Pre-Monsoon		Monsoon		Post-Monsoon		Rabi	
	trend	*p*-value	trend	*p*-value	trend	*p*-value	trend	*p*-value	trend	*p*-value	trend	*p*-value
Indo-Gangetic Plain												
APHRODITE	0.0073	0.0038	0.0036	0.0771	0.0155	0.0019	0.0106	0.0783	0.0033	0.2530	0.0031	0.0663
CRU	-0.0002	0.9409	0.0018	0.2794	0.0083	0.1591	-0.0106	0.1721	0.0008	0.7903	0.0015	0.3548
ERA-40	0.0053	0.0006	0.0021	0.0207	0.0106	0.0002	0.0093	0.0026	0.0013	0.2656	0.0013	0.0742
JRA-25	-0.0028	0.3636	0.0012	0.5648	0.0028	0.6704	-0.0145	0.0442	0.0015	0.6628	0.0018	0.3213
NCEP/NCAR	0.0040	0.1279	-0.0034	0.0458	0.0062	0.2155	0.0159	0.0066	-0.0018	0.4292	-0.0027	0.0581
Indus												
APHRODITE	0.0020	0.3653	0.0011	0.6021	0.0044	0.0743	0.0022	0.7072	0.0015	0.3782	0.0015	0.4044
CRU	0.0017	0.5272	0.0003	0.8776	0.0034	0.2408	0.0033	0.6681	0.0001	0.9237	0.0011	0.5166
ERA-40	0.0026	0.0648	0.0013	0.1250	0.0030	0.0428	0.0050	0.1704	0.0014	0.0799	0.0013	0.0859
JRA-25	-0.0002	0.9431	0.0000	0.9947	0.0017	0.5144	-0.0021	0.7812	0.0014	0.3841	0.0011	0.5083
NCEP/NCAR	-0.0006	0.8030	-0.0041	0.0044	-0.0035	0.1209	0.0042	0.5297	-0.0010	0.4731	-0.0029	0.0087
Ganges												
APHRODITE	0.0126	0.0069	0.0057	0.0458	0.0257	0.0059	0.0195	0.0639	0.0051	0.3468	0.0047	0.1031
CRU	-0.0015	0.7577	0.0032	0.1824	0.0124	0.2484	-0.0217	0.0586	0.0016	0.7799	0.0021	0.4817
ERA-40	0.0086	0.0001	0.0027	0.0258	0.0185	0.0001	0.0156	0.0001	0.0018	0.4235	0.0016	0.1986
JRA-25	-0.0043	0.4021	0.0022	0.4618	0.0045	0.7167	-0.0231	0.0346	0.0013	0.8440	0.0023	0.4928
NCEP/NCAR	0.0094	0.0365	-0.0033	0.2689	0.0172	0.0922	0.0293	0.0010	-0.0014	0.7317	-0.0022	0.3855
Himalaya												
APHRODITE	0.0014	0.5654	-0.0004	0.8954	0.0083	0.1085	0.0005	0.9350	0.0010	0.8140	-0.0004	0.8788

2.1.2 Mean temperature

Over the IGP, the CRU instrumentally-based dataset shows increasing trends that a
consistent with those reported by the IPCC (Working Group 1, Chapter 2), of appr
0.1 °C per decade for mean annual temperature (Table 2.3). Trends are positive for
seasons, though not statistically significant for the pre-monsoon and monsoon seas
reanalysis data show a much more mixed signal, which requires further investigati

The CRU dataset shows similar patterns over the sub-regions studied: the Ganges b
the Himalaya show warming in all seasons, while the Indus basin shows warming i
seasons except the monsoon. The Himalaya shows a greater warming trend than ot
regions, especially in the non-monsoon seasons, up to 0.2 °C per decade in some ir
Again a mixed picture emerges from the reanalysis data.

2.1.3 Maximum temperature

Table 2.4 shows the trends of maximum temperature. Over the wider IGP region, t
data show increasing trends, except in the monsoon season, while the reanalyses tr
more variable. This pattern is repeated for the different sub-regions. Not many of th
trends are statistically significant. For CRU, in nearly all cases, trends in maximum
temperature are lower than those for mean temperature.

2.1.4 Minimum temperature

With reference to Table 2.5, trends in the CRU estimates of minimum temperature
region are all positive, including for the monsoon season, with most results being s
significant. Trends are particularly large in the post-monsoon and rabi seasons, by
0.3 °C per decade, in the Ganges basin.

Table 2.3: Trends in seasonal climate from 1960-2001: Mean temperature

	Annual		Winter		Pre-Monsoon		Monsoon		Post-Monsoon		Rabi	
	trend	*p*-value	trend	*p*-value	trend	*p*-value	trend	*p*-value	trend	*p*-value	trend	*p*-value
Indo-Gangetic Plain												
CRU	0.0106	0.0056	0.0115	0.0531	0.0105	0.1090	0.0012	0.7604	0.0251	0.0001	0.0148	0.0049
ERA-40	-0.0065	0.1215	-0.0046	0.4376	-0.0172	0.0217	-0.0131	0.0099	0.0075	0.2651	-0.0002	0.9756
NCEP/NCAR	-0.0037	0.4449	-0.0143	0.0663	-0.0104	0.0861	0.0016	0.7413	0.0112	0.0993	-0.0047	0.4846
Indus												
CRU	0.0118	0.0174	0.0153	0.0338	0.0210	0.0397	-0.0037	0.4623	0.0254	0.0019	0.0149	0.0236
ERA-40	-0.0082	0.1944	0.0030	0.6960	-0.0123	0.2508	-0.0271	0.0012	0.0075	0.4063	0.0023	0.7571
NCEP/NCAR	0.0077	0.2247	0.0009	0.9067	0.0133	0.1482	0.0061	0.4010	0.0214	0.0335	0.0056	0.4981
Ganges												
CRU	0.0099	0.0117	0.0084	0.1631	0.0020	0.7774	0.0058	0.1193	0.0250	0.0001	0.0148	0.0030
ERA-40	-0.0048	0.1667	-0.0109	0.0635	-0.0209	0.0085	-0.0008	0.8460	0.0080	0.1676	-0.0018	0.6755
NCEP/NCAR	-0.0126	0.0097	-0.0265	0.0042	-0.0293	0.0002	-0.0018	0.6727	0.0037	0.5218	-0.0126	0.0606
Himalaya												
CRU	0.0123	0.0167	0.0165	0.0378	0.0100	0.1776	0.0022	0.6211	0.0196	0.0116	0.0178	0.0105
ERA-40	0.0037	0.4025	0.0035	0.6263	-0.0050	0.4389	-0.0012	0.6883	0.0159	0.0633	0.0090	0.1654
NCEP/NCAR	-0.0296	0.0004	-0.0346	0.0014	-0.0407	0.0013	-0.0236	0.0263	-0.0195	0.0830	-0.0293	0.0077

Note: Statistically significant values (p-value < 0.1) are coloured red

Table 2.4: Trends in seasonal climate from 1960-2001: Maximum temperature

	Annual		Winter		Pre-Monsoon		Monsoon		Post-Monsoon		Rabi	
	trend	*p*-value	trend	*p*-value	trend	*p*-value	trend	*p*-value	trend	*p*-value	trend	*p*-value
Indo-Gangetic Plain												
CRU	0.0061	0.1213	0.0043	0.5093	0.0071	0.3262	-0.0017	0.6736	0.0208	0.0009	0.0088	0.1285
ERA-40	-0.0085	0.1349	-0.0083	0.2804	-0.0176	0.0693	-0.0134	0.0773	0.0080	0.3012	-0.0037	0.5759
NCEP/NCAR	0.0042	0.4856	-0.0021	0.8325	0.0002	0.9767	0.0035	0.6356	0.0232	0.0083	0.0053	0.5224
Indus												
CRU	0.0101	0.0533	0.0141	0.0753	0.0202	0.0585	-0.0062	0.2289	0.0230	0.0069	0.0130	0.0711
ERA-40	-0.0109	0.2195	-0.0017	0.8706	-0.0113	0.3976	-0.0304	0.0129	0.0110	0.3422	-0.0016	0.8720
NCEP/NCAR	0.0196	0.0184	0.0180	0.0827	0.0307	0.0128	0.0106	0.3798	0.0402	0.0010	0.0204	0.0365
Ganges												
CRU	0.0028	0.5163	-0.0041	0.5636	-0.0037	0.6749	0.0025	0.5690	0.0190	0.0018	0.0051	0.3600
ERA-40	-0.0063	0.1478	-0.0139	0.0448	-0.0224	0.0375	0.0013	0.8027	0.0055	0.3436	-0.0053	0.2683
NCEP/NCAR	-0.0078	0.2378	-0.0177	0.1516	-0.0239	0.0471	-0.0019	0.7613	0.0092	0.2509	-0.0067	0.4618
Himalaya												
CRU	0.0080	0.1188	0.0093	0.2824	0.0049	0.5564	-0.0011	0.7931	0.0173	0.0458	0.0130	0.0919
ERA-40	0.0068	0.1250	0.0059	0.4394	-0.0062	0.4169	0.0003	0.9192	0.0268	0.0038	0.0148	0.0288
NCEP/NCAR	-0.0281	0.0022	-0.0344	0.0056	-0.0418	0.0030	-0.0233	0.0380	-0.0132	0.3369	-0.0266	0.0355

Note: Statistically significant values (p-value < 0.1) are coloured red

Table 2.5: Trends in seasonal climate from 1960-2001: Minimum temperature

	Annual		Winter		Pre-Monsoon		Monsoon		Post-Monsoon		Rabi	
	trend	*p*-value	trend	*p*-value	trend	*p*-value	trend	*p*-value	trend	*p*-value	trend	*p*-value
Indo-Gangetic Plain												
CRU	0.0151	0.0002	0.0186	0.0012	0.0139	0.0281	0.0041	0.3298	0.0294	0.0000	0.0208	0.0000
ERA-40	-0.0102	0.0430	-0.0050	0.4076	-0.0195	0.0124	-0.0185	0.0000	-0.0014	0.8774	-0.0029	0.6424
NCEP/NCAR	-0.0022	0.6684	-0.0159	0.0351	-0.0099	0.1699	0.0049	0.2367	0.0124	0.1384	-0.0037	0.5893
Indus												
CRU	0.0135	0.0058	0.0164	0.0146	0.0217	0.0273	-0.0012	0.8129	0.0278	0.0015	0.0168	0.0081
ERA-40	-0.0063	0.2365	0.0057	0.3455	-0.0140	0.1813	-0.0243	0.0001	0.0062	0.5346	0.0057	0.3907
NCEP/NCAR	0.0061	0.3733	-0.0055	0.4953	0.0060	0.5239	0.0092	0.1240	0.0165	0.1866	0.0027	0.7804
Ganges												
CRU	0.0169	0.0001	0.0209	0.0006	0.0077	0.2124	0.0090	0.0499	0.0309	0.0000	0.0244	0.0000
ERA-40	-0.0130	0.0193	-0.0138	0.0567	-0.0237	0.0009	-0.0130	0.0013	-0.0069	0.4508	-0.0096	0.1799
NCEP/NCAR	-0.0090	0.0558	-0.0248	0.0025	-0.0232	0.0009	0.0018	0.6222	0.0096	0.1467	-0.0089	0.1419
Himalaya												
CRU	0.0165	0.0042	0.0237	0.0027	0.0151	0.0429	0.0056	0.3321	0.0220	0.0089	0.0226	0.0014
ERA-40	-0.0066	0.3295	-0.0019	0.8219	-0.0067	0.4606	-0.0124	0.0313	-0.0057	0.5899	-0.0038	0.6524
NCEP/NCAR	-0.0369	0.0001	-0.0433	0.0006	-0.0477	0.0008	-0.0270	0.0173	-0.0268	0.0281	-0.0388	0.0024

Note: Statistically significant values (*p*-value < 0.1) are coloured red

2.2 Trends in extremes

Eight indices are used to study the trends of extreme events from 1960-2001. Datas
Table 2.1 except CRU[1] are used to calculate the indices. For rainfall-based indices
APHRODITE dataset is used in addition to reanalysis data; for temperature based i
only reanalysis data are used. The indices are:

- Consecutive dry days (CDD): the longest run of consecutive days where daily precipitation is less than 1mm, in each year and season.
- Consecutive wet days (CWD): the longest run of consecutive days where daily precipitation is at least 1mm.
- Consecutive dry periods of more than five days (CDD5): the total number of p more than five consecutive days with precipitation less than 1mm.
- Consecutive wet periods of more than days (CWD5): the total number of perio than five consecutive days with precipitation greater than 1mm.
- Cold nights (TN10p): number of days where daily minimum temperature is les 10th percentile of the daily minimum temperature for 1970-1999
- Warm nights (TN90p): number of days where daily minimum temperature is m the 90th percentile of the daily minimum temperature for 1970-1999
- Very cold days (TX10p): number of days where daily maximum temperature i the 10th percentile of the daily maximum temperature for 1970-1999
- Very warm days (TX90p): number of days where daily maximum temperature than the 90th percentile of the daily maximum temperature for 1970-1999

Tables C1–C8 in Appendix 3 provide a summary of the trends and significance of
these indices for different seasons for the IGP domain and its associated sub-regior

2.2.1 Consecutive dry days (CDD)

CDD (Table C1) show a largely negative trend for the IGP region, and most of the
domains for each season, suggesting the maximum length of dry spells has decreas
However, while 70% of the possible data-domain-season combinations show this d
trend, only a few are statistically significant. Of the sub-regions, the Indus shows tl
consistent picture.

[1] CRU data are monthly, whereas daily data are needed to calculate indices of extremes.

2.2.2 Number of dry periods > 5 days (CDD5)

While the length of the longest dry spells (CDD) has decreased quite widely, the number of extended dry periods in each season shows a more mixed signal (Table C2). No consistent picture emerges, and the lack of many statistically significant trends suggests that little can be concluded about any emerging signals for this agriculturally important critical index.

2.2.3 Consecutive wet days (CWD)

The trend of CWD over the IGP region is largely positive (Table C3) with approximately 65% of data-domain-season combinations showing increases. However, very few of these trends are statistically significant, and as with other rainfall indices, there appears to be no strong emerging signal.

2.2.4 Number of wet periods > 5 days (CWD5)

The IGP region sees a negative trend of CWD5 for the annual cycle and monsoon season (Table C4). Statistically significant trend values dominate the monsoon season with trends as large as -0.072 per year. Some statistically significant positive trends can be seen for the remaining seasons with a high and low of 0.0298 and 0.0033 per year, respectively. For the Indus sub-region, the annual cycle sees a predominantly negative trend while the rest of the seasons see two out of the four datasets projecting trends that go either way. The case for the Himalaya sub-region is characterized by largely negative trends for all seasons except the monsoon and post-monsoon, while for the Ganges sub-region, it is the annual cycle and monsoon season.

2.2.5 Temperature extremes

Trends for temperature extremes—cold nights (TN10p), warm nights (TN90p), cold days (TX10p) and warm days (TX90p)—are shown in Tables C5–C8. These trends are based on the NCEP and ERA reanalysis datasets, which were shown to exhibit less distinct trends in mean monthly temperatures than the station-based CRU dataset. While there is a tendency for decreasing trends for both the cold and hot extremes, very few of these trends are statistically significant, and in quite a few instances, for any one region or season, the two datasets show contrasting trends. The lack of significance in these extremes agrees with other work; for example Kothawale et al. (2010) showed that most stations in the north of India showed non-significant trends in temperature extremes in the pre-monsoon season.

3. Global Climate Model Evaluation

3.1 Previous work

A necessary, but not complete, gauge of the reliability of a climate change projection is a model's ability to simulate the present-day climatology and its variability; this forms an important part of model evaluation (Randall et al. 2007). Uncertainties in climate projections originate from several sources in climate models, commonly divided into (Hawkins and Sutton 2009):

- *Internal variability*: all climate models, as with the real world climate, have internal variability related to chaotic nature of weather and climate; thus, even a projection with a perfect model will have some variation for any time period in the future; in reality, this internal variability will have differences to that of the real world due to physics and structural errors described below.
- *Model structure*: differences in the ways models are "put together"—the components included and model resolution.
- *Model physics*: the ways that physical processes in the model are represented, most especially parameterisations, "sub-models" that represent physical processes that cannot be resolved by the fluid-dynamical equations.

Additional to these model-related uncertainties are forcing uncertainties—a lack of clarity on how natural and anthropogenic radiative forcing of the climate system will evolve in the future.

Over the Indian subcontinent, a major obstacle for deriving reliable projection arises from the difficulties that climate models have in simulating the Indian summer monsoon rainfall characteristics (Annamalai and Slingo 2001; Ashrit et al. 2005; Annamalai et al. 2007) and also the interaction of the monsoon and other circulation features with the Himalaya–Hindu-Kush and Tibetan Plateau.

The broad-scale features of the monsoon circulation, such as the establishment of the trough of low pressure along the Indo-Gangetic Plains, the cross-equatorial flow from the Southern Hemisphere across the east African coast, low level wind flow over south Asia, and the upper level large scale anti-cyclonic conditions are reasonably well captured by the recent coupled climate models (Kripalani et al. 2007; Stowasser et al. 2009). Consequently, the three relevant

intense rainfall or deep convection centres of the Asian summer monsoon—Indian monsoon, western north Pacific monsoon and equatorial Indian Ocean convection—are captured realistically (Annamalai et al. 2007).

However the simulation of the monsoon precipitation climatology has proven to be more difficult, and provides a severe test of the climate models. Studies have shown that compared to atmosphere-only GCMs, coupled atmosphere–ocean GCMs perform better in simulating the monsoon, but with a moderate skill (Krishna Kumar et al. 2005). Model inter-comparison studies have shown that there is a very wide variation in the quality of the simulation of the mean monsoon, even in the latest generation of models used in IPCC-AR4. Annamalai et al. (2007) found that, out of 18 models considered, only one third was able to reproduce a reasonable monsoon precipitation climatology; of these, four exhibited a robust ENSO–monsoon contemporaneous teleconnection, including the known inverse relationship between ENSO and rainfall variations over India. Further, only half of the six models were able to represent the timing of the teleconnection and only one model captured the observed phase lag with the strongest anti-correlation of SST peaking 2–3 months after the summer monsoon. The models which best capture the ENSO–monsoon teleconnection also do a better job in simulating the timing and location of sea-surface temperature and diabatic heating anomalies in the equatorial Pacific, and the associated changes to the equatorial Walker circulation during El Niño events.

When looking at specific models, a number of studies have identified shortcomings, with no model being particularly strong in all aspects of its simulation of the monsoon (for example, Ashrit et al. 2001; Ashrit et al. 2003; Meehl and Arblaster 2003; Ashrit et al. 2005; Turner et al. 2007). Thus the ability of different global climate models to represent both temperature and rainfall patterns over the south Asian region is quite variable—some models simulate patterns better than others overall, and many reproduce aspects within some sub-regions better than in others. Only a few capture some of the relationships that are known to affect interannual variability of monsoon rainfall.

3.2 Current analysis

In the analysis presented here, the ability of CMIP3 (IPCC AR4) coupled climate models (Table 3.1) to represent the basic climate over the IGP is assessed; this therefore extends previous work by focusing specifically on the IGP, and Ganges, Indus and Himalaya sub-

domains. We analyse a sub-set of the CMIP3 models, limited to those for which daily data are available. Daily data for precipitation and temperature (mean, maximum and minimum) are available for the "present day" period, that is 1960–1999, and two periods in the future, 2046–2065 and 2080–2099. Monthly data are available for all models for the period 1960–2099 but for precipitation and mean temperature only (not maximum and minimum temperatures). For the periods 2050s and 2090s, the years 2050–2059 and 2090–2099, respectively are extracted from the daily data. For the 2030s, monthly data from 2030–2039 are used. For analysis requiring a baseline, the years 1970–1999 are extracted and averaged to give the baseline values.

Table 3.1: Details of GCMs used

Data	Resolution (in degrees)	Originating group (*Country*)
bccr_bcm2_0	2.81 x 2.78	Bjerknes Centre for Climate Research (*Norway*)
cccma_cgcm3_1	3.75 x 3.70	Canadian Centre for Climate Modelling and Analysis (*Canada*)
cnrm_cm3	2.81 x 2.78	Centre National de Recherches Météorologiques (*France*)
csiro_mk3_0	1.87 x 1.86	CSIRO Atmospheric Research (*Australia*)
csiro_mk3_5	1.87 x 1.86	CSIRO Atmospheric Research (*Australia*)
gfdl_cm2_0	2.5 x 2	Geophysical Fluid Dynamics Laboratory (*USA*)
giss_model_e_r	5 x 4	NASA / Goddard Institute for Space Studies (*USA*)
ipsl_cm4	3.75 x 2.53	Institut Pierre Simon Laplace (*France*)
miroc3_2_medres	2.81 x 2.78	Center for Climate System Research (The University of Tokyo), National Institute for Environmental Studies, and Frontier Research Center for Global Change (JAMSTEC) (Japan)
miub_echo_g	3.75 x 3.70	Meteorological Institute of the University of Bonn, Meteorological Research Institute of KMA, and Model and Data group (*Germany/Korea*)
mpi_echam5	1.87 x 1.86	Max Planck Institute for Meteorology (*Germany*)
mri_cgcm2_3_2a	2.81 x 2.81	Meteorological Research Institute (*Japan*)
ncar_pcm1	2.81 x 2.78	National Center for Atmospheric Research (*USA*)

A number of observed datasets are used in the model evaluation (Table 3.1). To evaluate the performance of models in simulating the present climate, a series of analyses are performed. Firstly, maps of model bias—the difference between model and observed means—are used to show the spatial patterns of model performance (Section 0). Secondly, the mean absolute error between models and observations across the IGP is computed to quantitatively measure how close the models are to the observed dataset in terms of representing the present (1970–1999) climatology (Section 0). Thirdly, the spatial correlation is calculated to measure the strength

of the agreement in the spatial patterns of observed and model climatologies (Section0). Finally, the monsoon timing and over the IGP is compared to observations (Section 0).

3.2.1 Bias

CRU is used as the reference dataset for evaluating biases in models since it closely resembles the reality more than other datasets given the fact that it is based on a dense network of rain gauge and/or temperature data, that is, gridded datasets interpolated from meteorological station data. The average of the present period from 1970–1999 is obtained from both CRU and GCMs, after which the value of CRU is subtracted from each GCM on a grid-point basis. The procedure is repeated for each season: annual, winter, pre-monsoon, monsoon, post-monsoon and rabi for precipitation and temperature (mean, maximum, and minimum). To ensure a fair comparison, the resolution of CRU is interpolated to match the resolution of the corresponding model. For example, to evaluate bccr_bcm2_0 which has a resolution of 2.81° x 2.78°, the resolution of CRU is interpolated from 0.5° x 0.5° to 2.81° x 2.78°.

For precipitation, the average bias generated by the models is relatively small, ranging from -2 mm/day to 2 mm/day over much of South Asia (Appendix 4, Figures D1–D6). Large negative (dry) bias (> -5 mm/day) is consistently projected over Bangladesh during the annual (Figure D1), pre-monsoon (Figure D3), and monsoon (Figure D4) seasons. In many models the spatial extent of large negative bias is more widespread during the monsoon season (Figure D4). However, during the winter (Figure D2), post-monsoon (Figure D5) and rabi (Figure D6) seasons, the bias is significantly less over Bangladesh. Apart from the common dry bias over the Bangladesh region, and the IGP in the monsoon season for a large proportion of models, there is not any other systematic pattern of bias—different models have their largest biases in different parts of the South Asian region.

For mean temperature (Appendix 4, Figures D7–D12), most models have a tendency for negative (cold) bias over the entire region, and many of the models have a large negative bias of up to ~5 °C over the IGP region over all seasons. Three of the models, csiro_mk3_5, model_e_r and mpi_echam5 show positive biases over the IGP area. The situation is similar for minimum temperature (Appendix 4, Figures D13–D18) but with the addition of bccr_bcm2_0 and miub_echo_g which show a more positive bias over the IGP region. In the case of maximum temperature (Appendix 4, Figures D19–D24), a large bias (more than -5 °C) is apparent in many of the models especially bccr_bcm2_0 and ncar_pcm1 (note that for

ncar_PCM1, the large bias of over 15°C is likely due to a data transcoding error, and is being investigated at time of writing). More large positive biases (more than 5 °C) over the IGP area are present in several models (for example, cccma_cgcm3_1, csiro_mk3_5, giss_model_e_r, miroc3_2_medres, and mri_cgcm2_3_2a) during the pre-monsoon (Figure D21) and monsoon (Figure D22) seasons.

Both precipitation and temperature biases can, to some extent, be corrected for when developing climate change scenarios—and this is done in the generation of scenarios for this report. However, these 20th century biases may also effect the 21st century projected regional warming response—for example, a cold temperature bias would result in over-estimated snow cover at higher elevations, and potentially an incorrect snow-ice albedo feedback response in the 21st century scenarios. Thus while biases in basic state can be removed in the scenarios, biases in warming response cannot be easily accounted for.

3.2.2 Mean absolute error

The mean absolute error (MAE) is a measure average agreement between GCM and observed grid values, over a given domain. The error is calculated by adding the absolute values of the difference between the model and observed data, and averaging these differences across the geographical domain of interest. Lower MAE implies a closer match between the model and observations. The resolutions of some of the GCMs are too coarse to adequately capture the IGP domain, and especially the Indus and Ganges sub-domains, and so all datasets are re-gridded to 0.5° x 0.5° resolution, to match the CRU resolution. Tables 3.2–3.5 show the mean absolute error figures for the 13 GCMs for six seasons.

With reference to Table 3.2, the MAE for precipitation is largest for the monsoon, which is to be expected, given the higher mean rainfall amounts in this season. In the dry seasons, MAE is similar, and in the pre and post-monsoon seasons, intermediate values for MAE are reported. The spread in MAE across the models is quite variable, supporting the previous analysis suggesting that model performance with respect to precipitation is not consistent.

There are large MAEs for mean, maximum and minimum temperatures (Tables 3.3–3.5), but the degree of error from season to season is comparable with each other. For maximum temperature, the ncar_pcm1 and cccma_cgcm3_1 generates the largest MAE amongst models, but note that ncar_pcm1 maximum temperatures may be incorrectly archived.

Table 3.2: GCM mean absolute error for precipitation

Model	Annual	Winter	Pre-Monsoon	Monsoon	Post-Monsoon	Rabi
bccr_bcm2_0	1.11	0.44	1.39	3.02	0.80	0.59
cccma_cgcm3_1	1.06	0.31	1.51	2.53	0.39	0.24
cnrm_cm3	1.65	0.78	2.57	3.75	1.06	0.75
csiro_mk3_0	1.14	0.27	1.95	2.88	0.31	0.20
csiro_mk3_5	1.00	0.31	2.10	2.50	0.46	0.20
gfdl_cm2_0	0.81	0.27	1.69	1.77	0.37	0.21
giss_model_e_r	1.45	0.34	2.09	3.57	0.41	0.33
ipsl_cm4	1.65	0.47	2.06	4.94	0.50	0.42
miroc3_2_medres	0.59	0.22	0.84	1.29	0.58	0.29
miub_echo_g	1.20	0.24	1.65	3.30	0.37	0.23
mpi_echam5	0.97	0.28	1.03	2.43	0.32	0.22
mri_cgcm2_3_2a	1.38	0.34	1.80	3.58	0.45	0.31
ncar_pcm1	1.14	0.39	1.52	3.44	0.53	0.37
Ensemble mean	1.16	0.36	1.71	3.00	0.50	0.34

Table 3.3: GCM mean absolute error for mean temperature

Model	Annual	Winter	Pre-Monsoon	Monsoon	Post-Monsoon	Rabi
bccr_bcm2_0	4.26	4.97	4.65	3.16	4.56	4.86
cccma_cgcm3_1	6.82	8.72	4.79	4.33	9.2	9.07
cnrm_cm3	4.67	4.34	5.17	4.52	5.18	4.54
csiro_mk3_0	4.51	5.8	3.19	2.66	6.96	6.41
csiro_mk3_5	2.57	2.22	3.36	3.98	2.54	2.28
gfdl_cm2_0	4.59	5.44	2.86	3.29	6.79	6.04
giss_model_e_r	3.25	3.44	3.82	4.12	3.27	3.32
ipsl_cm4	4.79	5.7	5.59	3.29	5.5	5.53
miroc3_2_medres	4.19	4.52	3.67	3.91	4.72	4.62
miub_echo_g	5.61	6.21	5.95	4.39	6.47	6.24
mpi_echam5	2.47	2.07	3.02	3.19	2.12	2.05
mri_cgcm2_3_2a	5.74	6.23	5.61	4.78	6.8	6.46
ncar_pcm1	6.61	7.71	7.22	5.39	6.35	7.01
Ensemble mean	4.62	5.18	4.53	3.92	5.42	5.26

Table 3.4: GCM mean absolute error for maximum temperature

Model	Annual	Winter	Pre-Monsoon	Monsoon	Post-Monsoon	Rabi
bccr_bcm2_0	8.16	9.47	8.58	5.82	9.1	9.35
cccma_cgcm3_1	2.77	4.58	2.85	3.6	5.95	5.29
cnrm_cm3	4.71	4.11	5.05	4.6	5.95	4.63
csiro_mk3_0	3.92	5.24	2.9	2.61	7.17	6.14
csiro_mk3_5	2.54	2.11	4.15	4.69	2.71	2.1
gfdl_cm2_0	3.91	4.53	2.31	3.24	6.53	5.36
giss_model_e_r	3.34	3.74	4.32	5.1	3.73	3.66
ipsl_cm4	4.13	6.03	5.14	2.38	5.54	5.7
miroc3_2_medres	4.01	4.22	3.09	4.04	4.94	4.58
miub_echo_g	6.89	8.5	7.03	4.05	8.9	8.58
mpi_echam5	2.25	1.87	2.76	3.38	1.78	1.8
mri_cgcm2_3_2a	3.32	4.24	2.75	3.67	4.61	4.41
ncar_pcm1	19.43	21.91	21.41	16.06	19.15	20.52
Ensemble mean	5.34	6.20	5.56	4.86	6.62	6.32

Table 3.5: GCM Mean absolute error for minimum temperature

Model	Annual	Winter	Pre-Monsoon	Monsoon	Post-Monsoon	Rabi
bccr_bcm2_0	2.42	2.52	2.34	2.46	2.92	2.64
cccma_cgcm3_1	8.99	10.52	9.26	6.95	9.47	10.05
cnrm_cm3	3.64	3.51	4.43	3.64	3.54	3.46
csiro_mk3_0	5.31	6.39	4.9	3.58	6.37	6.44
csiro_mk3_5	2.41	2.51	2.4	2.8	2.78	2.62
gfdl_cm2_0	6.36	7.45	6.16	4.6	7.3	7.37
giss_model_e_r	3.38	3.61	3.71	3.42	3.53	3.53
ipsl_cm4	5.1	4.81	6.4	5.42	4.55	4.58
miroc3_2_medres	4.2	4.51	4.26	3.93	4.15	4.33
miub_echo_g	4.64	4.51	4.86	4.63	4.81	4.59
mpi_echam5	2.97	2.65	3.3	3.21	3.21	2.79
mri_cgcm2_3_2a	7.83	6.9	9.47	8.6	7.04	6.86
ncar_pcm1	6.51	7.03	7.97	6.46	4.93	5.95
Ensemble mean	4.90	5.15	5.34	4.59	4.97	5.02

3.2.3 Spatial correlation

Spatial correlation measures the extent to which a model captures the spatial pattern of the variable of interest, ignoring any systematic biases in absolute amount. The correlation is calculated on the basis of pairing each grid point of the observed dataset with its corresponding grid point from the modelled dataset and finding the correlation coefficient for the resulting paired data series. For this analysis, the datasets were re-gridded to 0.5° x 0.5° resolution, as some of the model resolutions are too coarse to adequately capture the IGP domain. Tables E1–E12 in Appendix 5 show the results of the spatial correlation of precipitation and mean temperature between the 13 GCMs and CRU datasets for different seasons and domains (see Appendix 6 for maximum and minimum temperatures).

For precipitation, results show that in general, the models generate positive correlations during all seasons and for different domains. Over the IGP region as a whole, a high correlation of at least 0.7 persists in all seasons, except during winter in which about half of the models have a correlation lower than 0.7. For the Indus region, the majority of the models show high positive correlation during the annual, winter and rabi seasons, whereas for the Ganges region, the high correlation dominates the pre-monsoon season. During the monsoon period, the correlation is high over the wider IGP and the Himalaya region as well as the entire south Asian domain. In all cases, the correlation is less good over the Himalaya, reflecting the difficulty that coarser resolution global models have in representing mountain climate. Several models have low or negative correlations in the monsoon season over the Indus basin; this is partly due to smaller spatial extent of this region, and the coarseness of these models, which are therefore unable to capture the finer detail of the patterns of monsoon rainfall. This would suggest that analyses at the scale of individual river basins, or the Himalayas as the source for these river basins, is pushing the limits of the skilful resolution of these models.

The case for mean temperature sees positive correlation of at least 0.7 for the IGP and Himalaya, and entire domain during all seasons. High correlation also exists for the Ganges during annual, winter, pre-monsoon, post-monsoon and rabi seasons. For the Indus region, the correlation is predominantly high except for during the pre-monsoon and monsoon seasons in which low correlation is registered by the models. Over the IGP region, the correlation is low during the post-monsoon season and to a certain extent, the annual cycle.

For maximum temperature, there is high correlation for all seasons and domains except Indus during pre-monsoon and monsoon. As for minimum temperature, consistently high correlation is found over the IGP + Himalaya and entire domain during all seasons. The majority of the models show high correlation during the winter season for the IGP region. Over the Indus, correlation is low for all seasons while over the Ganges, high correlation exists during annual, winter, pre-monsoon and rabi seasons.

3.2.4 Monsoon timing and extent

In this section, ability of climate models to represent the timing, duration and spatial extent of the monsoon over the IGP is evaluated through comparison with observations. Four observational datasets are used, all of which have daily data available: three reanalysis products (ERA-40, NCAR/NCEP and JRA-25) and one gauge-based dataset (APHRODITE). Monsoon onset and end are defined by the day where daily rainfall, averaged over the IGP between 1970–1990, and smoothed by passing a low-pass filter (1 month), exceeds the annual mean rainfall, expressed in mm/day (Table 3.6 and Figure 3.1).

Table 3.6: Monsoon timings and durations for present-day (1970–1999) simulations from observed/reanalysis and modelled (GCM) datasets

Observed/ Reanalysis	Start*	End*	Duration (months)	GCM	Start*	End*	Duration (months)
APHRODITE	150	283	4.4	bccr_bcm2_0	127	303	5.9
CRU	June	Sept	4	cccma_cgcm3_1	156	287	4.4
ERA-40	145	280	4.5	cnrm_cm3	133	310	5.9
JRA-25	144	277	4.4	csiro_mk3_0	175	288	3.8
NCAR/NCEP	203	329	4.2	csiro_mk3_5	178	296	3.9
				gfdl_cm2_0	166	284	3.9
				giss_model_e_r	164	265	3.4
				ipsl_cm4	11	320	10.3
				miroc3_2_medres	155	289	4.5
				miub_echo_g	155	291	4.5
				mpi_echam5	138	280	4.7
				mri_cgcm2_3_2a	153	280	4.2
				ncar_pcm1	140	276	4.5

* Start and end of monsoon season are expressed in terms of Julian day except CRU

Figure 3.1: Latitudinal mean daily precipitation (mm/day) averaged over the IGP region for the current period 1970-1999. Vertical lines indicate the onset (left) and termination (right) of the monsoon by respective datasets.

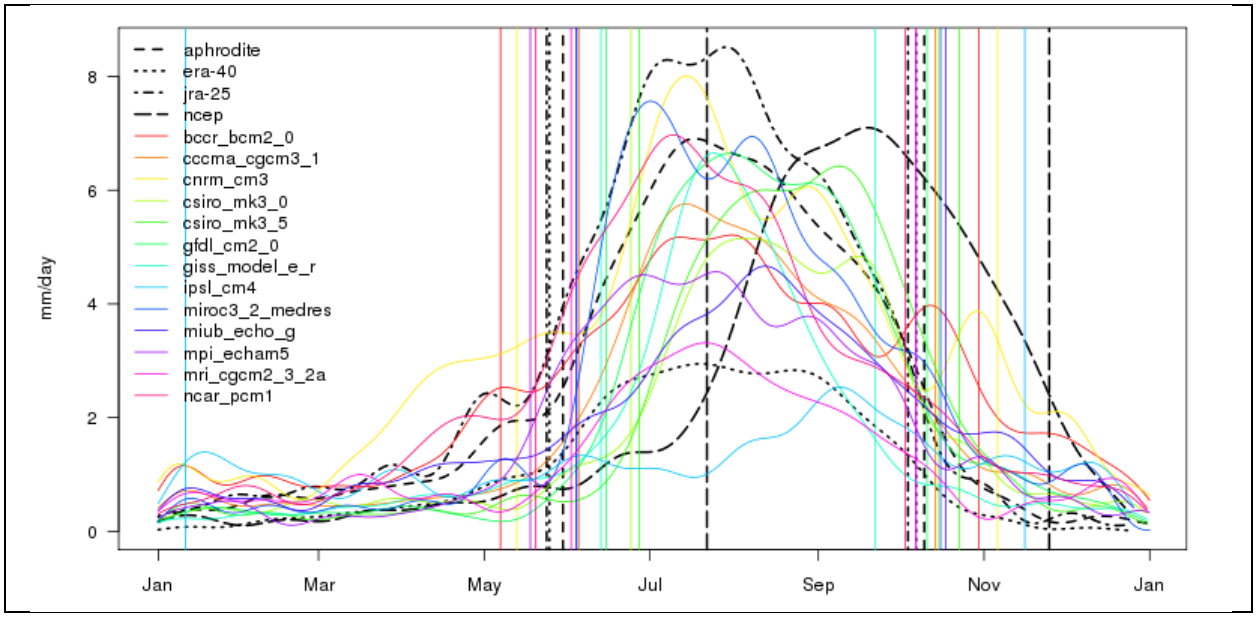

Three of the observed datasets are quite consistent in their representation of the onset and end of the monsoon; for APHRODITE, ERA-40 and JRA-25, the start and end of the monsoon period differ by a matter of a few days, with a similar duration of just over four months. The NCEP dataset exhibits a delayed onset and end date, but the correct duration. All the GCMs, except ipsl_cm4, have a distinct monsoon season, but none match the observations on all three criteria of start, end and duration. However, several match in terms of duration, and either start or end date. Most of the models generally simulate the start of monsoon to be the end of May or early June, while for the end of the monsoon season, models tend to predict a delayed end, giving, on average, a monsoon season that lasts longer than observed.

Figure 3.2 shows the spatial evolution of the monsoon in the IGP, through the use of latitude-month plots of precipitation. All models, except perhaps for IPSL show a monsoon-like pattern, with some progression northwards as the monsoon evolves and decays. However, the details of the monsoon evolution vary quite considerably, and so the specific characteristics of the monsoon rainfall across the IGP in each model should be treated cautiously.

Figure 3.2: Zonal mean precipitation (mm/day) for five observed/reanalysis and thirteen GCM datasets for the present period. Horizontal axis: months; vertical axis: latitude.

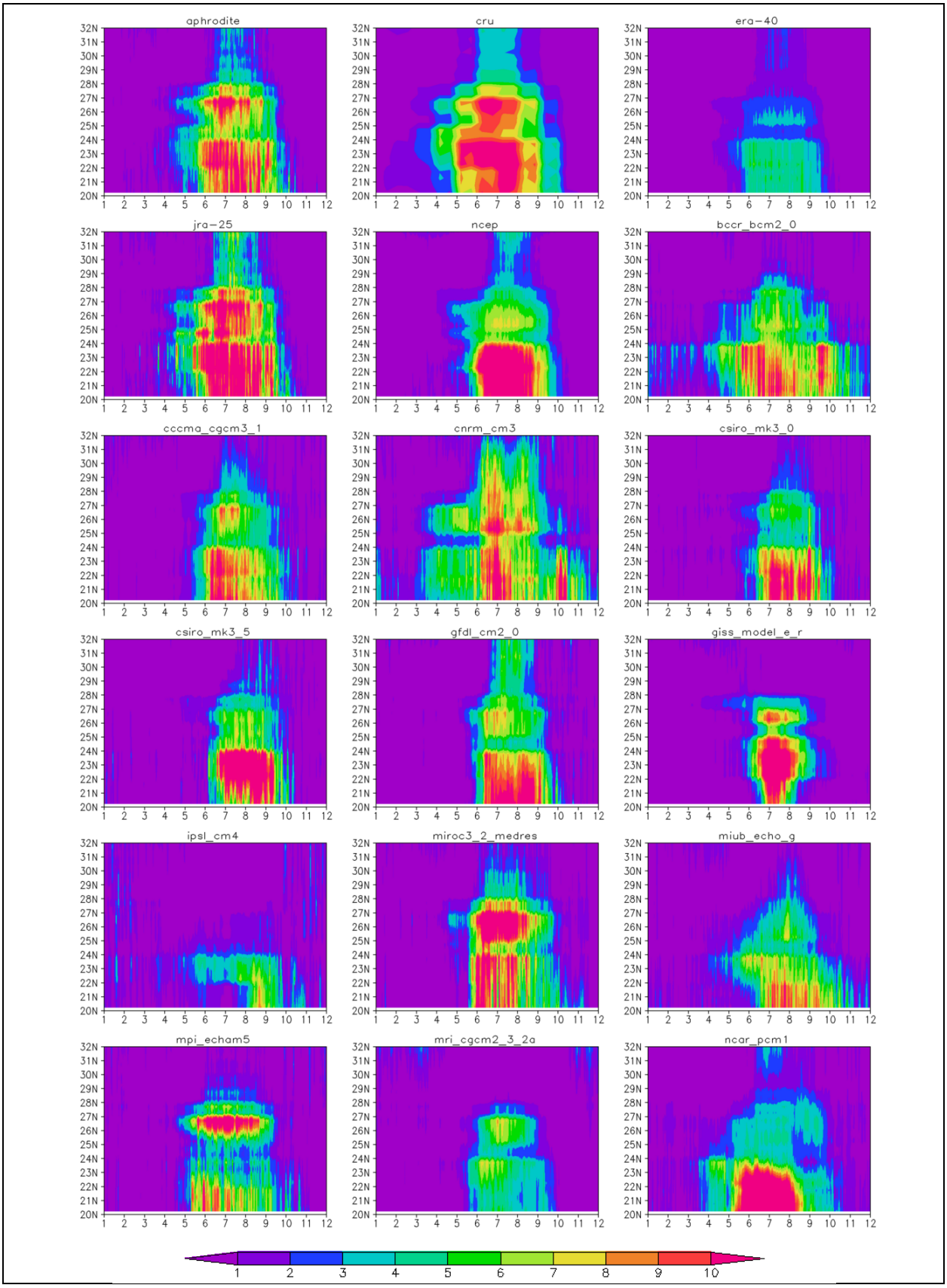

4. GCM projections

Projections for GCMs are calculated for three periods in the future, under three alternative emissions scenarios: 2030s, 2050s and 2090s, and SRES A1B, SRESA2 and SRES B1. The scenarios produce different rates of global and regional warming as a function of different possible future emissions, with the following "best guess" global temperature changes in the 2090s relative to 1980–1999: A2 – 3.4°C, A1B – 2.8°C , and B1 – 1.8°C (IPCC 2007).

Figures 4.1 and 4.2 show the trends of area-averaged mean temperature and precipitation, respectively, from 1960–2099, for different seasons for the IGP region (see Appendix 6 for the Indus, Ganges and Himalaya sub-domains). A summary of projected change for 2030s, 2050s and 2090s are given in Appendix 7 in Tables G1–G.12. Maps of changes (annual cycle) for the three future periods are shown in Figures 4.3 (precipitation) and 4.4 (mean temperature). Results for other variables (maximum and minimum temperatures) and seasons are available in Appendix 8.

Figure 4.1: Trends of annual and seasonal precipitation (mm/day) for the recent past and projected future for the Indo-Gangetic Plain. All values shown are anomalies, relative to the 1970-1999 mean climate. "20c3m: Re" represents the mean (black curve) and range (yellow shading) of five observed datasets from 1960-2001. "20c3m: Mo" represents the mean (brown curve) and range (pale brown shading) from 13 GCMs from 1960-1999. Coloured curves and shadings represent the ensemble projections of climate under three emission scenarios, SRESA1B (blue), SRESA2 (red) and SRESB1 (green).

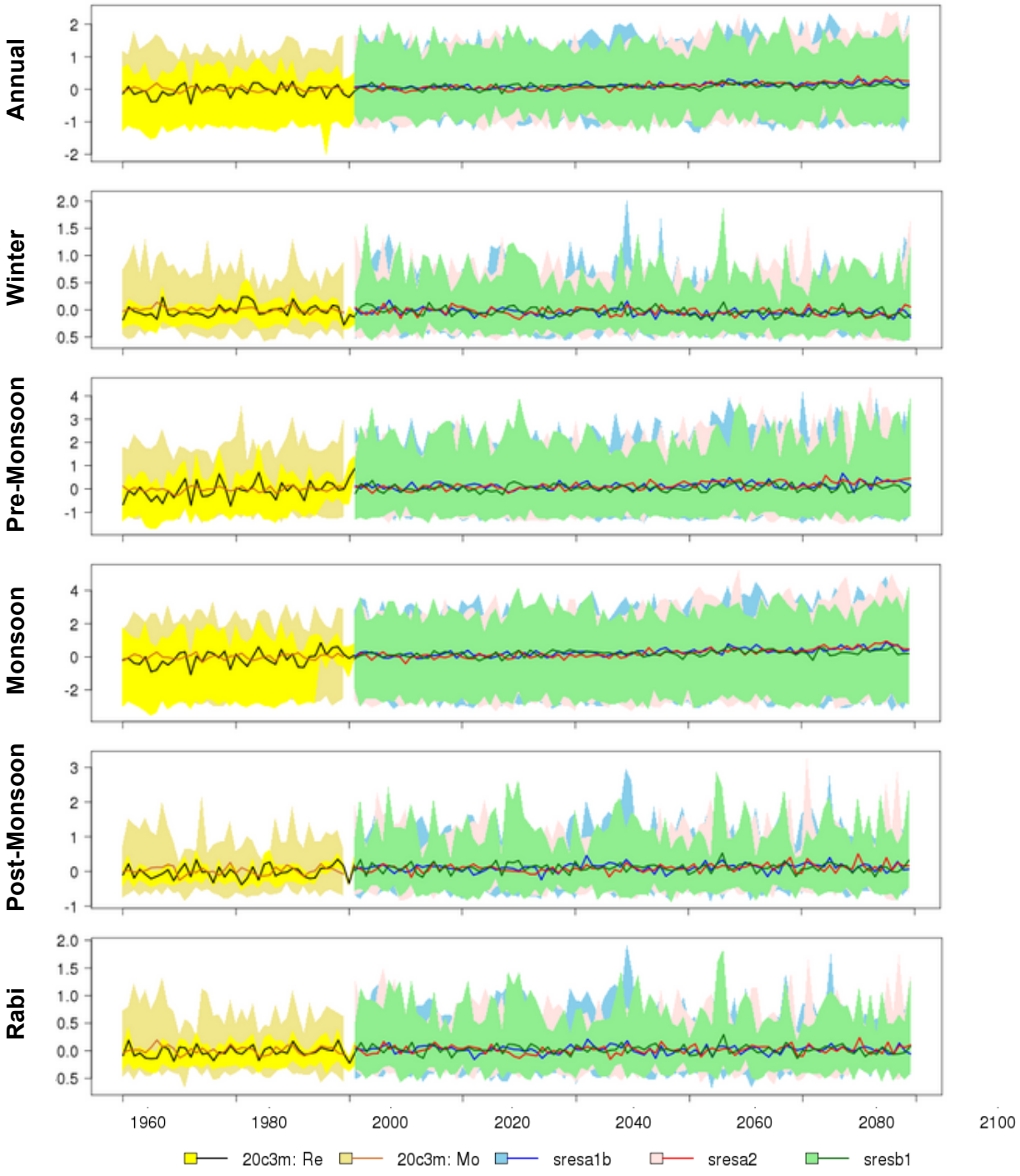

Figure 4.2: Trends of annual and seasonal mean temperature (°C) for the recent past and projected future for the Indo-Gangetic Plain. All values shown are anomalies, relative to the 1970-1999 mean climate. "20c3m: Re" represents the mean (black curve) and range (yellow shading) of three reanalysis datasets from 1960-2001. "20c3m: Mo" represents the mean (brown curve) and range (pale brown shading) from 13 GCMs from 1960-1999. Coloured curves and shadings represent the ensemble projections of climate under three emission scenarios, SRESA1B (blue), SRESA2 (red) and SRESB1 (green).

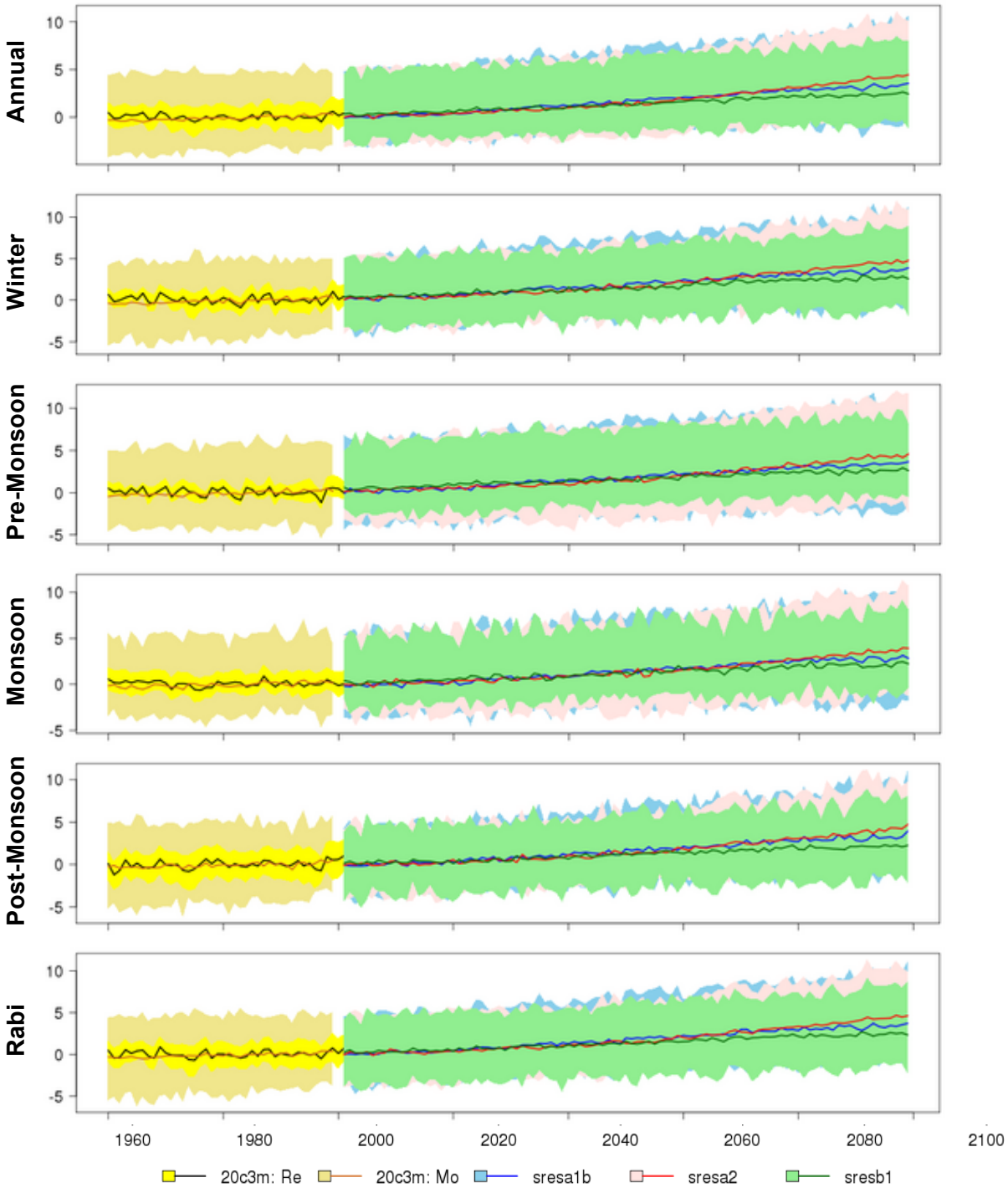

Figure 4.3: Ensemble mean precipitation anomalies (mm/day) relative to 1970-1999 for 2030s, 2050s and 2090s under the three emission scenarios. Figures shown are for annual cycle.

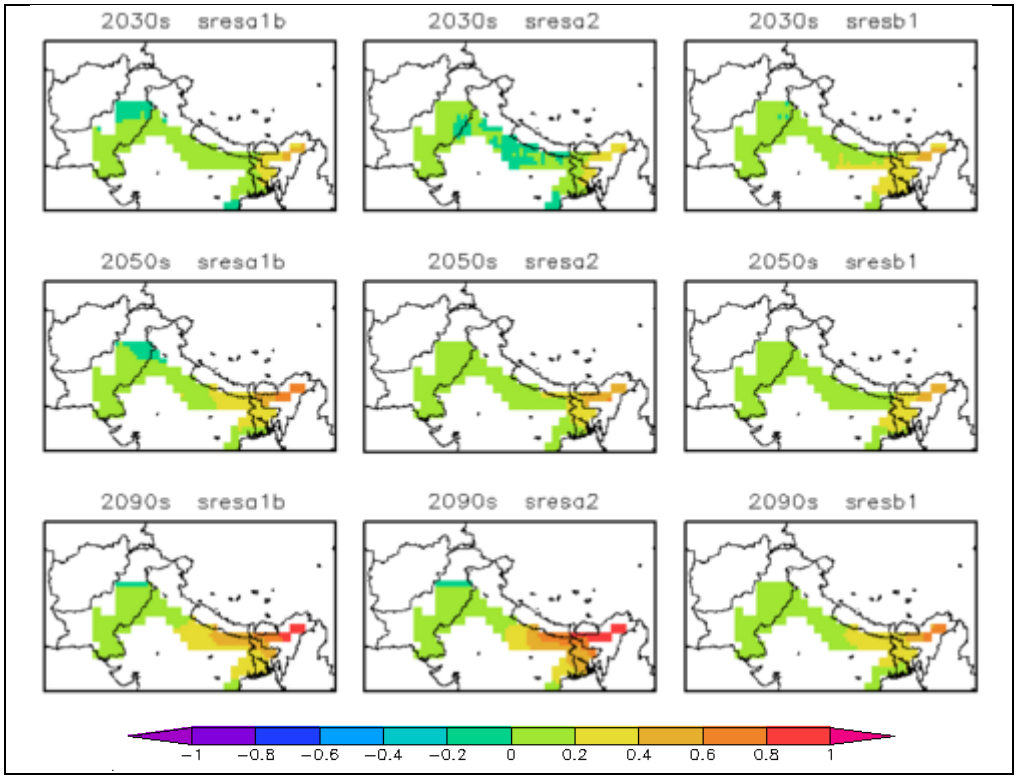

Figure 4.4: As Figure 4.3 but for mean temperature (°C)

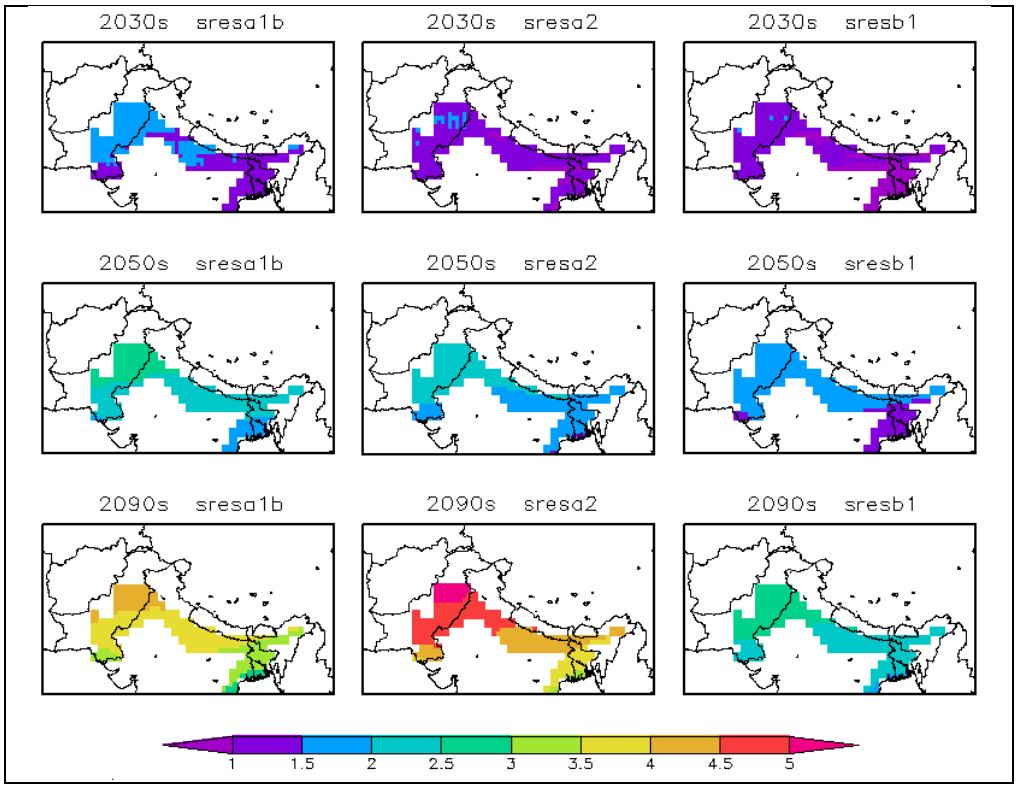

4.1 Precipitation

For all three emissions scenarios, the ensemble mean precipitation over each domain increases though the 21st century for the annual cycle, pre-monsoon, monsoon and post-monsoon seasons. In all cases, however, the inter-model spread is large, and the inter-model range spans zero, indicating that reductions in rainfall cannot be ruled out. For the winter season, ensemble mean rainfall shows small reductions, while the pre-monsoon, monsoon and post-monsoon seasons show increased rainfall. For the rabi season, the ensemble mean precipitation change over the wider IGP is negative for the 2030s, but becomes positive in the 2050s and 2090s. Again, the intermodal range is large, and spans zero. Comparing seasons, the change is less during rabi and winter seasons (not more than ±0.06 mm/day) and greatest during the monsoon season with the three periods registering a change of more than 0.1 mm/day for the three emission scenarios. When the Indus and Ganges are considered separately, the latter shows a larger increase in ensemble mean precipitation change in the monsoon season, with a greater number of models showing increased precipitation. Thus, if the climate model projections are taken at face value, there is a more consistent signal of increased precipitation for the Ganges than the Indus.

For mean temperature, there is a consistent increase in temperature for all seasons in the IGP region. Mean annual temperatures for each region are considerably warmer than the global average temperature change; for example, over the IGP, the ensemble mean temperature change for SRES A2 in the 2090s is 4.13°C, compared to 3.4 for the mean global temperature change. On average, temperature increases are lower in the monsoon season and larger in the dry periods.

4.2 Monsoon timing changes

Table 4.1 (see also Appendix 9) shows the change in mean start and end dates of monsoon season simulated by the 13 GCMs under the three emissions scenarios for 2050s and 2090s relative to the respective GCM's 1970–1999 value. Note that for the 2030s, daily data are not available, precluding an analysis of onset changes for this period.

Table 4.1: Projections of mean start and end monsoon season by 13 GCMS for 2050s and 2090s under the three emission scenarios. Figures are change values expressed in terms of number of days relative to respective GCM's 1970-1999 value.

	2050s						2090s					
	A1B		A2		B1		A1B		A2		B1	
	Start	End	Start	End	Start	End	Start	End	Start	End	Start	End
bccr_bcm2_0	12	25	-2	-10	-2	21	22	34	12	16	15	6
cccma_cgcm3_1	-2	-3	0	1	-4	3	-7	-1	-4	4	-3	-5
cnrm_cm3	1	9	5	5	24	-2	-1	-28	-24	-7	6	-3
csiro_mk3_0	5	7	-6	18	12	-1	7	-2	13	4	0	0
csiro_mk3_5	14	-6	14	-6	15	3	-2	3	16	2	14	1
gfdl_cm2_0	-5	10	1	3	0	5	2	10	-10	0	-8	17
giss_model_e_r	0	0	-6	11	-10	-4	-5	7	-7	9	-10	-8
ipsl_cm4	-4	-26	123	6	21	-32	-8	-18	-9	34	190	21
miroc3_2_medres	-5	5	-9	4	1	9	-11	3	1	9	6	7
miub_echo_g	-23	16	-18	-8	-6	22	-5	-1	14	7	15	12
mpi_echam5	4	13	3	7	2	13	0	9	0	10	3	6
mri_cgcm2_3_2a	3	0	2	-2	5	0	-4	6	-11	2	-3	10
ncar_pcm1	4	-12	7	-1	0	-21	4	6	4	15	3	5
Minimum	-23	-26	-18	-10	-10	-32	-11	-28	-24	-7	-10	-8
Maximum	14	25	123	18	24	22	22	34	16	34	190	21
Ensemble mean*	0.7	5.3	-0.8	1.8	3.1	4.0	0.0	3.8	0.3	5.9	3.2	4.0

Results suggest some evidence of a shift in monsoon timings (Table 4.1), although direction of change is variable between models. In both time periods, the ensemble onset date[2] under different emissions scenarios varies between a slight decrease to of several days, with a tendency for later onset to be clearer in the 2090s. The ense end date is later for all scenarios in the 2050s and 2090s, by several days.

Comparing the change in ensemble mean duration (excluding ipsl_cm4), results sh mean duration of monsoon increases under all scenarios, and that by the 2090s, gre warming produces a greater increase in monsoon length, of up to 5 days, for the wa scenario, A2.

5. Crop Thresholds and Projections

5.1 Crop climatic threshold

Table 5.1 provides a list of crops and their production values for the countries loca IGP, Pakistan, India, Nepal and Bangladesh (FAO 2008). Six crops—wheat, maize sugarcane, potato, onion and rice—are chosen based on their presence in the four c combined production values and perceived significance to food and economic secu Sections 5.1.1–5.1.6 describe the climatic requirements for individual crops, taken accounts of crop cultivation in various South Asian states.

5.1.1 Maize

Maize is a kharif crop although it is able to grow in other cropping seasons, for exa Kerala, India, where maize is grown in all three cropping seasons—kharif, rabi and India, maize is grown in areas with temperatures between 10–40 °C. In general, the requirements for maize lie between 250–2700 mm annually, although maize grown different rainfall regimes has different rainfall thresholds. For the kharif season, sea rainfall requirement is between 450–800 mm. Excessive rainfall and flood can how damage the crop and reduce yield. For optimum growth, the night temperature shou below minimum temperature requirement.

[2] Excluding the ipsl_cm4 model, which does not simulate a distinct monsoon

Table 5.1: Crop production for countries of the Indo-Gangetic Plain. (NA = Not grown)

Crop	Production (International Standardized Price $1000) [2008]				
	India	Pakistan	Nepal	Bangladesh	Total
rice, paddy	30246312	2162313	850799	9868753	43128177
wheat	11671546	3023994	206063	125407	15027010
sugar cane	6725632	1194856	49005	103510	8073003
vegetables fresh nes	5892585	NA	479070	206415	6578070
cotton lint	5621725	2983804	NA	NA	8605529
potatoes	4602900	347249	269041	905982	6125172
chillies and peppers, dry	3771670	386122	48597	349782	4556171
bananas	3736184	NA	NA	124998	3861182
mangoes, mangosteens, guavas	3323492	427005	26963	195461	3972921
groundnuts, with shell	3260903	NA	NA	NA	3260903
onions, dry	2499893	371381	NA	163881	3035155
tomatoes	2441089	NA	NA	NA	2441089
soybeans	2032695	NA	NA	NA	2032695
chick peas	1897235	NA	NA	NA	1897235
millet	1841508	NA	48782	NA	1890290
cottonseed	NA	449528	NA	NA	449528
maize	NA	311997	182086	146489	640572
oranges	NA	302448	NA	NA	302448
dates	NA	213193	NA	NA	213193
ginger	NA	NA	100558	NA	100558
fruit fresh nes	NA	NA	92515	NA	92515
mustard seed	NA	NA	41904	NA	41904
oilseed, nes	NA	NA	39343	NA	39343
lentils	NA	NA	35092	NA	35092
tangerines, mandarins, clem	NA	NA	34131	NA	34131
jute	NA	NA	NA	316604	316604
spices, nes	NA	NA	NA	180189	180189
garlic	NA	NA	NA	111772	111772
fruit, tropical fresh nes	NA	NA	NA	103014	103014

Source: FAO (2010)

5.1.2 Wheat

A rabi crop, wheat requires different temperatures at different stages of its growth and development. In general, temperature thresholds of wheat lie between 3.5–35 °C with optimum temperature between 20–25 °C. Below or above the optimum temperature, the germination of seed decreases slowly. The growth of wheat also favours areas where the annual rainfall is between 250–1750 mm.

5.1.3 Sugarcane

The thresholds for sugarcane which grows during the kharif season are between 10 and 40 °C for minimum and maximum temperatures, respectively, with optimum temperature at 30 °C. Sugarcane grows in areas with well-distributed annual rainfall of about 1200 mm.

5.1.4 Potato

Potato is commonly grown during the rabi season where a mean daily temperature between 18–20 °C is required for optimum growth. Night temperature of below 15 °C is required for tuber initiation which is significantly hindered when temperature drops below 10 °C and rises above 30 °C. Its water requirement is estimated to be between 150–750 mm during the growing season.

5.1.5 Onion

Onions are commonly grown during the rabi season. Based on onion growing locations in the Maharastra, Gujarat, Karnataka, Tamil Nadu, Andhra Pradesh, and Rajastan states of India, the minimum and maximum temperatures for onion cultivation are 13 and 30 °C, respectively with monthly rainfall between 38–128 mm during the growing season.

5.1.6 Rice

The cultivation of rice (kharif crop) requires high rainfall of at least 100 mm per month during its growing season. Being a tropical plant, it requires a fairly high temperature ranging from 20 to 40 °C with optimum at 30 °C (daytime) and 20 °C (night time).

5.2 Crop projections

The temperature and rainfall limits described above are used to estimate present day and future climatically suitable growing areas. For the present day, the CRU observed gridded data are used to define locations where the climatic conditions are suitable for each crop. This

is undertaken for two water availability conditions: (i) assuming the crops are rain-fed, where rainfall acts in combination with temperature to limit the growing conditions, and (ii) assuming crops are irrigated, in which case rainfall is not included as a limiting factor. This latter scenario assumes that *all* crop water demands can be satisfied by irrigation, and does not attempt to include any potential or actual limitations on irrigation water availability, which would require a much more detailed water and irrigation modelling approach than is possible here.

For each month in the designated growing season of a crop, a mask is created showing the grid points that have climatic values suitable for growth. Then, a composite map is created, adding together the masks from each month, showing for each 0.5 ° latitude/longitude location, the number of months in which suitable conditions occur.

Projections for the 2050s and 2090s are based on the GCM ensemble mean changes, applied as change factors to the CRU baseline data. As maximum and minimum temperature data are not available for the 2030s, the analysis could not be undertaken for this earlier time period. Results are presented in Appendix 10 in Figures J1–J12 and are supplemented with Tables J1 and J2 which show the total area of crop grown in the IGP region, under each of the scenarios.

5.2.1 Maize

Under rain-fed conditions for the present period, maize can be grown for at least one month over 31% of the IGP, mainly in the upper reaches of the Indus and Ganges rivers (Figure J1). The spatial extent of growth area for the two future periods under the three emission scenarios shows a significant increase between 96 and 153% relative to the present period, due to the general increase in rainfall projected by the GCM ensemble mean. Under the warmest scenarios, increases in rainfall even permit rain-fed maize for one month over much of the lower Indus.

Assuming an irrigated situation (Figure J2), the present day period sees the entire IGP area being climatically suitable for maize cultivation, for the full four months of the growing season. No marked difference can be seen in the change in growth area for the future periods which see 1-4% increase in coverage, indicating that increased temperature does not become a constraint on maize growth.

5.2.2 Wheat

The present day situation under rain-fed condition shows 69% of the IGP region being climatically suitable for wheat cultivation (Figure J3) for at least one month, with coverage largely confined to the Ganges and parts of the upper Indus basin. The extent of growth area sees an increase between 22 and 31% for the two future periods under the three emission scenarios, with longer periods of suitability in areas already suitable in the present day, and much of the Indus becoming suitable as rainfall increases in these areas. Note that using the ensemble mean rainfall hides significant inter-model uncertainty.

Under irrigation, suitable conditions for wheat exist for the present over the entire IGP region, with most areas having met the temperature thresholds for four and five months of the growing season (Figure J4). Under the three emission scenarios, the 2050s and 2090s do not show any evidence of change in spatial extent. However, it can be noted that there are now more areas with lesser number of months meeting the temperature thresholds, as the climate warms.

5.2.3 Sugarcane

Figure J5 shows the growth area for sugarcane for the present day and future periods under rain-fed conditions. For the present period, 67% of the IGP region is suitable for sugarcane cultivation, largely over the Ganges, and also part of the upper Indus, with a majority of the area being climatically suitable for three or four months of the growing season. Under the climate change scenarios, potential growth areas increase, extending further west, and into the lower Indus basin; total area suitable for at least one month of the year increases by 16 to 42% (Table J1).

For the irrigated scenario (Figure J6), 99% of the IGP region is suitable for sugarcane cultivation, although the length of the climatically suitable period is shorter in the Indus. In the future, little change in overall climatic suitability is projected, but the number of months that are suitable decreases in the Indus basin as temperatures increase; in the 2090s the growing season decreases in the upper Ganges as well.

5.2.4 Potato

Under rain-fed conditions (Figure J7), the spatial extent of growth area for the present day is rather limited, with only 27% of the region having sufficient rainfall and adequate

temperature conditions for at least one month; these areas are all in the lower Ganges, and small parts of the upper Indus. In the future, increased rainfall results in a larger area suitable for potatoes, but only for one month of the year.

Under irrigated conditions (Figure J8), the present day sees 88% of IGP region being suitable for potato cultivation for at least one month, with most of this area having satisfied the temperature criteria for at least two months of the growing season. Changes for the future periods see an increase of about 12% in the growth area under all three emission scenarios with more areas satisfying the temperature criteria for two months.

5.2.5 Onion

The estimated growth area for onion, using the generic climate conditions form the literature, is very limited for rain-fed conditions (Figure J9). For the present period, only 10% of the IGP region is considered suitable for cultivation. In the 2050s and 2090s the increases in rainfall allow for larger growing areas, increasing from the present day by over 200%, to cover much of the lower Ganges, and parts of the upper Indus.

Taking into consideration where irrigated cultivation can occur (Figure J10), a larger area of the IGP region (73%) is climatically suitable; this is mostly over the Ganges basin, but the upper Indus is also suitable. Projections for the future show a mean increase of 16–32%, with suitable conditions extending further west as temperatures rise.

5.2.6 Rice

Figure J11 shows that under rain-fed conditions, the entire Ganges region and upper section of the Indus region are suitable for rice cultivation; this corresponds to 71% of the IGP region. Most, if not all, of the Ganges region is climatically suitable for four months of the growing season. The climate change scenarios show that the total area suitable for cultivation increases by up to 37%, with much of the Indus basin becoming suitable as rainfall increases. However, under the warmer scenarios, the number of suitable months in the upper Ganges reduces.

For irrigated rice production (Figure J12), 99% of the IGP is climatically favourable for rice growth today, with the Ganges and much of the Indus regions having suitable conditions for three and four months of the growing season. In the projections for the future, the overall area suitable for rice does not decrease, but the length of the growing season decreases over much of the Indus and upper Ganges, especially under the warmest scenarios.

6. Summary and Discussion

6.1 Observed climate trends

Over the IGP, trends in station-based observed temperatures (CRU) since 1960 are consistent with those reported for the Indian sub-continent by the IPCC, around approximately 0.1 °C per decade. Trends in the reanalysis data are less consistent, suggesting that not all the regional warming signal is captured well in these model-based datasets. The warming trend in the Himalaya mountains is steeper than the surrounding IGP, at 0.2°C per decade, which has implications for the seasonality of snow cover and runoff into the Ganges and Indus rivers. Trends in maximum and minimum temperature generally follow those of mean temperature, except that minimum temperature trends are larger than maximum temperature, implying a reduction in the diurnal temperature range.

Trends in rainfall are inconclusive. The two datasets based on station data, CRU and APHRODITE, show opposite trends for the monsoon season and for annual precipitation, and across all datasets, there are a mixed set of trends, with very few statistically significant values. This is somewhat consistent with the GCM projections, where both positive and negative changes occur, depending on the model. Trends in rainfall extremes—dry and wet spell lengths—are also inconclusive, but with a tendency for increased dry spell length and decreased wet spell length.

Temperature extremes, which are based on the reanalysis data, do not show any consistent statistically significant trends over the region.

6.2 Climate model evaluation

There has been considerable previous work evaluating global climate models over the South Asia region, with a focus on the monsoon. Very few, if any, models capture both monsoon rainfall amount and timing accurately over the region, as well as known remote forcing of the monsoon in the Indian and Pacific oceans. The analysis undertaken in this report, which focuses specifically on model performance over the IGP, is consistent with this broader work. While all models, except ipsl_cm4, have a distinct monsoon rainfall season, they all have significant biases or mismatches between their simulated rainfall and temperature and that observed over the IGP. Thus it is hard to identify a model or models that are “better” than

others, and the most robust approach to assessing climate change over the IGP would involve using all model projections, as potential changes that cannot at this stage be ruled out.

6.3 Climate projections

Climate models all agree that mean temperature will rise, at a rate greater than the global mean temperature. The range of possible temperature increases for the IGP is 0.6–2.7, 0.5–3.1 and 1.0–5.4 °C above the 1070–1999 mean for the 2030s, 2050s and 2090s respectively. In general, temperatures in the monsoon period increase less than in the dry seasons.

The projections for changes in precipitation are varied. For any period and season, the projected changes span zero, but the ensemble mean changes are generally positive, and more consistently positive over the Ganges than the Indus. Changes in monsoon variability are not assessed, but any projections of such changes in future would have to be treated with even greater caution than changes in the mean because of the difficulties climate models have in representing remote drivers of monsoon variability.

6.4 Crop suitability scenarios

Scenarios for locations suitable for cultivation of key crops in the IGP show marked contrasts between irrigated and rain-fed situations. When using the ensemble mean projected changes in climate, suitability for rain-fed agriculture of all increases in the future, due to the general increase in precipitation. Areas in the western Ganges and lower Indus that were previously unsuitable become suitable for at least one month, and those areas that are suitable in the present climate become suitable for longer.

For irrigated agriculture, where temperature is the only constraint on crop suitability, the main crops of maize, wheat and rice are not affected in terms of areas that are suitable for growth, except in the warmest scenarios in the 2090s; here temperature changes could start to limit the number of months in which a crop can be cultivated, especially in the lower Indus valley. Although not assessed in this report, it is generally accepted that plant water demand will increase under warmer temperatures; the availability of water for irrigation therefore becomes an increasingly important factor in a warming world. The projections of increased rainfall for the Himalaya, the source for much of the surface irrigation water in the Indus and Ganges, may ameliorate this stress; however, the considerable inter-model range in projected changes in precipitation means that this outcome cannot be relied upon.

6.5 Prospects for climate modelling

The review and analysis presented in Section 0 showed that there remain large uncertainties in climate projections over the IGP from global models, as reflected in the differences between models in their ability to represent present day climate, and the range in changes projected under any single emissions scenario. These relate to a number of general issues in the models, such as climate sensitivity, representation of ENSO and other ocean-atmosphere processes, and also the specific challenges involved in modelling the regional climate of South Asia and the Himalaya–Hindu-Kush–Tibet topographic influences on climate. Here some key developments in models are discussed, along with new experiments emerging from the CMIP5 and CORDEX modelling programs.

6.5.1 Global climate model developments

Most major modelling centres have developed newer versions of their global models since the 4th IPCC assessment. Each model typically includes improvements in the representation of physical processes, and usually increases in resolution, which can be important for representation of ocean-atmosphere interactions, and simulations of processes in areas with complex topography and land-sea geography. For example the Canadian Centre for Climate Modelling and Analysis fourth generation model has a resolution of approximately 1.85 degrees latitude/longitude, whereas the previous version had a resolution of 3.75 degrees latitude/longitude; the ocean model shows a similar improvement in resolution, increased to 1.41/0.91 degrees[3]. Similarly, the Met Office Hadley Centre HadCM3 model had a resolution of 3.75/2.5 degrees longitude/latitude, while the HadGEM modelling system has a resolution of up to 1.85/1.25[4], and many changes to the model physics.

Despite these global climate model developments, it is unlikely that there will be step changes in the reliability of projections from these models. Careful evaluation of models will be required to identify models that satisfy basic performance characteristics over the IGP, including (i) monsoon circulation, moisture transport and rainfall characteristics; (ii) winter circulation and snow cover; (iii) hydrological budget over the Indus and Ganges basins and

3 http://www.ec.gc.ca/ccmac-cccma

4 http://www.metoffice.gov.uk/research/modelling-systems/unified-model

major sub-catchments; and (iv) representation of ENSO and Indian Ocean variability and teleconnections to the South Asian monsoon.

6.5.2 Asian brown cloud forcing of climate

Very few models used for centennial projections currently have sufficiently well represented atmospheric chemistry to represent the effects of Asian Brown Cloud pollution on the climate of South Asia, both in terms of local radiative effects on regional temperatures, and its effect on monsoon processes. While many modelling centres are developing models with improved chemistry, these are unlikely to be well represented in the next generation of centennial model runs. Most likely is a set of emerging research results where the sensitivity of South Asian climate to ABC is assessed in specific experiments, which can be used to inform the decadal and longer term climate change projections.

6.5.3 CMIP5 Global Climate Model Experiments

New global climate models simulations for the next IPCC assessment report are being undertaken under the auspices of the Coupled Model Intercomparison Project Phase 5 (CMIP5)[5]. Two types of simulations are underway, with data due to be available for analysis from 2011 onwards. The first set of simulations are centennial length simulations similar to those undertaken under CMIP3 in advance of the IPCC AR4, but driven by a new set of radiative forcing scenarios, the Representative Concentration Profiles (RCPs) (Moss et al. 2010). The RCPs represent a range of possible future greenhouse gas and aerosol concentrations, from a business as usual scenario (RCP 8.5) similar to the old SRES A1FI scenario to a fairly stringent mitigation scenario (RCP 3) where emissions peak in about 2020. It is expected that about 20 global climate models will contribute simulations for this experiment.

The second experiment is a set of "decadal prediction and hindcast" simulations (Taylor et al. 2009). The aim here is to produce a set of GCM simulations which are initialized using observations of the climate system in 2005, and then predict climate evolution 10 and 30 years forward. The skill of the model predictions can be assessed through evaluation of a set of hindcast experiments, namely 10 and 30 year simulations initialised in 1960, 1965, and so

[5] http://cmip-pcmdi.llnl.gov

on through to 2000 for the 10 year simulations, and initialised in 1960 and 1980 for the 30 year simulations. These model simulations have the potential to provide improved forecasts of climate over the near-term, out to 2035, but the approach is relatively new, and much evaluation of model skill from the hindcasts will be required before the forecasts can be used with any confidence.

6.5.4 CORDEX – the Coordinated Regional Downscaling Experiment

Given the complex geography of the IGP, higher resolution simulations with Regional Climate Models (RCMs) have the potential to add considerable detail to the outputs from coarser resolution GCMs discussed in this report. The CORDEX[6] initiative aims to encourage the development of regionally downscaled climate projections in a consistent manner, over a predefined set of regional domains, each with a spatial resolution of 50 km, or approximately 0.5° latitude by longitude. For the IGP, the West Asia domain is of relevance, as it includes the Indian sub-continent. International modelling groups are encouraged to undertake climate change simulations with RCMs over each of these domains, driven by CMIP5 global climate model data. The coordinating institute for the West Asia domain is the Indian Institute for Tropical Meteorology (IITM). As of early 2011, various staffing changes at IITM have meant that CORDEX experiments have not been initiated, but these can be expected to begin in 2011, with results becoming available over the next few years.

A major challenge for the West Asia domain will be finding the computational resources and qualified people to undertake a comprehensive set of RCM simulations. In the past, RCM simulations over South Asia, and other developing country regions, have been limited to a few RCMs, usually the UK Met Office PRECIS and the ICTP RegCM3 models; both these centres have invested considerable resources into making their models simple to run by third parties. However, each of these RCMs has been driven by one or only a few GCMs; this rather small sample of the full set of possible RCM-GCM combinations has made it difficult to undertake comprehensive assessments of climate change impacts using the downscaled data, in a manner similar to the multi-model assessments undertaken with the CMIP GCMs. It remains to be seen whether there will be a sufficiently large set of RCM simulations over the West Asian CORDEX region.

[6] http://wcrp.ipsl.jussieu.fr/SF_RCD_CORDEX.html

Appendix 1

Figure A1: 0.5° x 0.5° masks over the Indo-Gangetic Plain and its sub regions; Indus, Ganges and Himalaya. Values in parenthesis show the number of grid points.

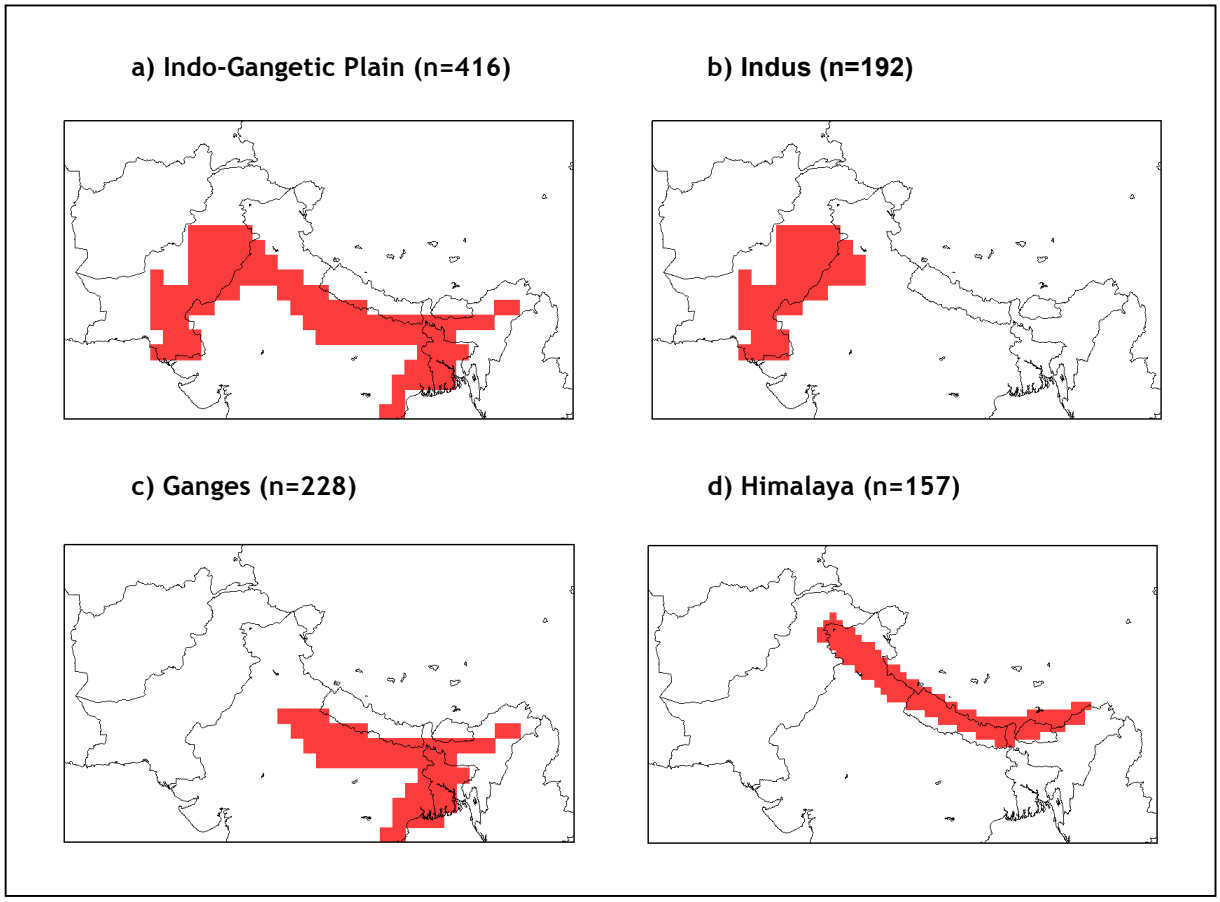

Appendix 2

Table B1: Spatial correlation of minimum temperature between respective GCMs and CRU dataset for annual cycle

Model	IGP	Indus	Ganges	Himalaya	IGP + Himalaya	Domain
bccr_bcm2_0	0.58	0.64	0.75	0.84	0.92	0.95
cccma_cgcm3_1	0.62	0.56	0.82	0.42	0.83	0.87
cnrm_cm3	0.70	0.68	0.81	0.81	0.92	0.95
csiro_mk3_0	0.67	0.68	0.80	0.81	0.90	0.92
csiro_mk3_5	0.68	0.72	0.77	0.86	0.91	0.95
gfdl_cm2_0	0.70	0.63	0.87	0.76	0.91	0.94
giss_model_e_r	0.64	0.62	0.54	0.67	0.86	0.90
ipsl_cm4	0.67	0.48	0.86	0.64	0.86	0.90
miroc3_2_medres	0.53	0.46	0.83	0.71	0.84	0.87
miub_echo_g	0.54	0.44	0.83	0.54	0.80	0.85
mpi_echam5	0.57	0.72	0.71	0.81	0.94	0.97
mri_cgcm2_3_2a	0.56	0.42	0.85	0.60	0.76	0.77
ncar_pcm1	0.75	0.57	0.86	0.51	0.83	0.87
Ensemble mean	0.63	0.59	0.79	0.69	0.87	0.90

Table B2: As B1 but for winter season

Model	IGP	Indus	Ganges	Himalaya	IGP + Himalaya	Domain
bccr_bcm2_0	0.74	0.73	0.76	0.81	0.92	0.96
cccma_cgcm3_1	0.68	0.62	0.83	0.38	0.83	0.90
cnrm_cm3	0.74	0.75	0.76	0.81	0.92	0.95
csiro_mk3_0	0.71	0.72	0.79	0.74	0.89	0.94
csiro_mk3_5	0.78	0.77	0.79	0.82	0.90	0.96
gfdl_cm2_0	0.71	0.68	0.86	0.78	0.91	0.95
giss_model_e_r	0.76	0.65	0.59	0.58	0.84	0.89
ipsl_cm4	0.78	0.63	0.87	0.62	0.85	0.92
miroc3_2_medres	0.62	0.57	0.82	0.65	0.84	0.90
miub_echo_g	0.65	0.57	0.88	0.48	0.80	0.88
mpi_echam5	0.73	0.81	0.71	0.75	0.93	0.97
mri_cgcm2_3_2a	0.61	0.56	0.89	0.73	0.78	0.82
ncar_pcm1	0.86	0.66	0.89	0.46	0.81	0.88
Ensemble mean	0.72	0.67	0.80	0.66	0.86	0.92

Table B3: As B1 but for pre-monsoon season

Model	IGP	Indus	Ganges	Himalaya	IGP + Himalaya	Domain
bccr_bcm2_0	0.75	0.63	0.91	0.81	0.93	0.95
cccma_cgcm3_1	0.66	0.59	0.74	0.56	0.86	0.86
cnrm_cm3	0.77	0.65	0.88	0.79	0.93	0.95
csiro_mk3_0	0.72	0.68	0.81	0.85	0.91	0.92
csiro_mk3_5	0.78	0.71	0.87	0.87	0.93	0.95
gfdl_cm2_0	0.71	0.66	0.77	0.72	0.91	0.94
giss_model_e_r	0.55	0.64	0.61	0.58	0.84	0.88
ipsl_cm4	0.65	0.48	0.80	0.69	0.88	0.91
miroc3_2_medres	0.63	0.49	0.79	0.75	0.87	0.88
miub_echo_g	0.59	0.45	0.73	0.59	0.83	0.85
mpi_echam5	0.77	0.70	0.88	0.82	0.95	0.97
mri_cgcm2_3_2a	0.49	0.39	0.59	0.64	0.77	0.74
ncar_pcm1	0.64	0.58	0.74	0.60	0.85	0.87
Ensemble mean	0.67	0.59	0.78	0.71	0.88	0.90

Table B4: As B1 but for monsoon season

Model	IGP	Indus	Ganges	Himalaya	IGP + Himalaya	Domain
bccr_bcm2_0	0.67	0.55	0.79	0.87	0.93	0.94
cccma_cgcm3_1	0.52	0.41	0.59	0.42	0.84	0.83
cnrm_cm3	0.63	0.51	0.75	0.83	0.93	0.93
csiro_mk3_0	0.64	0.62	0.70	0.88	0.90	0.90
csiro_mk3_5	0.70	0.67	0.77	0.90	0.92	0.94
gfdl_cm2_0	0.59	0.53	0.68	0.67	0.91	0.92
giss_model_e_r	0.49	0.55	0.62	0.75	0.86	0.88
ipsl_cm4	0.40	0.19	0.60	0.63	0.87	0.85
miroc3_2_medres	0.48	0.26	0.61	0.83	0.84	0.81
miub_echo_g	0.41	0.21	0.58	0.60	0.81	0.79
mpi_echam5	0.72	0.62	0.83	0.88	0.93	0.96
mri_cgcm2_3_2a	0.22	0.12	0.36	0.44	0.72	0.66
ncar_pcm1	0.47	0.40	0.60	0.53	0.84	0.84
Ensemble mean	0.53	0.43	0.65	0.71	0.87	0.87

Table B5: As B1 but for post-monsoon season

Model	IGP	Indus	Ganges	Himalaya	IGP + Himalaya	Domain
bccr_bcm2_0	0.55	0.71	0.52	0.81	0.90	0.95
cccma_cgcm3_1	0.62	0.64	0.69	0.36	0.81	0.86
cnrm_cm3	0.60	0.75	0.54	0.79	0.90	0.94
csiro_mk3_0	0.64	0.75	0.59	0.71	0.87	0.91
csiro_mk3_5	0.64	0.78	0.54	0.79	0.88	0.93
gfdl_cm2_0	0.58	0.69	0.68	0.83	0.90	0.94
giss_model_e_r	0.65	0.65	0.40	0.66	0.85	0.90
ipsl_cm4	0.64	0.60	0.69	0.65	0.84	0.90
miroc3_2_medres	0.56	0.60	0.66	0.62	0.82	0.86
miub_echo_g	0.49	0.55	0.73	0.51	0.78	0.85
mpi_echam5	0.52	0.81	0.52	0.79	0.92	0.96
mri_cgcm2_3_2a	0.55	0.54	0.77	0.56	0.76	0.79
ncar_pcm1	0.75	0.68	0.68	0.52	0.82	0.87
Ensemble mean	0.60	0.67	0.62	0.66	0.85	0.90

Table B6: As B1 but for rabi season

Model	IGP	Indus	Ganges	Himalaya	IGP + Himalaya	Domain
bccr_bcm2_0	0.68	0.73	0.67	0.81	0.91	0.95
cccma_cgcm3_1	0.66	0.62	0.78	0.36	0.82	0.89
cnrm_cm3	0.69	0.75	0.66	0.80	0.91	0.95
csiro_mk3_0	0.68	0.74	0.70	0.73	0.89	0.93
csiro_mk3_5	0.73	0.78	0.68	0.82	0.90	0.95
gfdl_cm2_0	0.64	0.68	0.78	0.81	0.91	0.95
giss_model_e_r	0.71	0.65	0.49	0.63	0.85	0.90
ipsl_cm4	0.73	0.61	0.80	0.63	0.85	0.92
miroc3_2_medres	0.59	0.58	0.75	0.63	0.83	0.89
miub_echo_g	0.58	0.55	0.82	0.49	0.79	0.87
mpi_echam5	0.64	0.82	0.63	0.77	0.93	0.97
mri_cgcm2_3_2a	0.58	0.54	0.84	0.66	0.77	0.81
ncar_pcm1	0.82	0.66	0.82	0.48	0.82	0.89
Ensemble mean	0.67	0.67	0.72	0.66	0.86	0.91

Table B7: Spatial correlation of maximum temperature between respective GCMs and CRU dataset for annual cycle

Model	IGP	Indus	Ganges	Himalaya	IGP + Himalaya	Domain
bccr_bcm2_0	0.81	0.75	0.86	0.88	0.96	0.96
cccma_cgcm3_1	0.79	0.71	0.81	0.71	0.87	0.89
cnrm_cm3	0.69	0.68	0.63	0.86	0.95	0.95
csiro_mk3_0	0.75	0.77	0.77	0.83	0.93	0.93
csiro_mk3_5	0.76	0.66	0.86	0.89	0.95	0.96
gfdl_cm2_0	0.80	0.78	0.81	0.88	0.95	0.96
giss_model_e_r	0.54	0.67	0.77	0.60	0.84	0.88
ipsl_cm4	0.71	0.68	0.80	0.66	0.90	0.91
miroc3_2_medres	0.73	0.60	0.77	0.83	0.88	0.85
miub_echo_g	0.67	0.66	0.66	0.70	0.86	0.87
mpi_echam5	0.76	0.66	0.85	0.90	0.96	0.96
mri_cgcm2_3_2a	0.80	0.70	0.84	0.72	0.85	0.84
ncar_pcm1	0.37	0.70	0.51	0.59	0.82	0.84
Ensemble mean	0.71	0.69	0.76	0.77	0.90	0.91

Table B8: As B7 but for winter season

Model	IGP	Indus	Ganges	Himalaya	IGP + Himalaya	Domain
bccr_bcm2_0	0.82	0.85	0.88	0.88	0.96	0.97
cccma_cgcm3_1	0.85	0.81	0.87	0.45	0.81	0.91
cnrm_cm3	0.63	0.82	0.69	0.87	0.95	0.96
csiro_mk3_0	0.74	0.87	0.82	0.88	0.93	0.94
csiro_mk3_5	0.78	0.79	0.85	0.89	0.96	0.97
gfdl_cm2_0	0.85	0.84	0.89	0.86	0.95	0.96
giss_model_e_r	0.76	0.74	0.80	0.60	0.85	0.91
ipsl_cm4	0.79	0.73	0.88	0.71	0.91	0.94
miroc3_2_medres	0.62	0.67	0.83	0.75	0.89	0.90
miub_echo_g	0.74	0.71	0.81	0.68	0.86	0.90
mpi_echam5	0.80	0.84	0.83	0.87	0.96	0.97
mri_cgcm2_3_2a	0.78	0.76	0.88	0.66	0.86	0.90
ncar_pcm1	0.74	0.77	0.79	0.66	0.83	0.87
Ensemble mean	0.76	0.78	0.83	0.75	0.90	0.93

Table B9: As B7 but for pre-monsoon season

Model	IGP	Indus	Ganges	Himalaya	IGP + Himalaya	Domain
bccr_bcm2_0	0.85	0.69	0.88	0.86	0.96	0.95
cccma_cgcm3_1	0.80	0.62	0.85	0.53	0.87	0.92
cnrm_cm3	0.75	0.70	0.63	0.85	0.94	0.92
csiro_mk3_0	0.70	0.68	0.72	0.85	0.94	0.93
csiro_mk3_5	0.73	0.64	0.84	0.89	0.96	0.95
gfdl_cm2_0	0.75	0.73	0.84	0.85	0.96	0.96
giss_model_e_r	0.31	0.62	0.58	0.46	0.79	0.86
ipsl_cm4	0.65	0.56	0.75	0.64	0.91	0.91
miroc3_2_medres	0.79	0.58	0.80	0.83	0.91	0.88
miub_echo_g	0.57	0.58	0.59	0.67	0.87	0.86
mpi_echam5	0.86	0.64	0.89	0.89	0.96	0.96
mri_cgcm2_3_2a	0.83	0.60	0.90	0.68	0.87	0.85
ncar_pcm1	0.19	0.57	0.29	0.60	0.82	0.84
Ensemble mean	0.68	0.63	0.74	0.74	0.90	0.91

Table B10: As B7 but for monsoon season

Model	IGP	Indus	Ganges	Himalaya	IGP + Himalaya	Domain
bccr_bcm2_0	0.87	0.52	0.82	0.86	0.95	0.94
cccma_cgcm3_1	0.90	0.59	0.82	0.56	0.76	0.64
cnrm_cm3	0.72	0.21	0.39	0.85	0.94	0.92
csiro_mk3_0	0.86	0.58	0.74	0.75	0.91	0.88
csiro_mk3_5	0.87	0.53	0.84	0.82	0.92	0.91
gfdl_cm2_0	0.90	0.67	0.74	0.89	0.94	0.92
giss_model_e_r	0.58	0.53	0.78	0.59	0.80	0.81
ipsl_cm4	0.71	0.47	0.80	0.52	0.89	0.83
miroc3_2_medres	0.89	0.68	0.65	0.68	0.83	0.70
miub_echo_g	0.76	0.53	0.65	0.75	0.88	0.79
mpi_echam5	0.86	0.47	0.79	0.86	0.94	0.93
mri_cgcm2_3_2a	0.89	0.51	0.82	0.53	0.78	0.65
ncar_pcm1	0.20	0.34	0.26	0.45	0.81	0.77
Ensemble mean	0.77	0.51	0.70	0.70	0.87	0.82

Table B11: As B7 but for post-monsoon season

Model	IGP	Indus	Ganges	Himalaya	IGP + Himalaya	Domain
bccr_bcm2_0	0.78	0.82	0.83	0.88	0.95	0.96
cccma_cgcm3_1	0.73	0.75	0.77	0.64	0.83	0.88
cnrm_cm3	0.71	0.80	0.68	0.87	0.96	0.97
csiro_mk3_0	0.71	0.85	0.77	0.86	0.92	0.93
csiro_mk3_5	0.72	0.81	0.82	0.90	0.94	0.96
gfdl_cm2_0	0.77	0.81	0.81	0.89	0.94	0.95
giss_model_e_r	0.58	0.74	0.72	0.63	0.84	0.87
ipsl_cm4	0.73	0.72	0.80	0.70	0.89	0.91
miroc3_2_medres	0.63	0.63	0.78	0.81	0.86	0.87
miub_echo_g	0.66	0.68	0.68	0.65	0.84	0.88
mpi_echam5	0.74	0.81	0.84	0.89	0.96	0.97
mri_cgcm2_3_2a	0.74	0.74	0.78	0.73	0.85	0.85
ncar_pcm1	0.53	0.76	0.67	0.65	0.81	0.83
Ensemble mean	0.69	0.76	0.77	0.78	0.89	0.91

Table B12: As B7 but for rabi season

Model	IGP	Indus	Ganges	Himalaya	IGP + Himalaya	Domain
bccr_bcm2_0	0.80	0.84	0.86	0.89	0.95	0.97
cccma_cgcm3_1	0.80	0.79	0.87	0.53	0.83	0.90
cnrm_cm3	0.69	0.82	0.73	0.87	0.96	0.97
csiro_mk3_0	0.70	0.87	0.81	0.87	0.93	0.94
csiro_mk3_5	0.72	0.81	0.83	0.90	0.95	0.97
gfdl_cm2_0	0.80	0.83	0.88	0.88	0.95	0.96
giss_model_e_r	0.70	0.74	0.74	0.63	0.85	0.90
ipsl_cm4	0.77	0.73	0.87	0.71	0.90	0.93
miroc3_2_medres	0.58	0.65	0.82	0.77	0.88	0.89
miub_echo_g	0.73	0.70	0.82	0.68	0.85	0.89
mpi_echam5	0.75	0.83	0.82	0.88	0.96	0.97
mri_cgcm2_3_2a	0.75	0.76	0.85	0.70	0.86	0.88
ncar_pcm1	0.72	0.77	0.82	0.65	0.83	0.86
Ensemble mean	0.73	0.78	0.82	0.77	0.90	0.93

oAppendix 3

Table C1: Trends of extreme events from 1960-2001: Consecutive dry days (CDD)

	Annual		Winter		Pre-Monsoon		Monsoon		Post-Monsoon		Rabi	
	trend	*p*-value	trend	*p*-value	trend	*p*-value	trend	*p*-value	trend	*p*-value	trend	*p*-value
Indo-Gangetic Plain												
APHRODITE	-0.0088	0.9563	-0.2676	0.0665	-0.1026	0.2293	-0.0220	0.4482	0.0105	0.9514	-0.0079	0.9605
ERA-40	-0.0952	0.7631	-0.0781	0.8472	-0.3077	0.0314	-0.0800	0.0425	0.0751	0.6360	-0.0316	0.8832
JRA-25	0.1448	0.3893	-0.0988	0.4442	-0.1724	0.0025	-0.0459	0.0638	0.0367	0.8420	0.1448	0.3893
NCEP/NCAR	0.1250	0.4508	0.0622	0.7768	-0.0403	0.6790	0.0361	0.2933	0.0444	0.8119	0.1268	0.4482
Indus												
APHRODITE	-0.3440	0.2741	0.3162	0.1897	-0.1977	0.2329	-0.0710	0.5451	-0.1355	0.6405	0.0242	0.9472
ERA-40	-0.8302	0.0574	-0.6299	0.1725	-0.1807	0.4587	-0.3409	0.0343	-0.0625	0.7611	-1.0070	0.0376
JRA-25	-0.2035	0.4181	-0.1894	0.3649	-0.0553	0.7671	-0.1503	0.0692	-0.0962	0.7230	-0.2185	0.3978
NCEP/NCAR	0.2950	0.2855	0.3236	0.0415	0.2374	0.3002	-0.1236	0.3527	0.3360	0.1731	0.3014	0.2863
Ganges												
APHRODITE	-0.1100	0.5235	-0.0951	0.5431	-0.0279	0.6377	-0.0141	0.5484	-0.1057	0.5686	-0.1009	0.5680
ERA-40	-0.0975	0.6889	-0.1071	0.7325	-0.2821	0.0012	-0.0350	0.2493	-0.0810	0.6243	-0.0327	0.8792
JRA-25	0.1224	0.4501	0.0311	0.8014	-0.1679	0.0001	-0.0684	0.0103	0.1023	0.5354	0.1254	0.4400
NCEP/NCAR	-0.0344	0.8767	-0.1561	0.5327	-0.0596	0.5706	0.0126	0.5619	-0.1256	0.4274	-0.0140	0.9430
Himalaya												
APHRODITE	-0.1071	0.5819	-0.0409	0.6700	0.0309	0.4445	-0.0266	0.2831	-0.0819	0.6902	-0.0976	0.6185
ERA-40	-0.5461	0.0064	-0.5927	0.0338	-0.3105	0.0024	-0.0355	0.3996	-0.0676	0.6985	-0.5439	0.0236
JRA-25	-0.1542	0.3786	-0.0061	0.9410	-0.0505	0.0713	-0.0492	0.0498	-0.1603	0.3841	-0.1542	0.3786
NCEP/NCAR	0.4608	0.0249	0.2337	0.1866	0.1454	0.0060	0.0714	0.0342	0.1702	0.4794	0.4590	0.0259

Note: Statistically significant values (p-value < 0.1) are coloured red

)		l		r		n		n		n	
	d	e	d	e	d	e	d	e	d	e	d
n											
	1	2	3	4	8	4	1	2	1	2	6
	9	7	2	0	4	6	8	2	6	3	6
5	0	4	9	0	3	4	0	3	2	9	0
	0	2	3	9	9	4	4	8	0	0	0
s											
	7	9	9	3	1	6	6	4	8	7	4
	9	3	0	8	7	7	0	7	3	3	2
5	9	2	3	8	6	7	6	0	1	0	1
	6	8	1	4	8	8	3	7	2	4	0
s											
	6	5	5	3	9	4	6	7	7	0	1
	9	7	1	6	9	3	1	5	2	7	3
5	7	2	0	1	7	9	7	8	8	1	5
	4	0	7	9	0	5	2	3	3	8	8
a											
	3	7	3	2	9	1	9	7	8	1	7
	9	8	9	0	7	0	0	6	7	5	6
5	1	4	4	1	5	1	9	2	0	1	5
	1	3	7	4	6	1	3	3	6	6	8

d

Table C3: Trends of extreme events from 1960-2001: Consecutive wet days (CWD)

	Annual		Winter		Pre-Monsoon		Monsoon		Post-Monsoon		Rabi	
	trend	*p*-value	trend	*p*-value	trend	*p*-value	trend	*p*-value	trend	*p*-value	trend	*p*-value
Indo-Gangetic Plain												
APHRODITE	-0.1650	0.4292	0.0317	0.4923	-0.0238	0.8335	-0.1429	0.4190	-0.0066	0.8641	0.0250	0.5874
ERA-40	0.4094	0.3162	0.0294	0.1694	0.2413	0.0129	0.6108	0.0969	0.0237	0.6515	0.0177	0.7203
JRA-25	1.7196	0.0000	-0.0092	0.7613	0.1252	0.1613	1.6865	0.0000	0.0310	0.3100	0.0286	0.3870
NCEP/NCAR	0.3727	0.1129	-0.0780	0.1883	0.1888	0.2751	0.1359	0.1651	0.0061	0.9259	0.0009	0.9892
Indus												
APHRODITE	-0.0252	0.6748	0.0003	0.9880	0.0105	0.6598	-0.0290	0.6368	0.0385	0.0463	0.0117	0.5942
ERA-40	0.0399	0.5304	0.0305	0.1195	0.0096	0.6729	0.0660	0.3031	0.0321	0.0517	0.0263	0.1430
JRA-25	-0.0057	0.8902	0.0199	0.2637	0.0139	0.5297	-0.0078	0.8537	0.0342	0.0147	0.0261	0.1399
NCEP/NCAR	0.0807	0.6099	-0.0320	0.2206	-0.0030	0.9175	0.0780	0.6225	0.0019	0.9367	-0.0485	0.0353
Ganges												
APHRODITE	0.5154	0.0347	0.0633	0.1906	0.2088	0.2191	0.3274	0.0249	-0.0263	0.6661	-0.0384	0.5495
ERA-40	1.0331	0.0096	0.0202	0.5859	0.2141	0.1876	1.1193	0.0002	0.0615	0.3338	0.0412	0.5159
JRA-25	1.8837	0.0000	0.0405	0.2331	0.1586	0.1533	1.7582	0.0000	0.0336	0.2853	0.0685	0.0724
NCEP/NCAR	0.1351	0.5978	-0.1069	0.1338	0.1367	0.5425	-0.0050	0.9059	-0.0111	0.8861	0.0164	0.8434
Himalaya												
APHRODITE	0.1542	0.4613	-0.0586	0.0899	0.0724	0.5948	0.0553	0.7280	-0.0314	0.4034	-0.0657	0.0607
ERA-40	-0.1301	0.4675	0.1201	0.0008	0.0552	0.5515	-0.1101	0.5428	-0.0120	0.5669	-0.0062	0.7493
JRA-25	0.4447	0.0900	-0.0186	0.4543	0.1121	0.1446	0.4453	0.0812	0.0150	0.5716	-0.0007	0.9789
NCEP/NCAR	-0.6672	0.1169	-0.0673	0.3336	-0.0341	0.8805	-0.7234	0.0291	-0.2175	0.0001	-0.1908	0.0002

Note: Statistically significant values (p-value < 0.1) are coloured red

Table C4: Trends of extreme events from 1960-2001: Number of wet periods > 5 days (CWD5)

	Annual		Winter		Pre-Monsoon		Monsoon		Post-Monsoon		Rabi	
	trend	*p*-value	trend	*p*-value	trend	*p*-value	trend	*p*-value	trend	*p*-value	trend	*p*-value
Indo-Gangetic Plain												
APHRODITE	0.0224	0.1459	0.0171	0.0970	0.0135	0.2774	0.0052	0.6238	-0.0040	0.6130	-0.0019	0.8481
ERA-40	-0.0030	0.8809	0.0033	0.0910	0.0298	0.0119	-0.0355	0.0439	0.0040	0.5495	0.0090	0.2027
JRA-25	-0.0567	0.0177	0.0160	0.2312	-0.0139	0.2599	-0.0720	0.0006	0.0178	0.0165	0.0287	0.0141
NCEP/NCAR	-0.0078	0.5484	-0.0060	0.5578	0.0077	0.3889	-0.0122	0.0340	-0.0059	0.3994	-0.0116	0.1261
Indus												
APHRODITE	-0.0206	0.2456	-0.0037	0.4898	-0.0033	0.4327	-0.0195	0.2277	0.0027	0.1765	-0.0015	0.7875
ERA-40	-0.0008	0.9608	0.0004	0.8395	-0.0023	0.5744	0.0005	0.9751	0.0028	0.1795	0.0027	0.1765
JRA-25	0.0113	0.4602	0.0047	0.2182	0.0062	0.1974	0.0064	0.6612	0.0000	-	0.0043	0.1993
NCEP/NCAR	-0.0061	0.7404	-0.0060	0.3060	0.0011	0.8745	-0.0084	0.6167	0.0002	0.9538	-0.0053	0.2108
Ganges												
APHRODITE	-0.0134	0.4560	0.0094	0.4050	-0.0053	0.6843	-0.0071	0.4108	0.0001	0.9927	0.0028	0.7683
ERA-40	-0.0398	0.0516	0.0146	0.0317	0.0172	0.1041	-0.0479	0.0007	-0.0070	0.4266	-0.0065	0.4984
JRA-25	-0.0545	0.0285	0.0264	0.0434	0.0250	0.0383	-0.0838	0.0001	0.0176	0.0208	0.0225	0.0136
NCEP/NCAR	-0.0277	0.0614	-0.0001	0.9951	-0.0027	0.7892	-0.0025	0.2048	-0.0156	0.1133	-0.0263	0.0250
Himalaya												
APHRODITE	-0.0352	0.0533	-0.0314	0.0389	-0.0060	0.6412	0.0026	0.7602	0.0010	0.8996	-0.0212	0.1102
ERA-40	0.0864	0.0014	0.0288	0.0014	0.0770	0.0000	0.0481	0.0158	-0.0016	0.4539	-0.0029	0.2933
JRA-25	-0.0386	0.0871	-0.0088	0.4594	-0.0026	0.8553	-0.0344	0.0515	0.0027	0.6591	-0.0077	0.4345
NCEP/NCAR	-0.0459	0.0386	-0.0338	0.0018	-0.0309	0.0345	0.0179	0.2456	-0.0293	0.0019	-0.0451	0.0004

Note: Statistically significant values (p-value < 0.1) are coloured red

Table C5: Trends of extreme events from 1960-2001: Cold nights (TN10p)

	Annual		Winter		Pre-Monsoon		Monsoon		Post-Monsoon		Rabi	
	trend	*p*-value	trend	*p*-value	trend	*p*-value	trend	*p*-value	trend	*p*-value	trend	*p*-value
Indo-Gangetic Plain												
ERA-40	-0.1224	0.2077	-0.1441	0.0570	0.1060	0.0258	0.0993	0.1306	-0.0865	0.1604	-0.1566	0.0553
NCAR/NCEP	-0.0279	0.7945	-0.0550	0.4657	0.1074	0.0102	-0.0985	0.1186	-0.1142	0.0286	-0.0655	0.4289
Indus												
ERA-40	-0.3751	0.0005	-0.2970	0.0020	0.0913	0.1066	0.1054	0.1467	-0.1948	0.0088	-0.3421	0.0008
NCAR/NCEP	-0.1381	0.2736	-0.1384	0.0984	0.0348	0.4818	-0.0926	0.1637	-0.1414	0.0249	-0.1579	0.0915
Ganges												
ERA-40	0.0932	0.4308	-0.0091	0.9119	0.1179	0.0213	0.0812	0.3056	0.0070	0.9187	0.0060	0.9466
NCAR/NCEP	0.0732	0.4982	0.0137	0.8597	0.1691	0.0001	-0.1240	0.1223	-0.0867	0.1156	0.0136	0.8710
Himalaya												
ERA-40	-0.0383	0.7566	-0.0368	0.6606	0.0408	0.4141	0.1288	0.0962	-0.0537	0.4098	-0.0399	0.6660
NCAR/NCEP	0.2880	0.0261	0.1357	0.0714	0.2159	0.0000	0.2524	0.0276	-0.0225	0.6548	0.1614	0.0604

Note: Statistically significant values (p-value < 0.1) are coloured red

Table C6: Trends of extreme events from 1960-2001: Warm nights (TN90p)

	Annual		Winter		Pre-Monsoon		Monsoon		Post-Monsoon		Rabi	
	trend	*p*-value	trend	*p*-value	trend	*p*-value	trend	*p*-value	trend	*p*-value	trend	*p*-value
Indo-Gangetic Plain												
ERA-40	-0.6858	0.0000	-0.1195	0.0283	-0.2477	0.0001	-0.4195	0.0000	-0.0813	0.1500	-0.1168	0.1135
NCAR/NCEP	0.0574	0.5338	-0.1497	0.0003	-0.0268	0.4545	0.0290	0.5163	0.0223	0.5478	-0.0428	0.4321
Indus												
ERA-40	-0.6024	0.0001	-0.0680	0.2865	-0.1956	0.0017	-0.4245	0.0000	-0.1062	0.1081	-0.1333	0.1096
NCAR/NCEP	0.1602	0.0827	-0.0260	0.5337	0.0220	0.5953	0.0747	0.1058	0.0504	0.3943	0.0094	0.9136
Ganges												
ERA-40	-0.7631	0.0001	-0.1641	0.0078	-0.2961	0.0004	-0.4072	0.0001	-0.0564	0.4076	-0.0935	0.2733
NCAR/NCEP	-0.0339	0.7625	-0.2590	0.0000	-0.0741	0.1231	-0.0043	0.9425	0.0104	0.8428	-0.0731	0.2626
Himalaya												
ERA-40	-0.3079	0.0323	-0.0345	0.5719	-0.0721	0.1510	-0.2390	0.0110	-0.0654	0.2613	-0.1028	0.1543
NCAR/NCEP	-0.2708	0.0648	-0.2960	0.0001	-0.0939	0.0698	-0.0737	0.3557	-0.2144	0.0024	-0.3250	0.0025

Note: Statistically significant values (p-value < 0.1) are coloured red

Table C7: Trends of extreme events from 1960-2001: Very cold days (TX10p)

	Annual		Winter		Pre-Monsoon		Monsoon		Post-Monsoon		Rabi	
	trend	*p*-value	trend	*p*-value	trend	*p*-value	trend	*p*-value	trend	*p*-value	trend	*p*-value
Indo-Gangetic Plain												
ERA-40	-0.0610	0.5739	-0.0326	0.6853	0.0610	0.2082	-0.0335	0.5218	-0.0643	0.2908	-0.0362	0.6795
NCAR/NCEP	-0.1712	0.1707	-0.1093	0.1770	0.0252	0.4904	-0.1240	0.1107	-0.1672	0.0034	-0.1372	0.1293
Indus												
ERA-40	-0.1836	0.1894	-0.1469	0.1261	0.0552	0.3998	0.0981	0.2830	-0.1097	0.1545	-0.1494	0.1536
NCAR/NCEP	-0.3026	0.0378	-0.2155	0.0322	-0.0912	0.1237	-0.0149	0.8755	-0.2484	0.0014	-0.2406	0.0287
Ganges												
ERA-40	0.0567	0.6022	0.0710	0.4263	0.0643	0.2989	-0.1524	0.0027	-0.0173	0.7784	0.0696	0.4646
NCAR/NCEP	-0.0623	0.6661	-0.0194	0.8336	0.1122	0.0366	-0.2410	0.0084	-0.0970	0.1359	-0.0521	0.6119
Himalaya												
ERA-40	-0.2431	0.0591	-0.1477	0.1229	0.0161	0.7614	-0.0501	0.3088	-0.1785	0.0211	-0.1647	0.1094
NCAR/NCEP	0.2484	0.1058	0.0681	0.4583	0.2438	0.0000	0.2144	0.1192	-0.0518	0.3963	0.0879	0.3952

Note: Statistically significant values (p-value < 0.1) are coloured red

Table C8: Trends of extreme events from 1960-2001: Very warm days (TX90p)

	Annual		Winter		Pre-Monsoon		Monsoon		Post-Monsoon		Rabi	
	trend	*p*-value	trend	*p*-value	trend	*p*-value	trend	*p*-value	trend	*p*-value	trend	*p*-value
Indo-Gangetic Plain												
ERA-40	-0.2824	0.0283	-0.0781	0.2529	-0.1704	0.0212	-0.1370	0.0427	0.0068	0.8892	-0.0841	0.2321
NCAR/NCEP	-0.0024	0.9763	-0.0274	0.6682	0.0064	0.8886	0.0086	0.8245	0.1005	0.0707	-0.0108	0.8965
Indus												
ERA-40	-0.3575	0.0321	-0.0213	0.8085	-0.0945	0.1826	-0.2797	0.0019	-0.0315	0.6474	-0.1269	0.2199
NCAR/NCEP	0.3011	0.0128	0.1369	0.0608	0.1664	0.0040	0.0914	0.1398	0.1094	0.1087	0.1041	0.3042
Ganges												
ERA-40	-0.2296	0.1159	-0.1327	0.1144	-0.2422	0.0094	-0.0122	0.8589	0.0426	0.3896	-0.0449	0.4664
NCAR/NCEP	-0.2421	0.0534	-0.1456	0.0893	-0.1220	0.0609	-0.0646	0.2218	0.1062	0.0811	-0.0938	0.2971
Himalaya												
ERA-40	0.0486	0.6066	-0.0262	0.6855	-0.0662	0.2514	-0.0195	0.6976	0.0572	0.3031	0.0745	0.2989
NCAR/NCEP	-0.2868	0.0349	-0.2664	0.0018	-0.1554	0.0110	-0.1194	0.0760	-0.1037	0.2501	-0.2227	0.0952

Note: Statistically significant values (p-value < 0.1) are coloured red

Appendix 4

Figure D1: Precipitation bias (mm/day) for the annual cycle

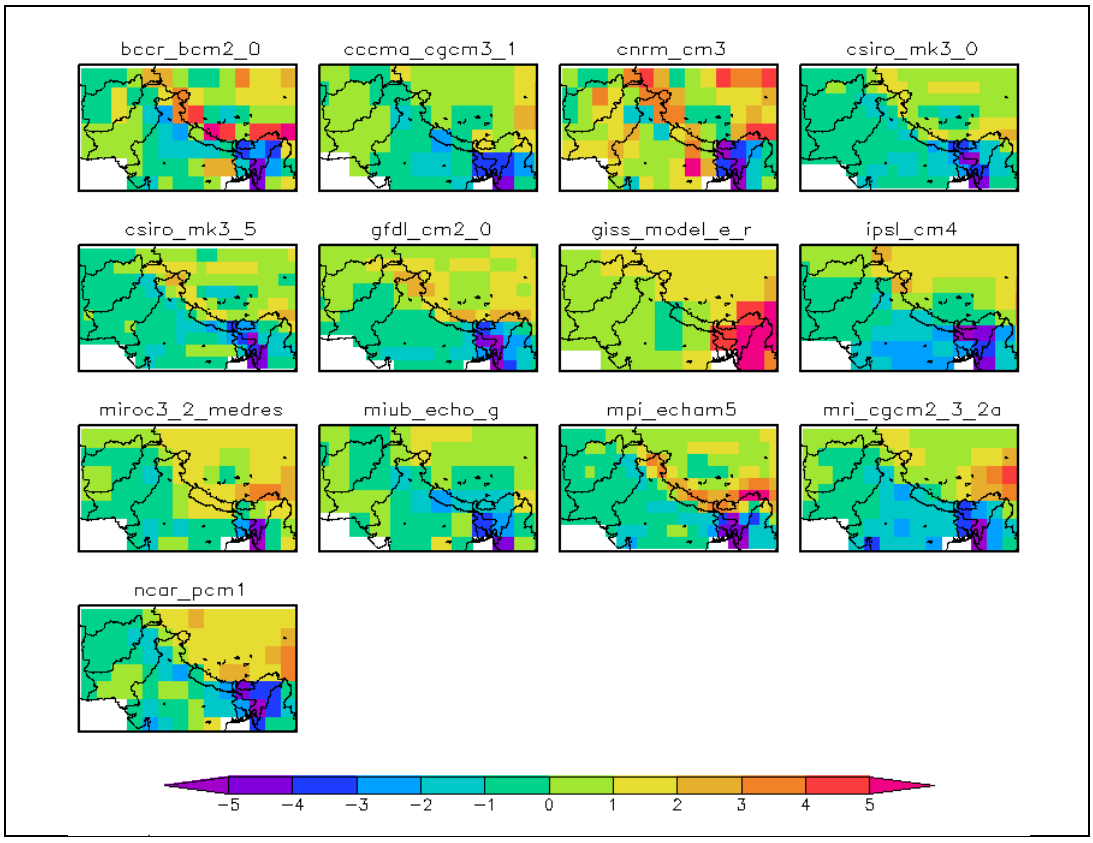

Figure D2: Precipitation bias (mm/day) for winter season

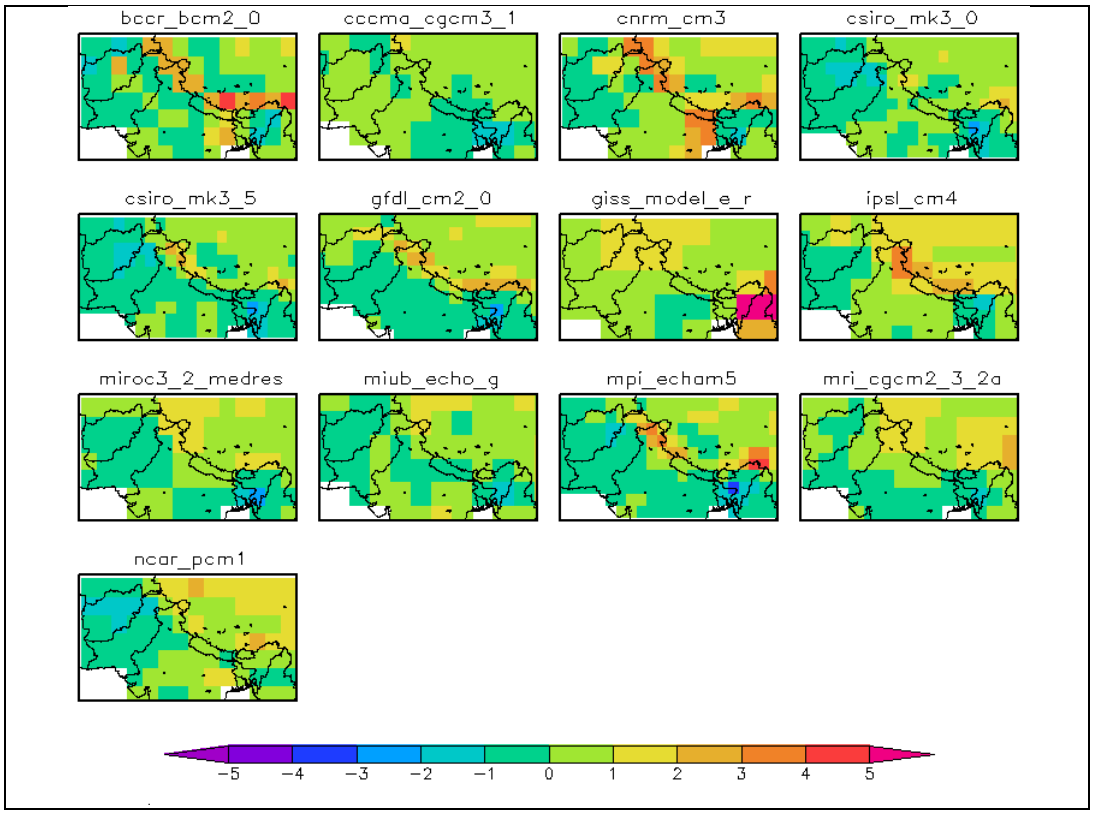

Figure D3: GCM Precipitation bias (mm/day) for pre-monsoon season

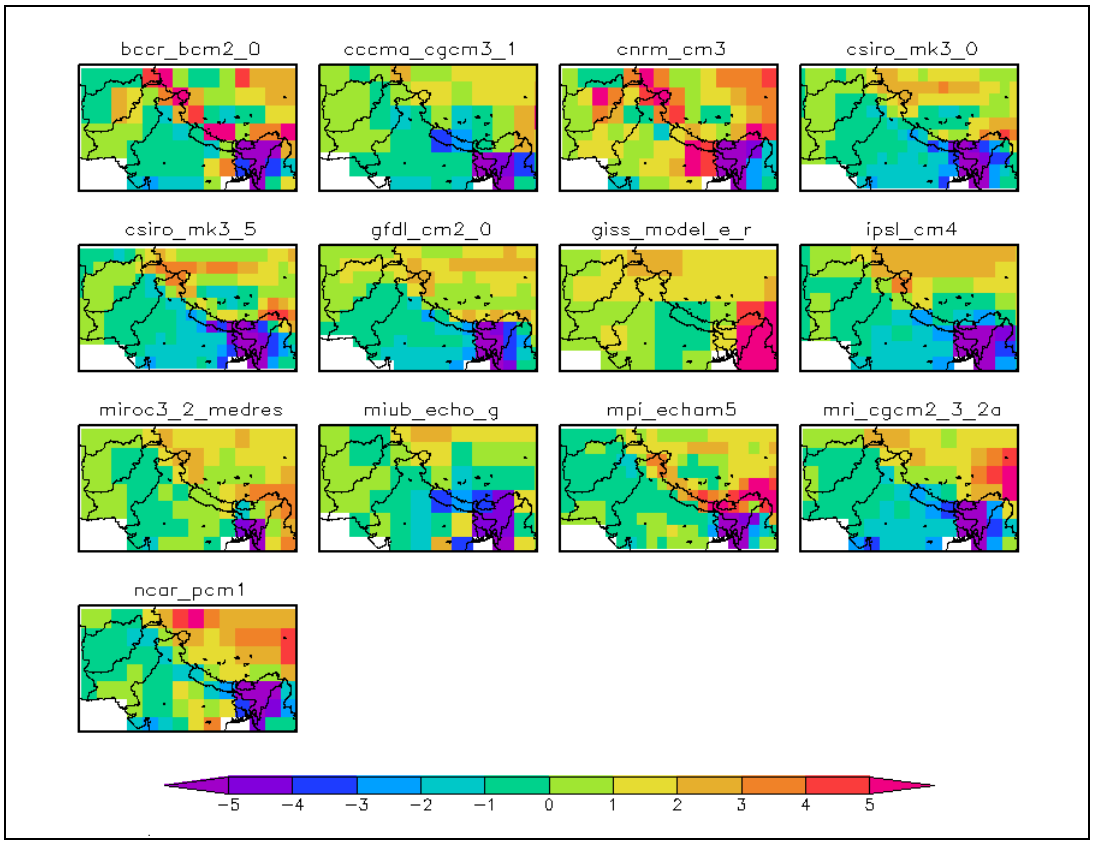

Figure D4: GCM Precipitation bias (mm/day) for monsoon season

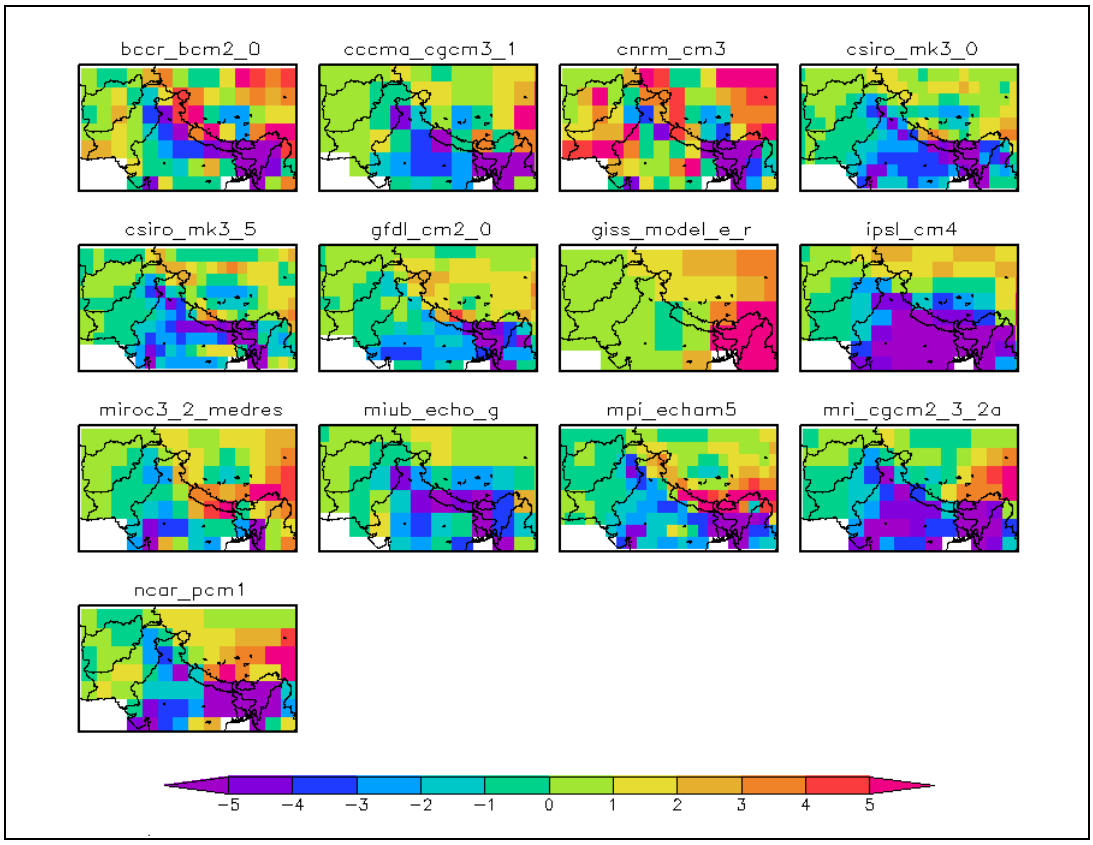

Figure D5: GCM Precipitation bias (mm/day) for post-monsoon season

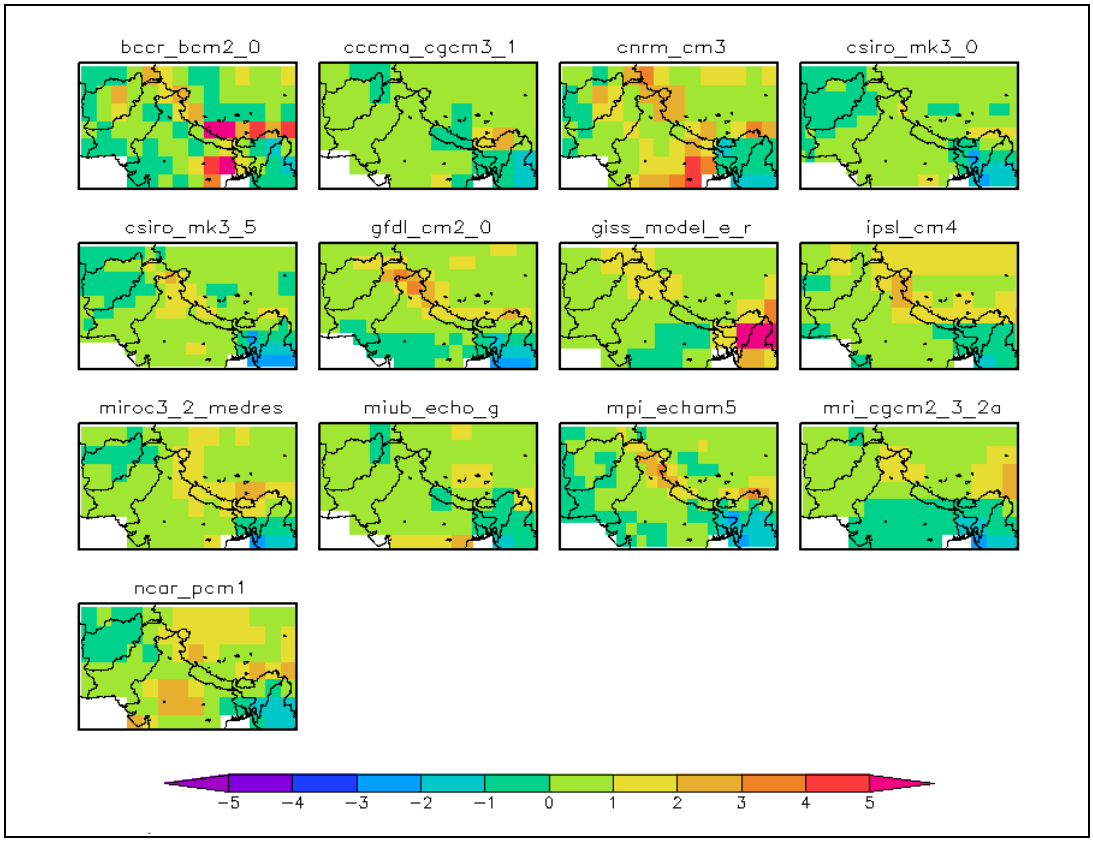

Figure D6: GCM Precipitation bias (mm/day) for rabi season

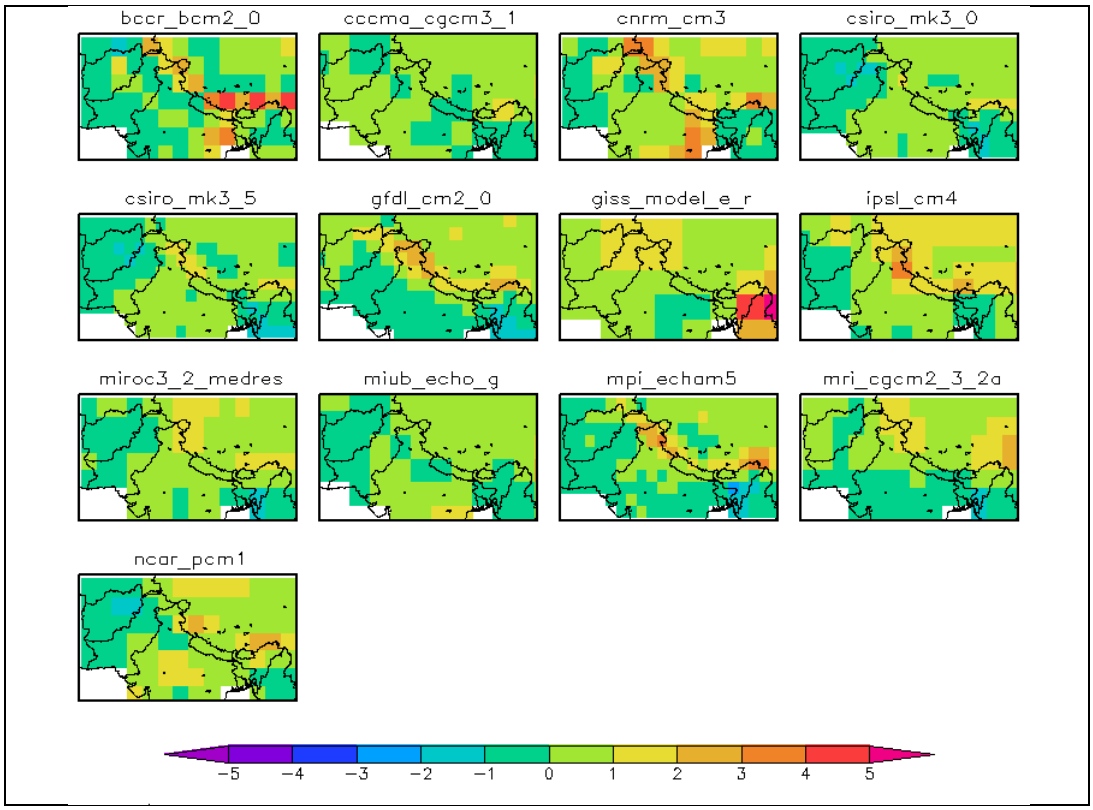

Figure D7: mean temperature bias (°C) for annual cycle

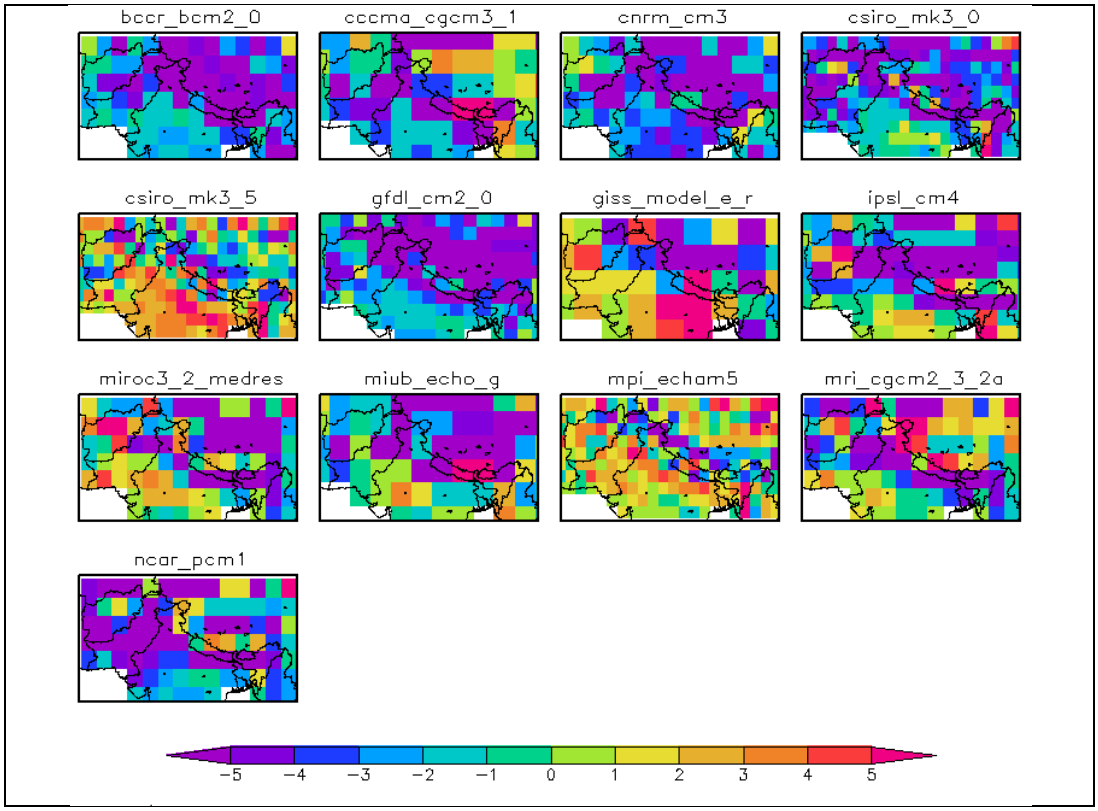

Figure D8: GCM mean temperature bias (°C) for winter season

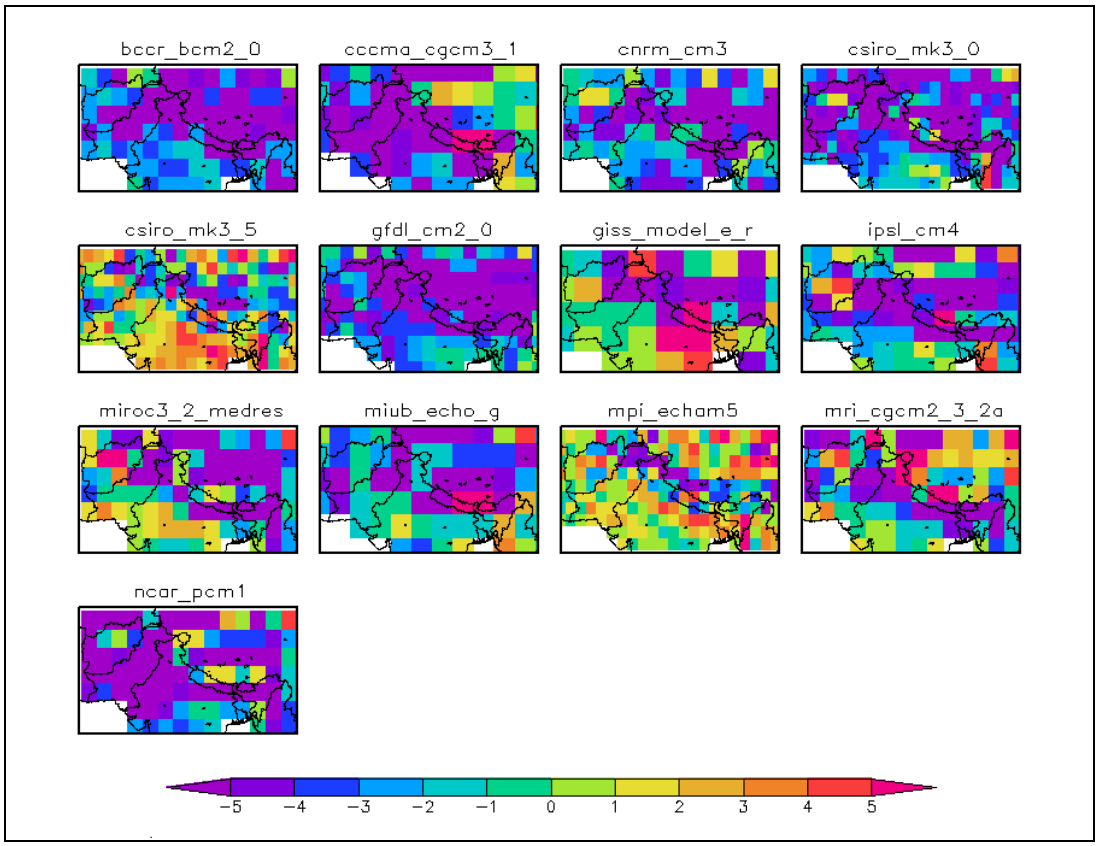

Figure D9: GCM mean temperature bias (°C) for pre-monsoon season

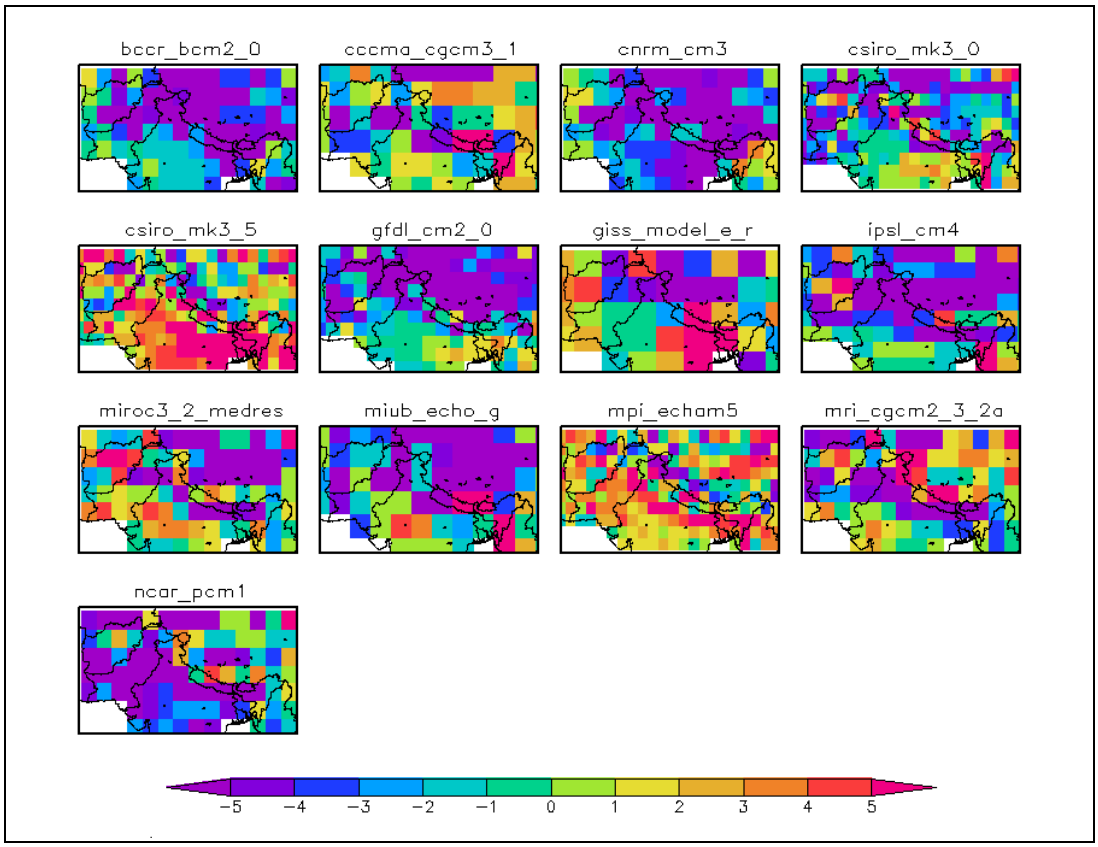

Figure D10: GCM mean temperature bias (°C) for monsoon season

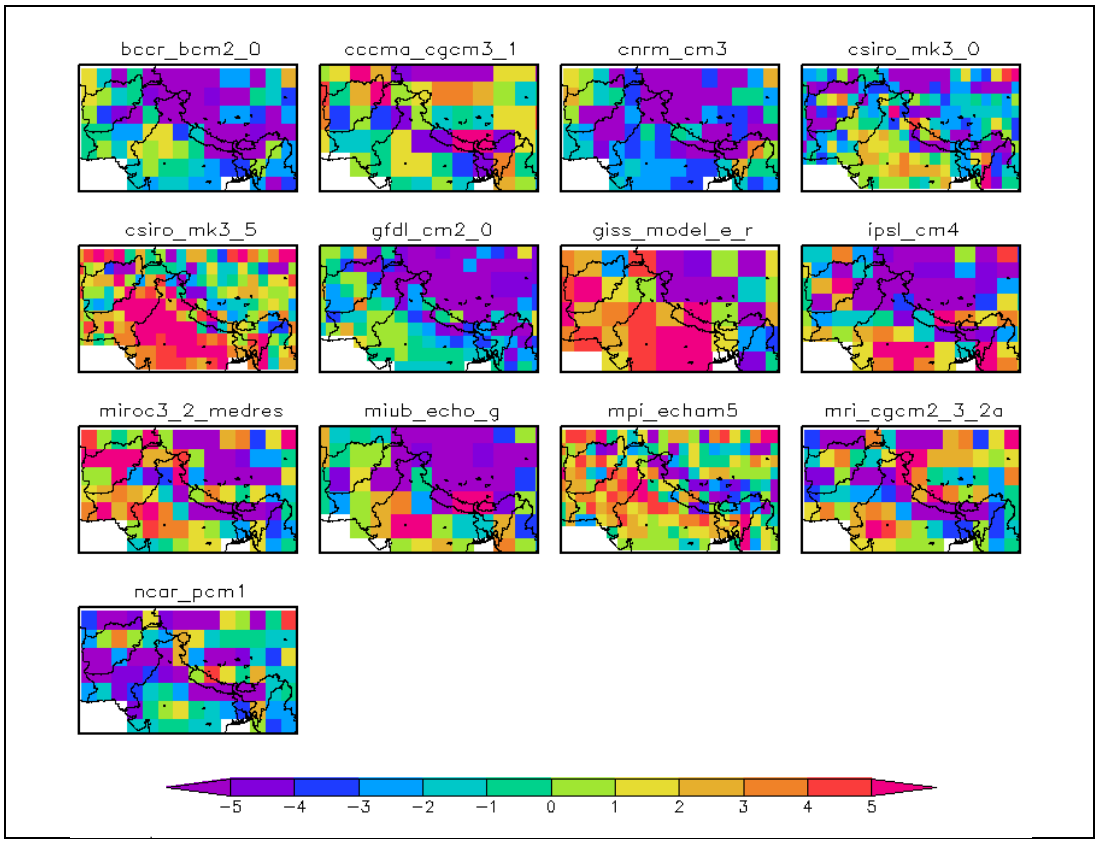

Figure D11: GCM mean temperature bias (°C) for post-monsoon season

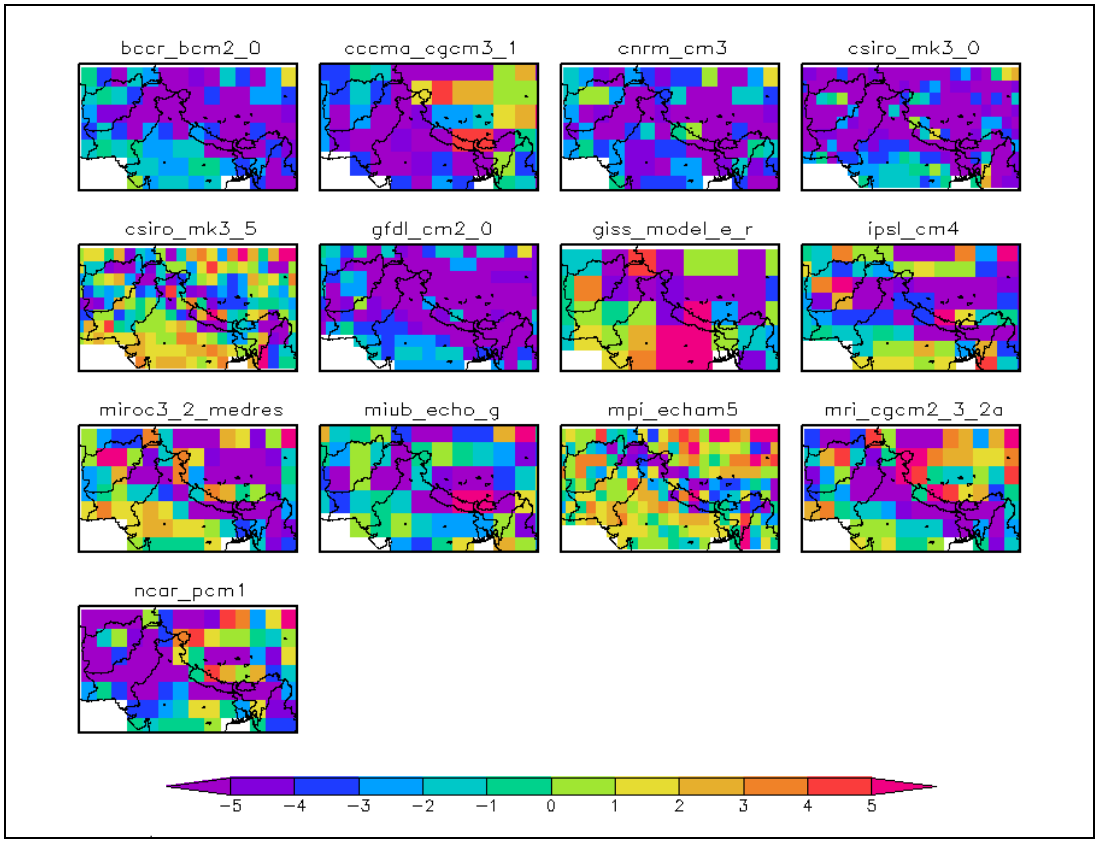

Figure D12: GCM mean temperature bias (°C) for rabi season

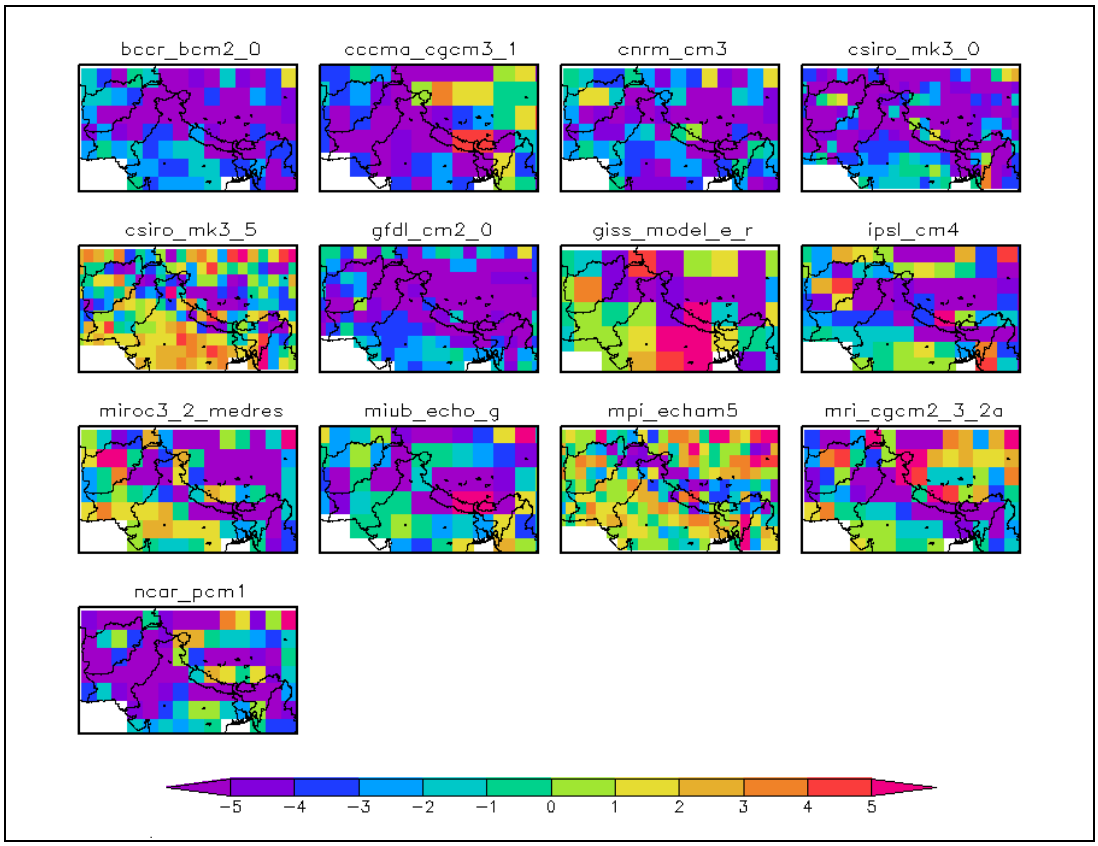

Figure D13: GCM minimum temperature bias (°C) for annual cycle

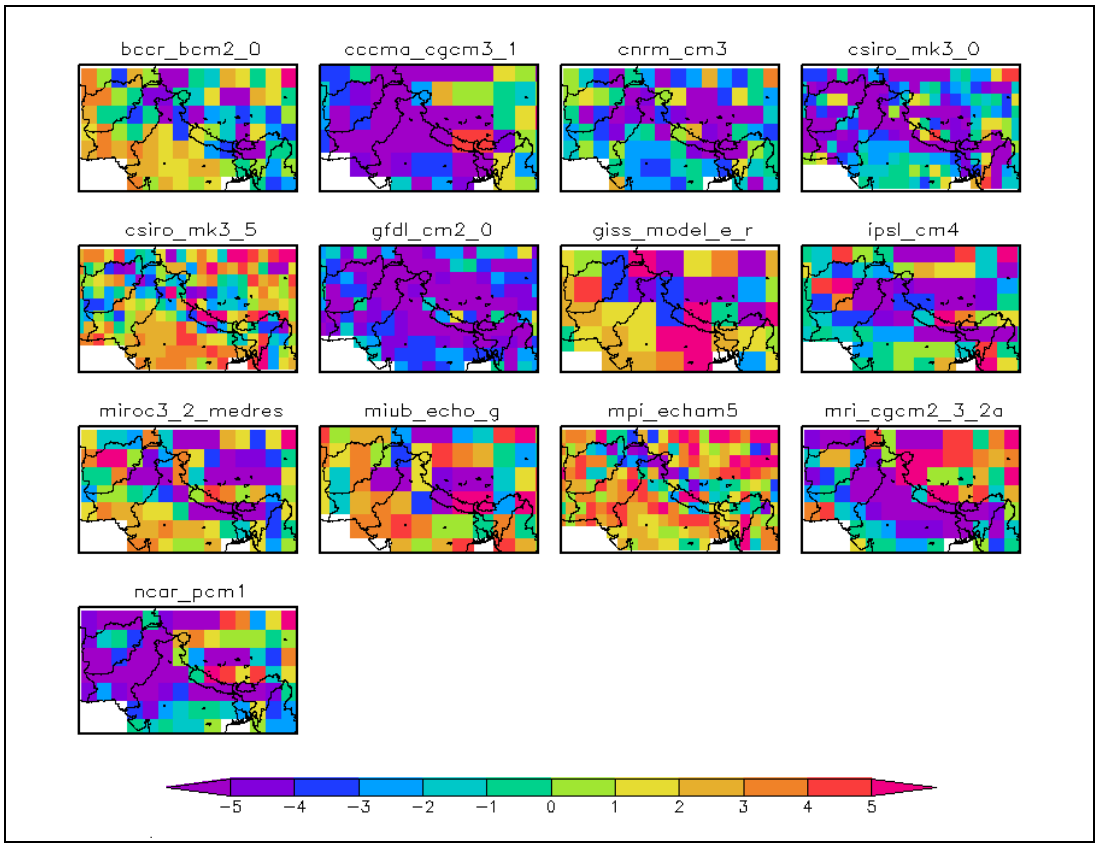

Figure D14: GCM minimum temperature bias (°C) for winter season

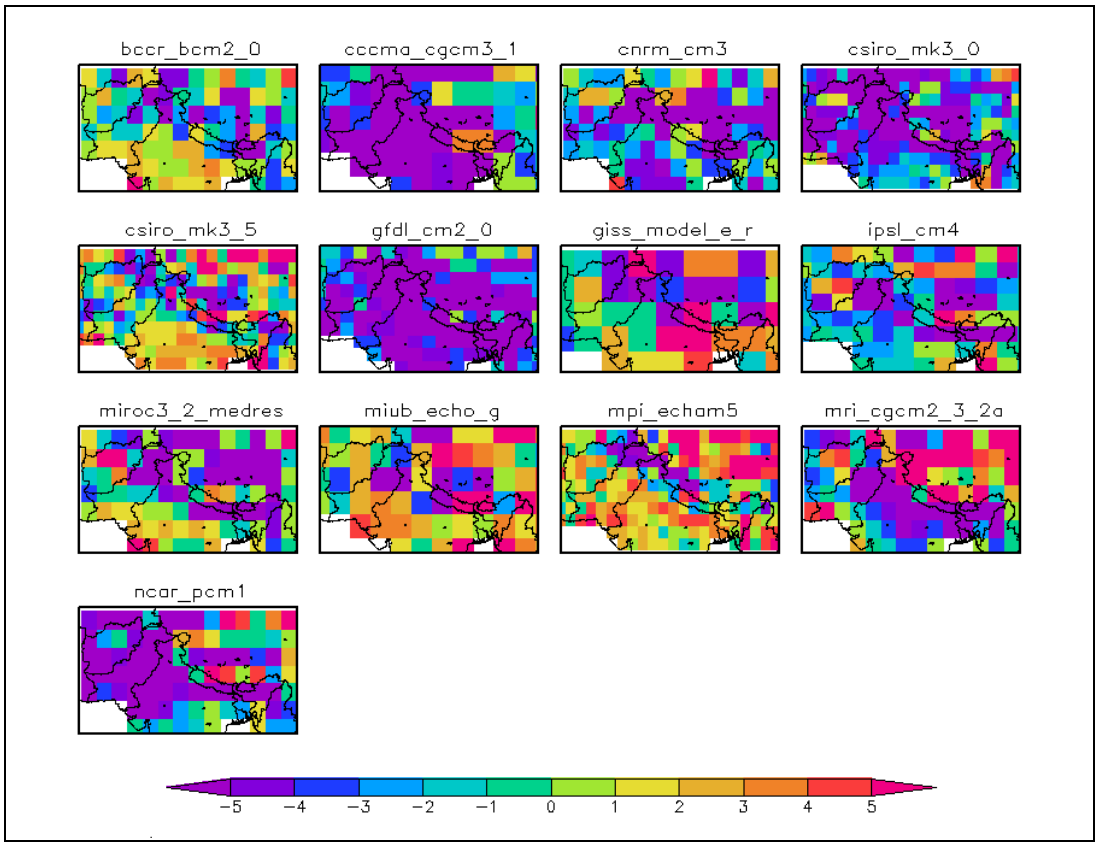

Figure D15: GCM minimum temperature bias (°C) for pre-monsoon season

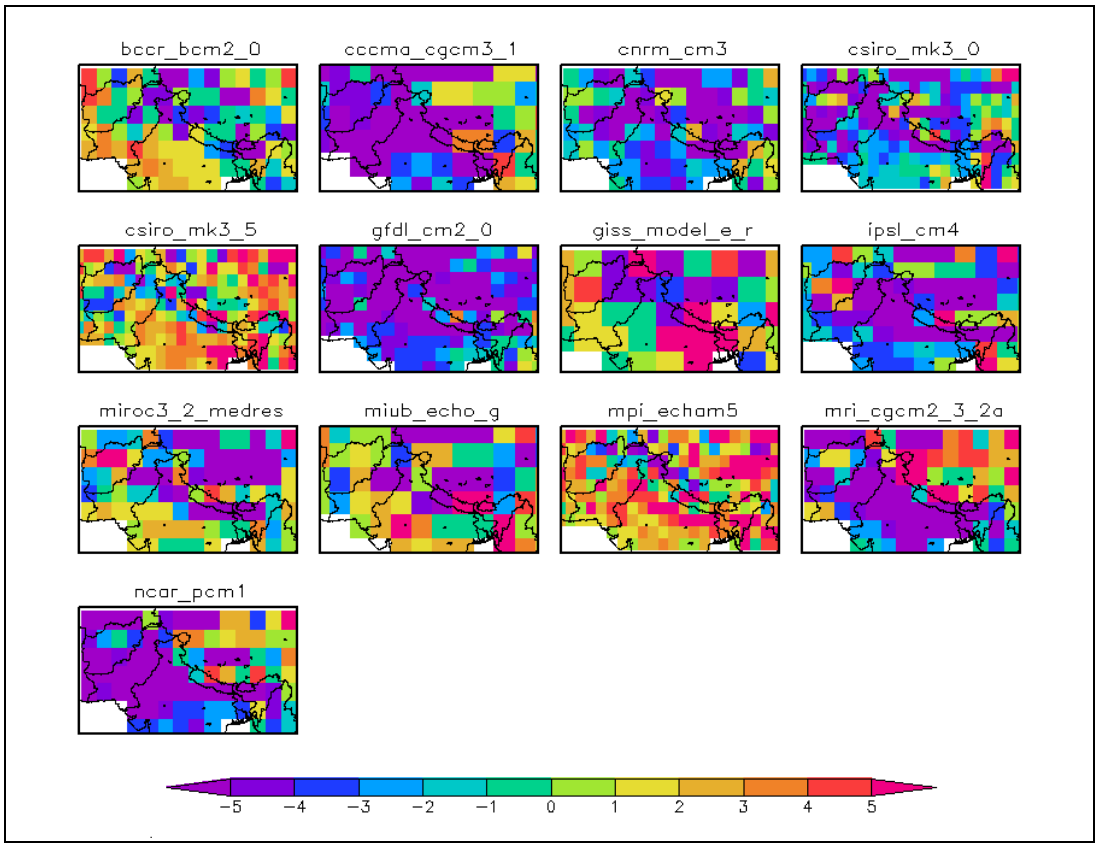

Figure D16: GCM minimum temperature bias (°C) for monsoon season

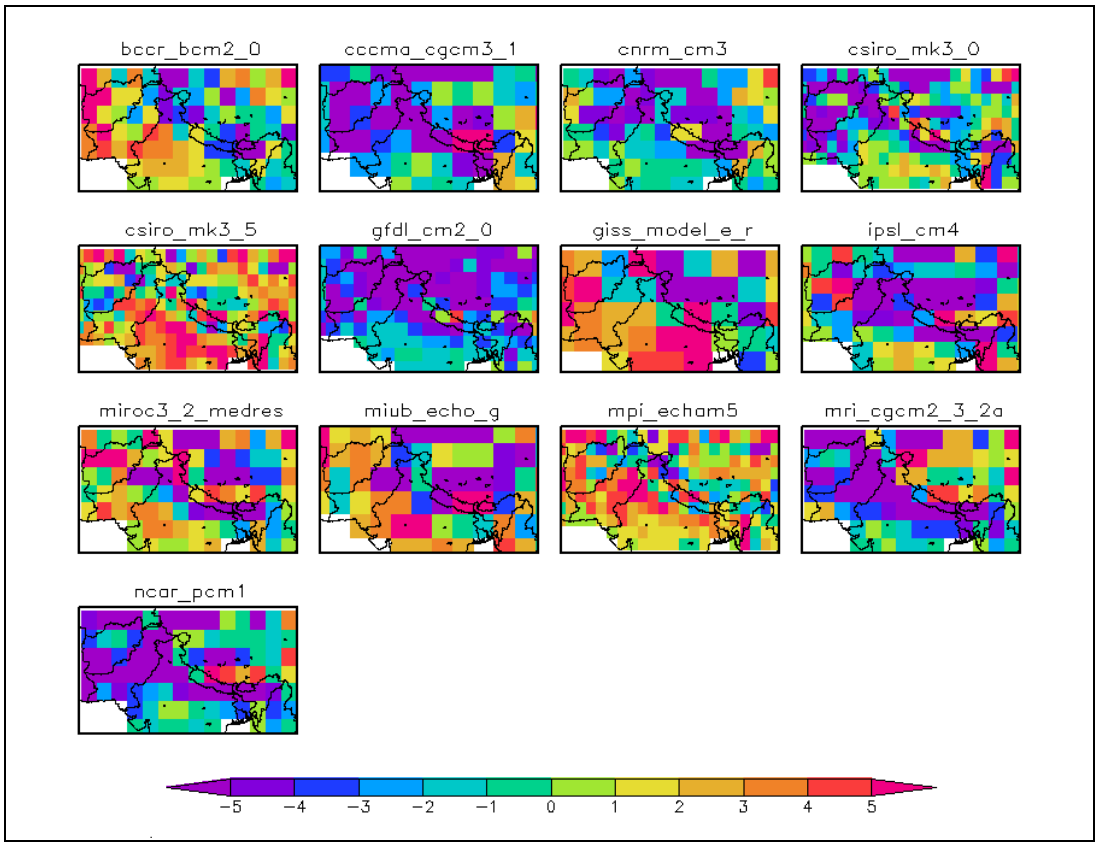

Figure D17: GCM minimum temperature bias (°C) for post-monsoon season

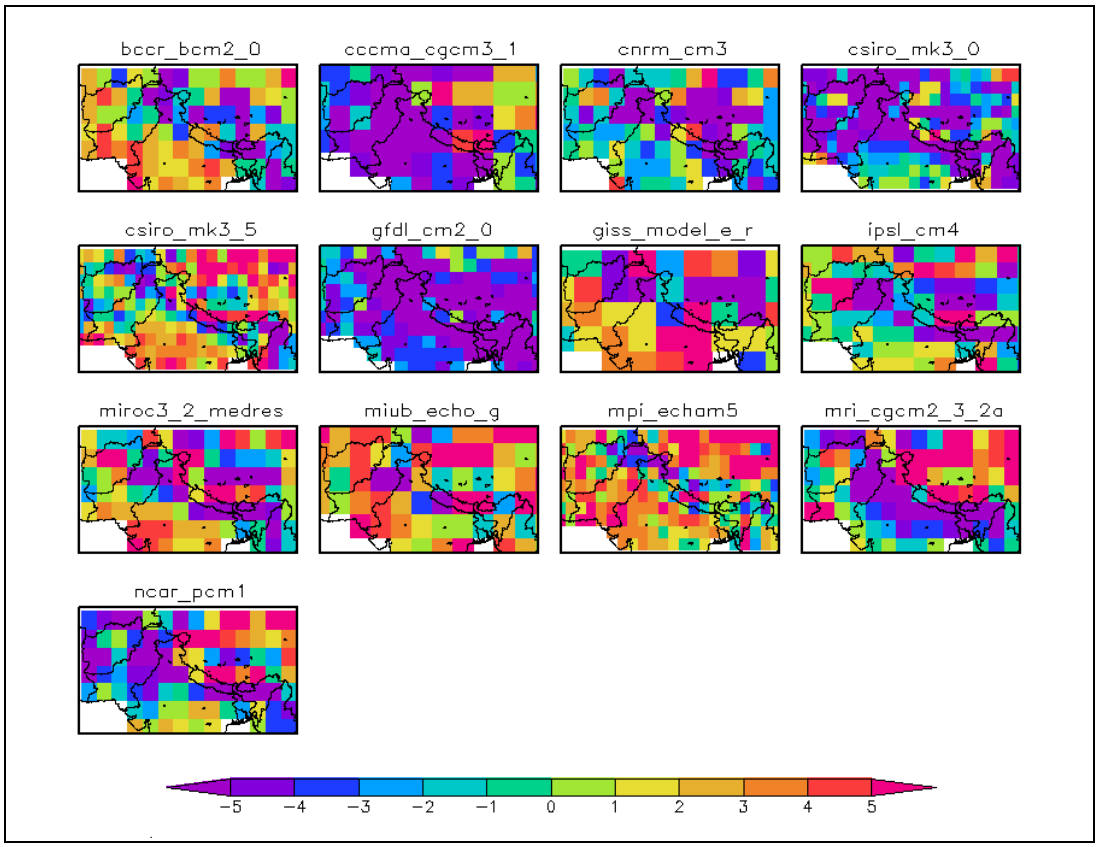

Figure D18: GCM minimum temperature bias (°C) for rabi season

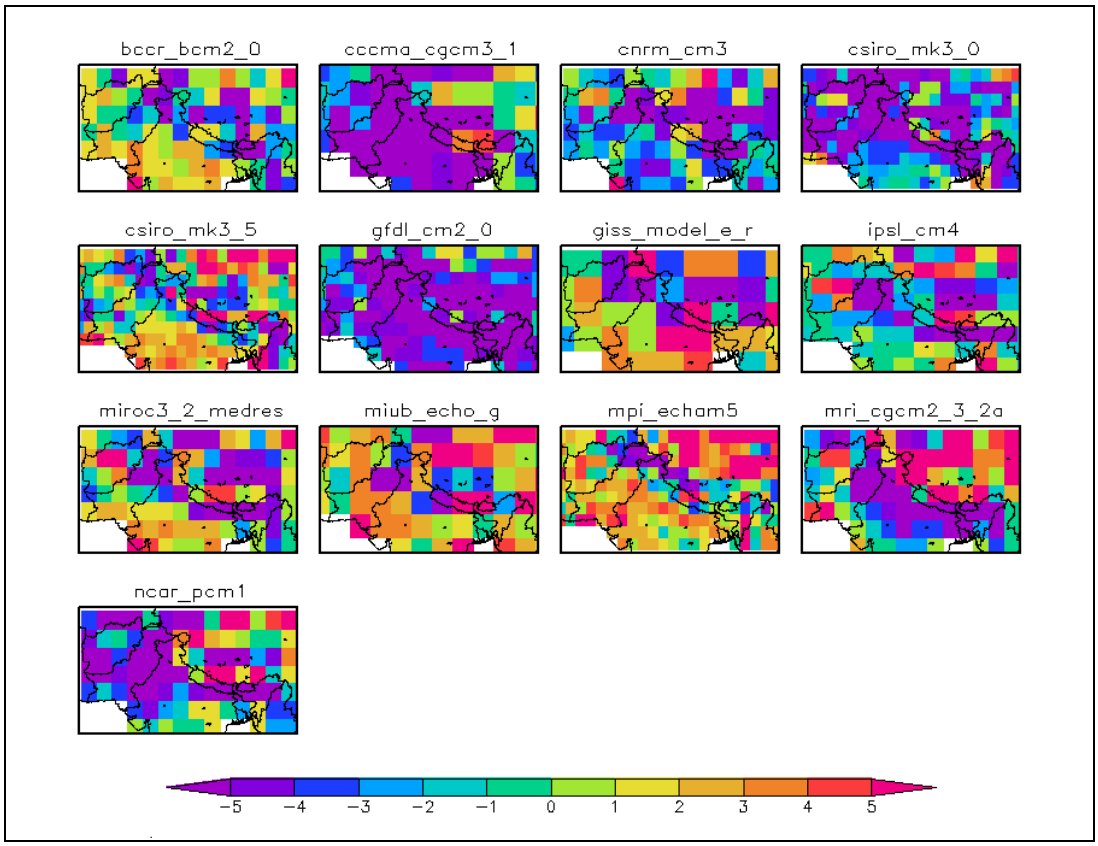

Figure D19: GCM maximum temperature bias (°C) for annual cycle

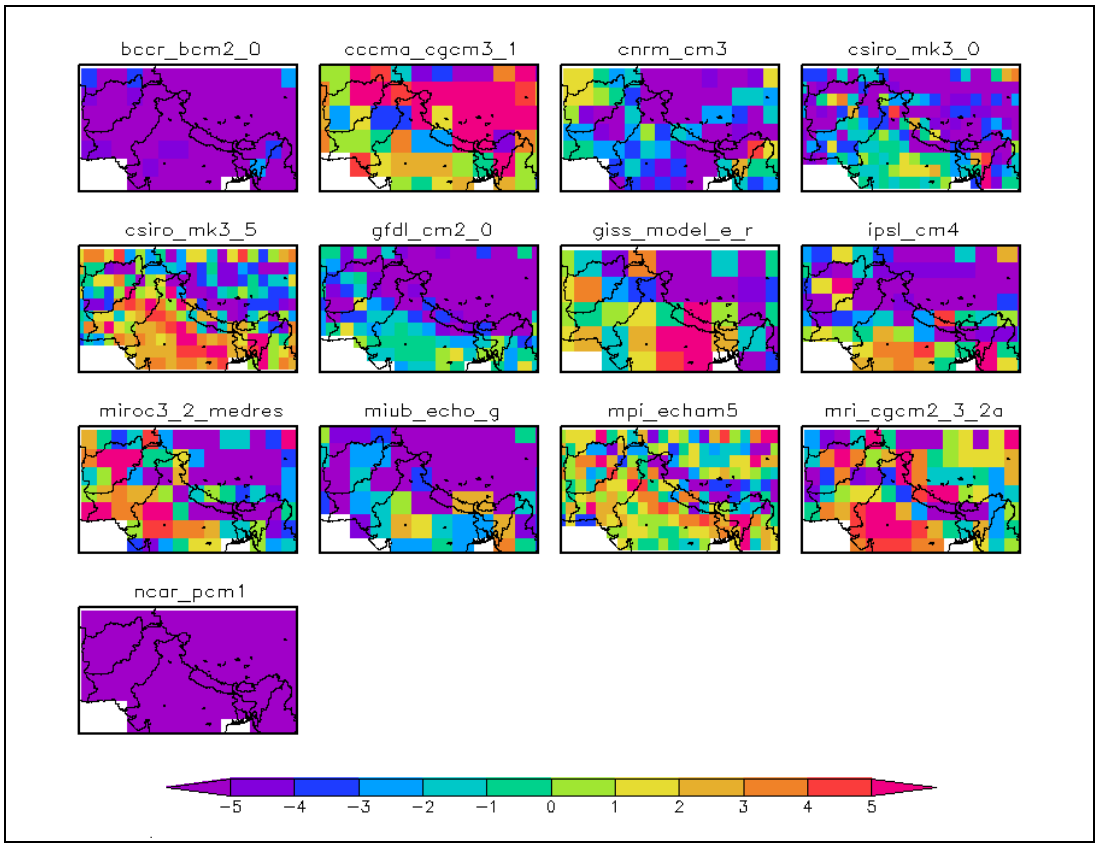

Figure D20: GCM maximum temperature bias (°C) for winter season

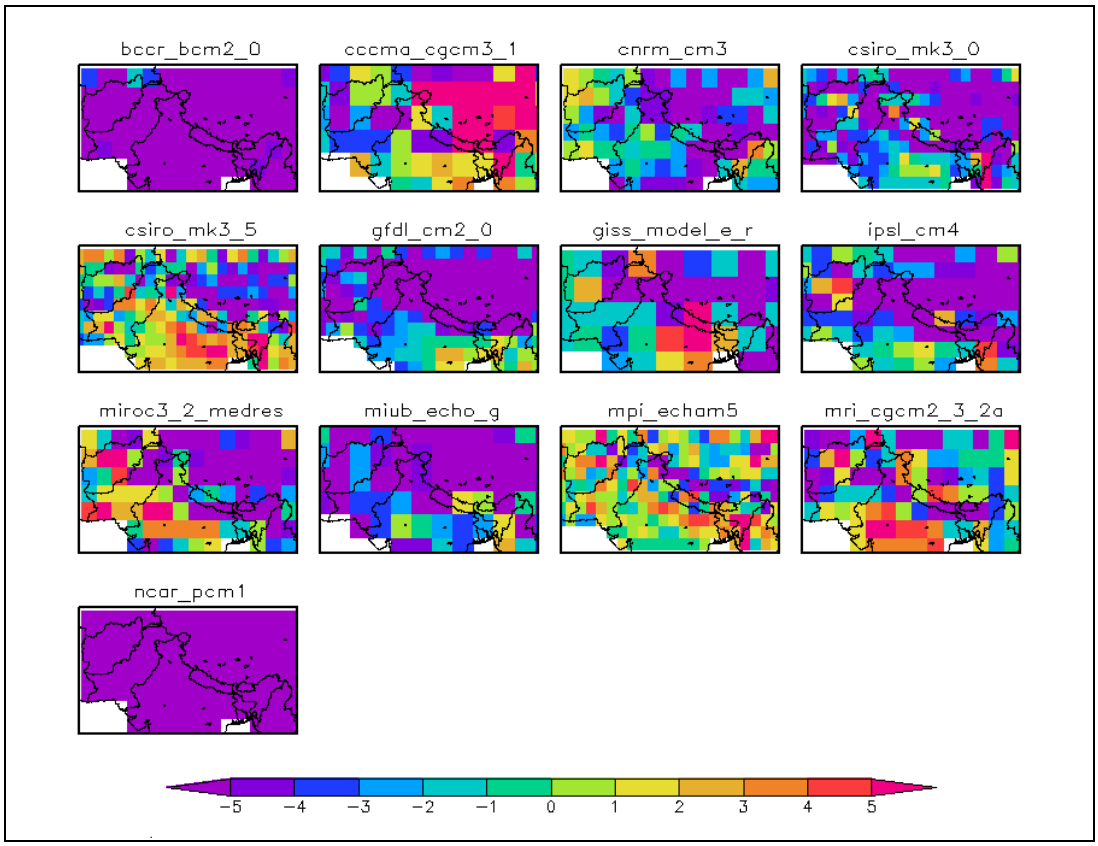

Figure D21: GCM maximum temperature bias (°C) for pre-monsoon season

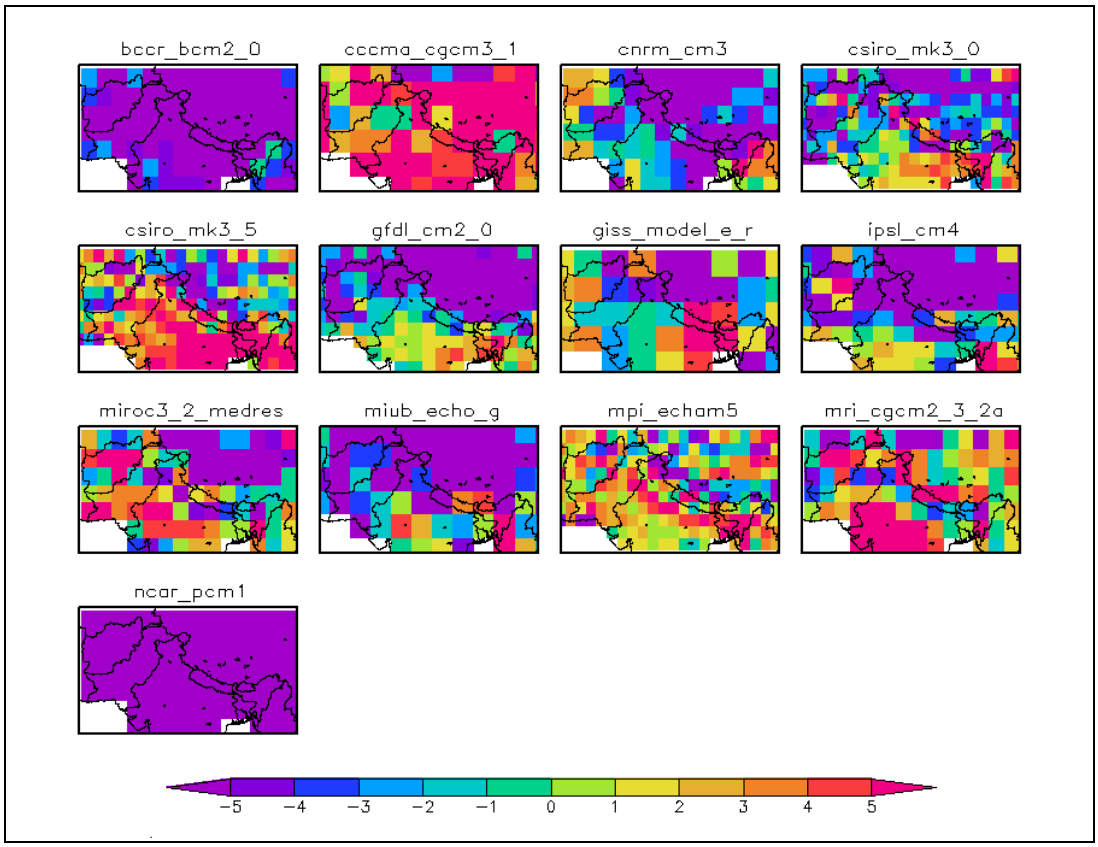

Figure D22: GCM maximum temperature bias (°C) for monsoon season

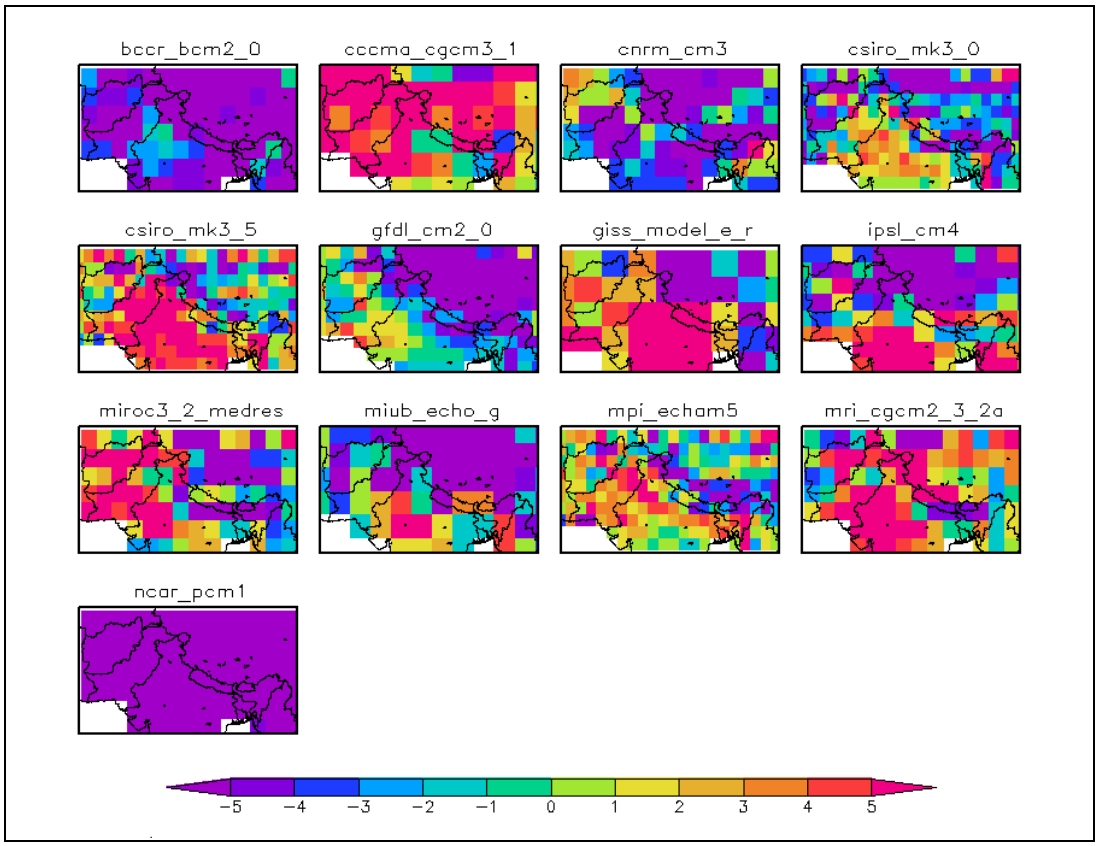

Figure D23: GCM maximum temperature bias (°C) for post-monsoon season

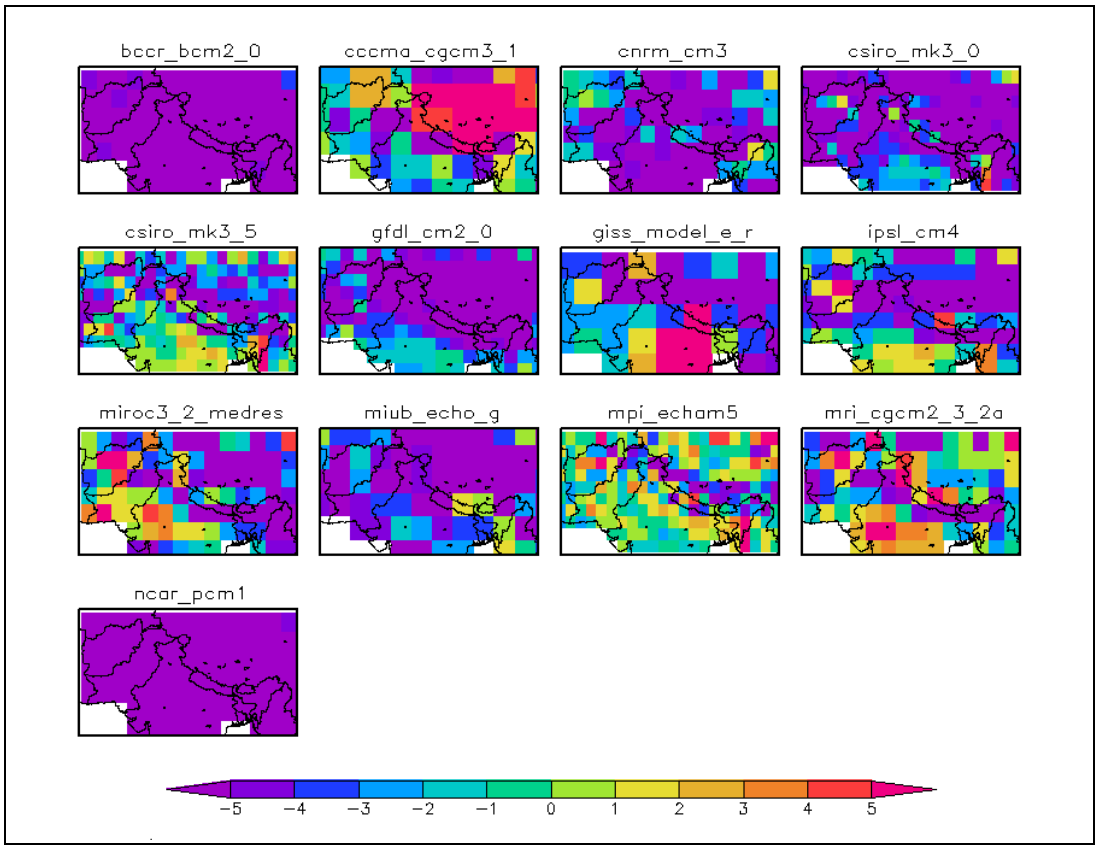

Figure D24: GCM maximum temperature bias (°C) for rabi season

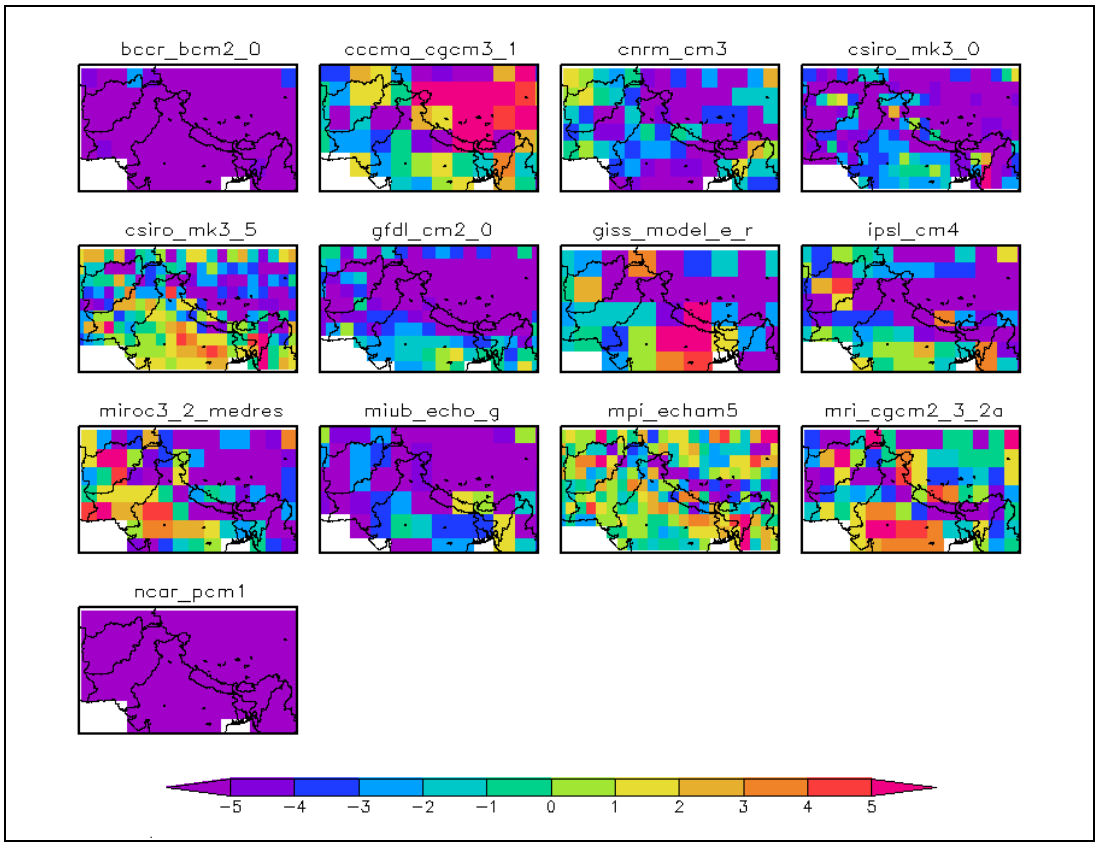

Appendix 5

Table E1: Spatial correlation of precipitation between respective GCMs and CRU for annual cycle

Model	IGP	Indus	Ganges	Himalaya	IGP + Himalaya	Domain
bccr_bcm2_0	0.76	-0.56	0.47	0.18	0.61	0.68
cccma_cgcm3_1	0.91	-0.35	0.82	0.47	0.77	0.80
cnrm_cm3	0.37	-0.63	-0.26	0.17	0.34	0.61
csiro_mk3_0	0.93	0.83	0.79	0.37	0.81	0.83
csiro_mk3_5	0.91	0.71	0.75	0.27	0.81	0.75
gfdl_cm2_0	0.88	0.97	0.65	0.22	0.69	0.65
giss_model_e_r	0.75	0.62	0.78	0.12	0.68	0.22
ipsl_cm4	0.86	0.96	0.62	-0.77	0.62	0.32
miroc3_2_medres	0.89	0.89	0.62	0.64	0.82	0.73
miub_echo_g	0.79	0.40	0.44	0.51	0.75	0.72
mpi_echam5	0.84	0.83	0.65	0.63	0.66	0.64
mri_cgcm2_3_2a	0.92	0.91	0.79	0.48	0.78	0.72
ncar_pcm1	0.70	-0.27	0.25	0.39	0.65	0.70
Ensemble mean	0.81	0.41	0.57	0.28	0.69	0.64

Table E2: As Table E1 but for winter season

Model	IGP	Indus	Ganges	Himalaya	IGP + Himalaya	Domain
bccr_bcm2_0	0.59	0.71	0.48	-0.52	0.44	0.60
cccma_cgcm3_1	0.51	0.84	0.63	0.18	0.50	0.82
cnrm_cm3	0.26	0.75	-0.12	-0.01	0.34	0.56
csiro_mk3_0	0.69	0.65	0.69	-0.17	0.57	0.70
csiro_mk3_5	0.77	0.65	0.80	0.25	0.61	0.69
gfdl_cm2_0	0.76	0.93	0.66	0.29	0.59	0.79
giss_model_e_r	0.68	0.92	0.67	0.50	0.66	0.71
ipsl_cm4	0.42	0.79	-0.14	0.31	0.51	0.80
miroc3_2_medres	0.72	0.93	0.56	0.09	0.62	0.77
miub_echo_g	0.66	0.90	0.42	0.68	0.72	0.77
mpi_echam5	0.70	0.82	0.63	0.26	0.54	0.74
mri_cgcm2_3_2a	0.60	0.89	0.59	0.44	0.63	0.79
ncar_pcm1	0.75	0.88	0.86	-0.56	0.57	0.60
Ensemble mean	0.62	0.82	0.52	0.13	0.56	0.72

Table E3: As Table E1 but for pre-monsoon season

Model	IGP	Indus	Ganges	Himalaya	IGP + Himalaya	Domain
bccr_bcm2_0	0.76	0.12	0.59	0.47	0.68	0.70
cccma_cgcm3_1	0.87	0.51	0.79	0.46	0.77	0.78
cnrm_cm3	0.35	-0.05	-0.15	0.49	0.36	0.60
csiro_mk3_0	0.89	0.81	0.82	0.38	0.69	0.51
csiro_mk3_5	0.79	0.71	0.73	0.21	0.60	0.27
gfdl_cm2_0	0.89	0.88	0.80	0.51	0.71	0.54
giss_model_e_r	0.58	0.05	0.62	0.10	0.54	-0.27
ipsl_cm4	0.77	0.87	0.63	-0.73	0.56	0.40
miroc3_2_medres	0.90	0.91	0.82	0.74	0.85	0.79
miub_echo_g	0.80	0.36	0.69	-0.05	0.73	0.61
mpi_echam5	0.83	0.63	0.72	0.76	0.71	0.75
mri_cgcm2_3_2a	0.93	0.91	0.89	0.45	0.81	0.70
ncar_pcm1	0.66	-0.01	0.36	0.68	0.66	0.72
Ensemble mean	0.77	0.52	0.64	0.34	0.67	0.55

Table E4: As Table E1 but for monsoon season

Model	IGP	Indus	Ganges	Himalaya	IGP + Himalaya	Domain
bccr_bcm2_0	0.74	-0.63	0.33	0.17	0.56	0.71
cccma_cgcm3_1	0.91	-0.43	0.82	0.66	0.81	0.80
cnrm_cm3	0.14	-0.57	-0.46	0.09	0.13	0.52
csiro_mk3_0	0.93	0.81	0.73	0.54	0.84	0.84
csiro_mk3_5	0.89	0.77	0.66	0.54	0.83	0.79
gfdl_cm2_0	0.90	0.95	0.52	0.68	0.84	0.83
giss_model_e_r	0.72	-0.39	0.74	0.37	0.67	0.42
ipsl_cm4	0.77	0.52	0.59	0.44	0.72	0.50
miroc3_2_medres	0.91	0.84	0.59	0.78	0.86	0.73
miub_echo_g	0.78	-0.06	0.30	0.63	0.74	0.72
mpi_echam5	0.83	0.67	0.66	0.77	0.71	0.75
mri_cgcm2_3_2a	0.89	0.69	0.71	0.68	0.80	0.77
ncar_pcm1	0.51	-0.50	0.03	0.51	0.51	0.64
Ensemble mean	0.76	0.21	0.48	0.53	0.69	0.69

Table E5: As Table E1 but for post-monsoon season

Model	IGP	Indus	Ganges	Himalaya	IGP + Himalaya	Domain
bccr_bcm2_0	0.77	0.33	0.56	0.35	0.68	0.79
cccma_cgcm3_1	0.86	0.51	0.76	0.04	0.68	0.81
cnrm_cm3	0.56	0.33	0.16	0.16	0.54	0.81
csiro_mk3_0	0.86	0.49	0.66	-0.21	0.74	0.80
csiro_mk3_5	0.81	0.20	0.67	-0.34	0.69	0.64
gfdl_cm2_0	0.76	0.81	0.56	-0.48	0.41	0.35
giss_model_e_r	0.67	0.87	0.68	-0.43	0.51	0.06
ipsl_cm4	0.64	0.62	0.28	-0.70	0.34	0.36
miroc3_2_medres	0.84	0.51	0.60	0.25	0.72	0.78
miub_echo_g	0.78	0.87	0.61	0.48	0.77	0.83
mpi_echam5	0.70	0.70	0.38	-0.60	0.30	0.31
mri_cgcm2_3_2a	0.53	0.79	0.70	-0.64	0.29	0.23
ncar_pcm1	0.70	0.10	0.11	-0.19	0.61	0.21
Ensemble mean	0.73	0.55	0.52	-0.18	0.56	0.54

Table E6: As Table E1 but for rabi season

Model	IGP	Indus	Ganges	Himalaya	IGP + Himalaya	Domain
bccr_bcm2_0	0.72	0.61	0.56	-0.50	0.50	0.65
cccma_cgcm3_1	0.80	0.77	0.76	-0.48	0.50	0.81
cnrm_cm3	0.51	0.57	0.10	0.02	0.48	0.67
csiro_mk3_0	0.81	0.51	0.75	-0.38	0.65	0.74
csiro_mk3_5	0.82	0.24	0.85	0.14	0.69	0.72
gfdl_cm2_0	0.79	0.89	0.58	0.31	0.56	0.68
giss_model_e_r	0.71	0.91	0.74	0.33	0.64	0.49
ipsl_cm4	0.63	0.75	0.11	0.16	0.51	0.67
miroc3_2_medres	0.79	0.83	0.53	-0.73	0.60	0.76
miub_echo_g	0.77	0.88	0.58	0.42	0.73	0.75
mpi_echam5	0.71	0.77	0.46	0.18	0.47	0.62
mri_cgcm2_3_2a	0.55	0.88	0.55	0.29	0.52	0.61
ncar_pcm1	0.76	0.40	0.63	-0.72	0.52	0.36
Ensemble mean	0.72	0.69	0.55	-0.07	0.57	0.66

Table E7: Spatial correlation of mean temperature between respective GCMs and CRU dataset for the annual cycle

Model	IGP	Indus	Ganges	Himalaya	IGP + Himalaya	Domain
bccr_bcm2_0	0.74	0.72	0.87	0.86	0.94	0.96
cccma_cgcm3_1	0.69	0.65	0.81	0.66	0.86	0.88
cnrm_cm3	0.75	0.73	0.85	0.86	0.95	0.96
csiro_mk3_0	0.70	0.74	0.82	0.87	0.92	0.93
csiro_mk3_5	0.71	0.71	0.85	0.90	0.94	0.96
gfdl_cm2_0	0.76	0.72	0.88	0.85	0.94	0.95
giss_model_e_r	0.63	0.66	0.70	0.65	0.86	0.90
ipsl_cm4	0.70	0.59	0.85	0.65	0.88	0.91
miroc3_2_medres	0.60	0.55	0.83	0.81	0.86	0.87
miub_echo_g	0.65	0.57	0.77	0.62	0.83	0.86
mpi_echam5	0.68	0.70	0.84	0.88	0.95	0.97
mri_cgcm2_3_2a	0.65	0.58	0.82	0.76	0.82	0.82
ncar_pcm1	0.71	0.64	0.83	0.68	0.87	0.89
Ensemble mean	0.69	0.66	0.82	0.77	0.89	0.91

Table E8: As Table E7 but for winter season

Model	IGP	Indus	Ganges	Himalaya	IGP + Himalaya	Domain
bccr_bcm2_0	0.80	0.81	0.86	0.86	0.94	0.97
cccma_cgcm3_1	0.80	0.75	0.89	0.46	0.84	0.91
cnrm_cm3	0.75	0.83	0.83	0.86	0.95	0.97
csiro_mk3_0	0.74	0.82	0.83	0.85	0.92	0.94
csiro_mk3_5	0.79	0.82	0.83	0.87	0.94	0.97
gfdl_cm2_0	0.82	0.79	0.91	0.82	0.93	0.96
giss_model_e_r	0.78	0.72	0.72	0.59	0.85	0.91
ipsl_cm4	0.79	0.70	0.91	0.67	0.88	0.93
miroc3_2_medres	0.63	0.66	0.87	0.70	0.87	0.91
miub_echo_g	0.73	0.67	0.89	0.58	0.83	0.89
mpi_echam5	0.78	0.85	0.78	0.83	0.95	0.98
mri_cgcm2_3_2a	0.70	0.68	0.89	0.67	0.83	0.87
ncar_pcm1	0.85	0.73	0.91	0.57	0.85	0.90
Ensemble mean	0.77	0.76	0.86	0.72	0.89	0.93

Table E9: As Table E7 but for pre-monsoon season

Model	IGP	Indus	Ganges	Himalaya	IGP + Himalaya	Domain
bccr_bcm2_0	0.83	0.67	0.89	0.84	0.95	0.95
cccma_cgcm3_1	0.74	0.62	0.77	0.70	0.89	0.89
cnrm_cm3	0.76	0.69	0.74	0.85	0.95	0.95
csiro_mk3_0	0.71	0.70	0.75	0.88	0.93	0.93
csiro_mk3_5	0.76	0.67	0.86	0.90	0.95	0.96
gfdl_cm2_0	0.74	0.72	0.81	0.84	0.95	0.96
giss_model_e_r	0.39	0.64	0.59	0.53	0.82	0.87
ipsl_cm4	0.64	0.53	0.74	0.67	0.90	0.92
miroc3_2_medres	0.72	0.54	0.77	0.82	0.89	0.89
miub_echo_g	0.55	0.52	0.58	0.62	0.85	0.85
mpi_echam5	0.83	0.65	0.90	0.89	0.96	0.97
mri_cgcm2_3_2a	0.68	0.52	0.76	0.74	0.85	0.83
ncar_pcm1	0.69	0.60	0.75	0.73	0.90	0.90
Ensemble mean	0.70	0.62	0.76	0.77	0.91	0.91

Table E10: As Table E7 but for monsoon season

Model	IGP	Indus	Ganges	Himalaya	IGP + Himalaya	Domain
bccr_bcm2_0	0.84	0.58	0.83	0.87	0.94	0.94
cccma_cgcm3_1	0.80	0.51	0.68	0.83	0.86	0.81
cnrm_cm3	0.70	0.43	0.58	0.86	0.95	0.94
csiro_mk3_0	0.79	0.61	0.72	0.82	0.91	0.89
csiro_mk3_5	0.82	0.58	0.83	0.87	0.92	0.93
gfdl_cm2_0	0.82	0.59	0.73	0.89	0.94	0.93
giss_model_e_r	0.54	0.57	0.73	0.69	0.84	0.86
ipsl_cm4	0.59	0.37	0.70	0.57	0.88	0.85
miroc3_2_medres	0.78	0.45	0.61	0.80	0.84	0.77
miub_echo_g	0.61	0.37	0.59	0.69	0.85	0.79
mpi_echam5	0.83	0.52	0.84	0.89	0.94	0.94
mri_cgcm2_3_2a	0.70	0.32	0.64	0.72	0.81	0.71
ncar_pcm1	0.71	0.54	0.64	0.86	0.90	0.84
Ensemble mean	0.73	0.50	0.70	0.80	0.89	0.86

Table E11: As Table E7 but for post-monsoon season

Model	IGP	Indus	Ganges	Himalaya	IGP + Himalaya	Domain
bccr_bcm2_0	0.67	0.78	0.70	0.85	0.93	0.96
cccma_cgcm3_1	0.64	0.71	0.74	0.55	0.83	0.87
cnrm_cm3	0.71	0.82	0.75	0.85	0.94	0.96
csiro_mk3_0	0.64	0.82	0.69	0.84	0.90	0.92
csiro_mk3_5	0.65	0.83	0.68	0.88	0.92	0.95
gfdl_cm2_0	0.63	0.76	0.76	0.86	0.92	0.94
giss_model_e_r	0.66	0.71	0.54	0.65	0.85	0.90
ipsl_cm4	0.69	0.67	0.77	0.67	0.86	0.90
miroc3_2_medres	0.53	0.64	0.72	0.73	0.84	0.88
miub_echo_g	0.62	0.63	0.78	0.58	0.80	0.86
mpi_echam5	0.62	0.84	0.68	0.85	0.94	0.97
mri_cgcm2_3_2a	0.60	0.64	0.76	0.69	0.80	0.82
ncar_pcm1	0.77	0.72	0.80	0.60	0.84	0.88
Ensemble mean	0.65	0.74	0.72	0.74	0.87	0.91

Table E12: As Table E7 but for rabi season

Model	IGP	Indus	Ganges	Himalaya	IGP + Himalaya	Domain
bccr_bcm2_0	0.75	0.81	0.79	0.86	0.94	0.96
cccma_cgcm3_1	0.74	0.73	0.85	0.49	0.84	0.90
cnrm_cm3	0.74	0.83	0.79	0.85	0.94	0.97
csiro_mk3_0	0.69	0.83	0.76	0.85	0.91	0.94
csiro_mk3_5	0.72	0.83	0.75	0.88	0.93	0.96
gfdl_cm2_0	0.73	0.78	0.84	0.85	0.93	0.96
giss_model_e_r	0.72	0.71	0.61	0.63	0.86	0.91
ipsl_cm4	0.75	0.69	0.86	0.67	0.87	0.92
miroc3_2_medres	0.58	0.64	0.80	0.71	0.86	0.90
miub_echo_g	0.69	0.66	0.86	0.58	0.82	0.88
mpi_echam5	0.71	0.85	0.72	0.84	0.95	0.97
mri_cgcm2_3_2a	0.65	0.66	0.85	0.69	0.82	0.86
ncar_pcm1	0.82	0.73	0.87	0.58	0.85	0.90
Ensemble mean	0.71	0.75	0.80	0.73	0.89	0.93

Appendix 6

Figure F1: As Figure 4.1 but for Indus region

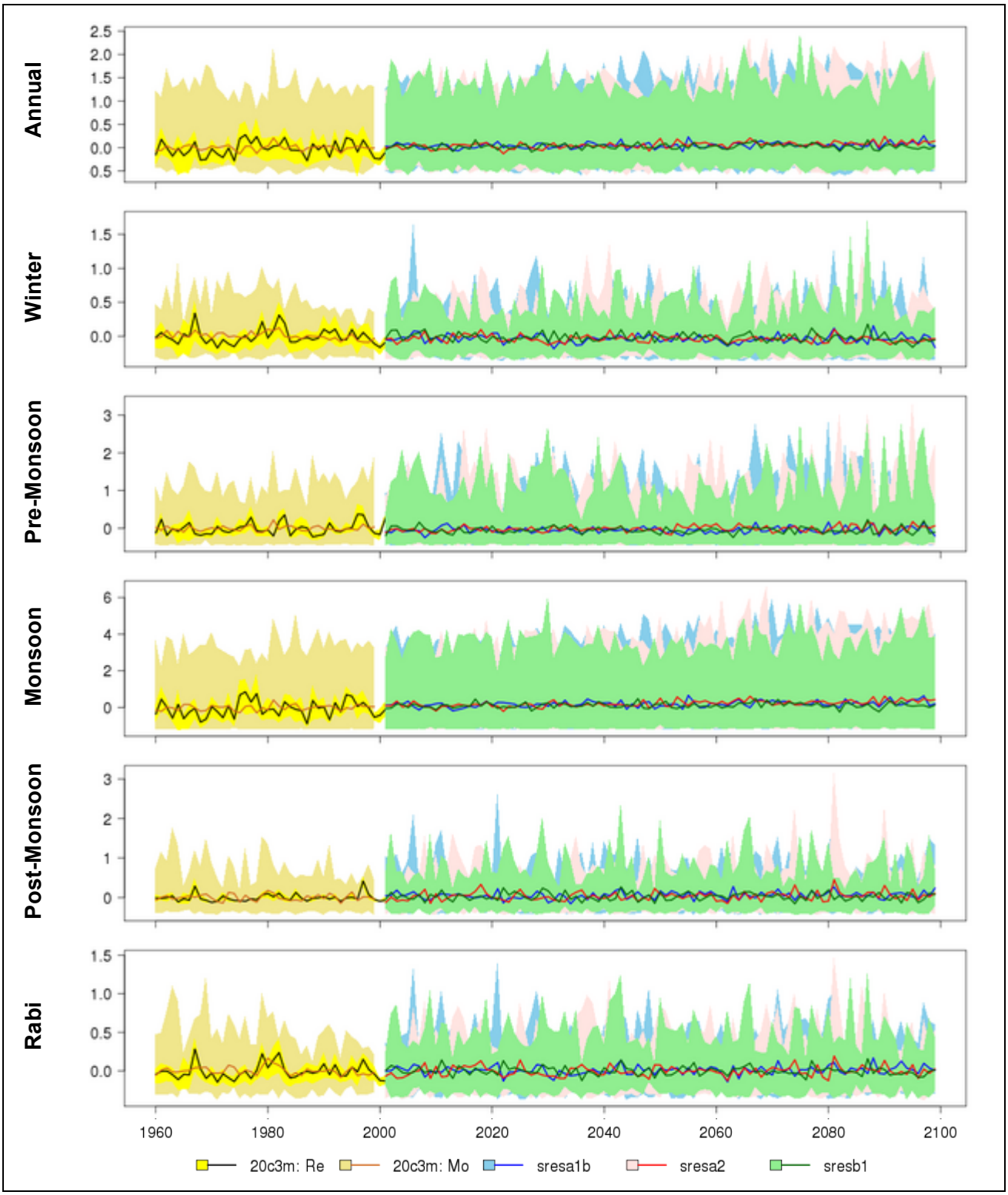

Figure F2: As Figure 4.1 but for Ganges region

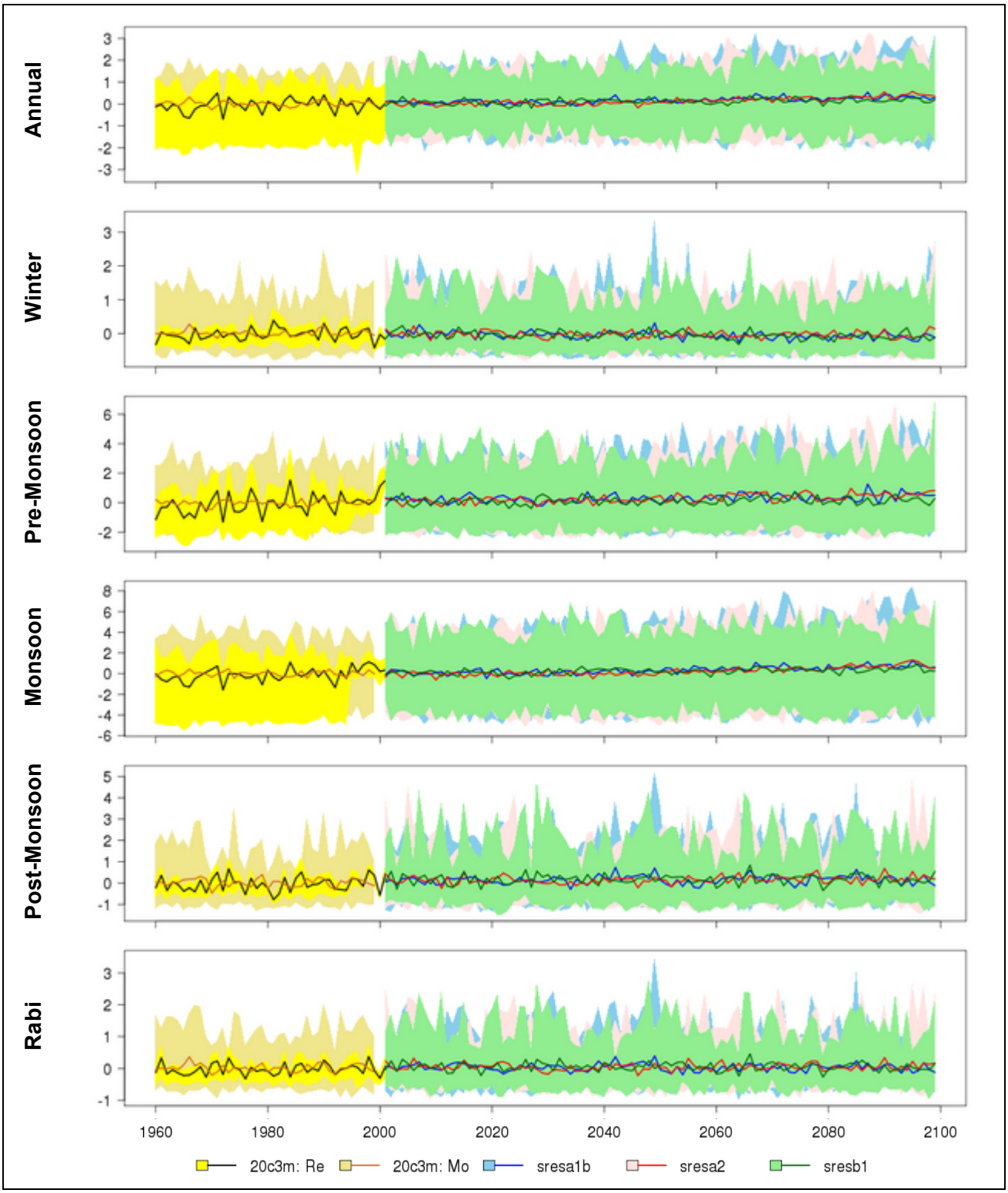

Figure F3: As Figure 4.1 but for Himalaya region

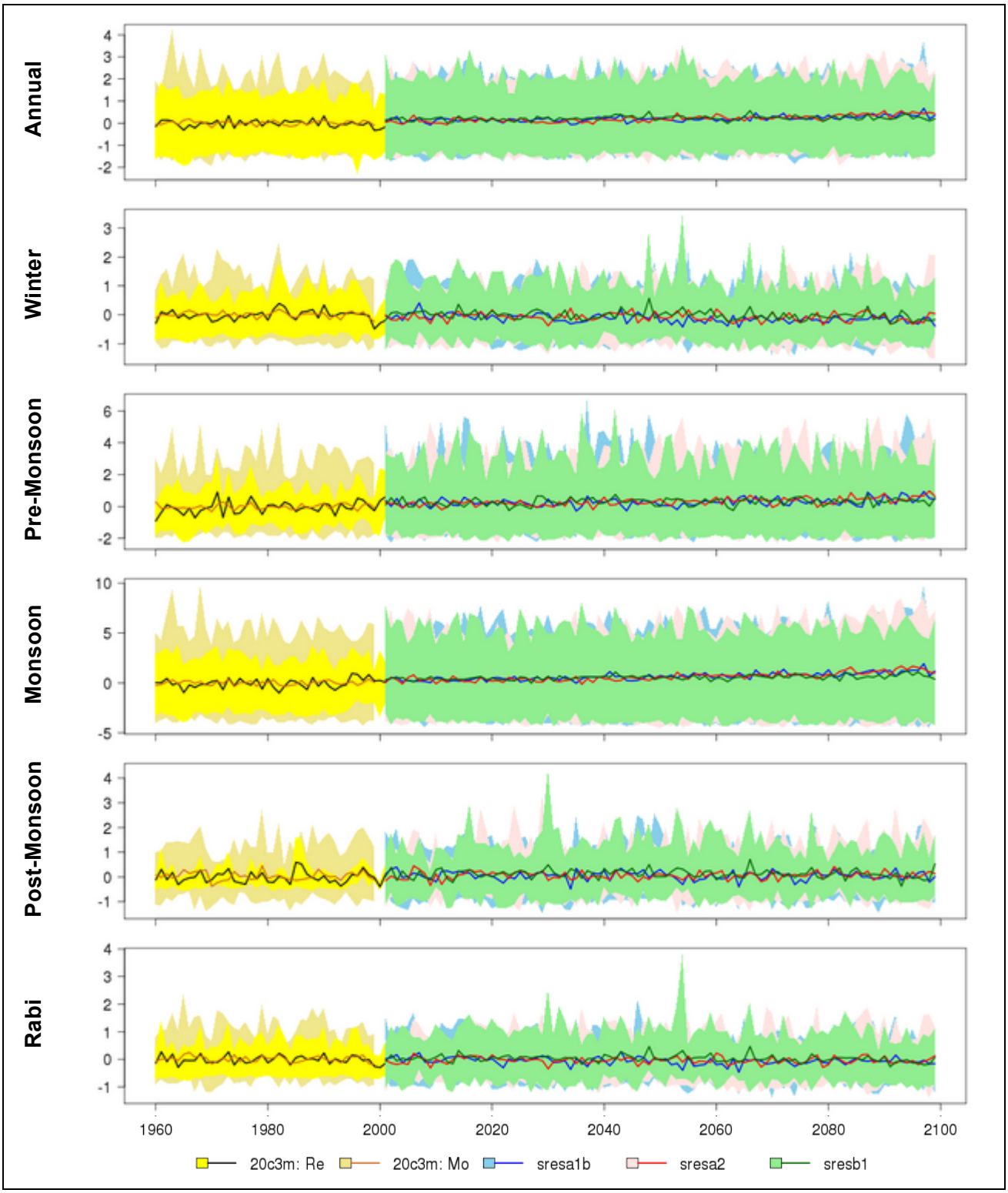

Figure F4: As Figure 4.2 but for Indus region

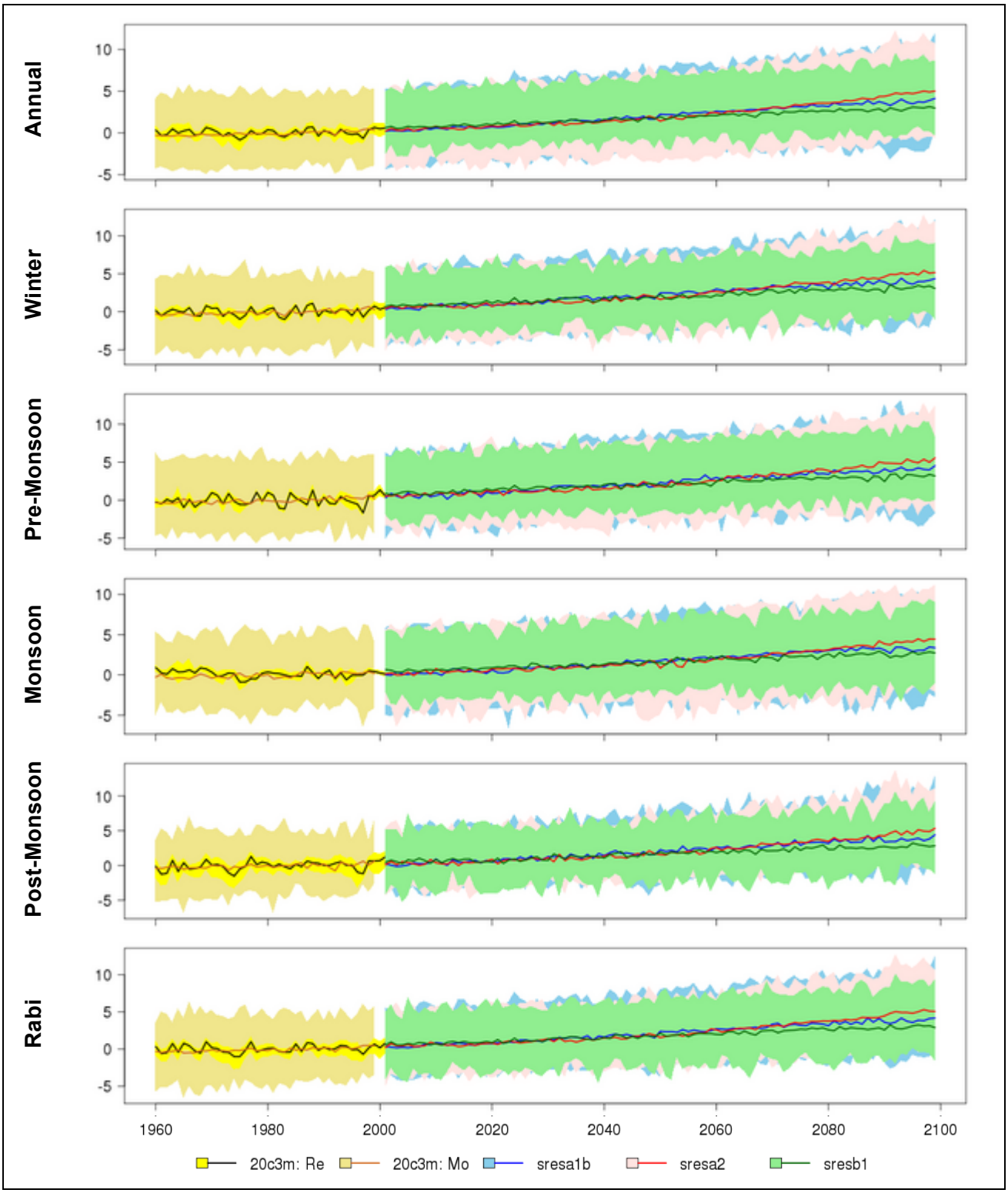

Figure F5: As Figure 4.2 but for Ganges region

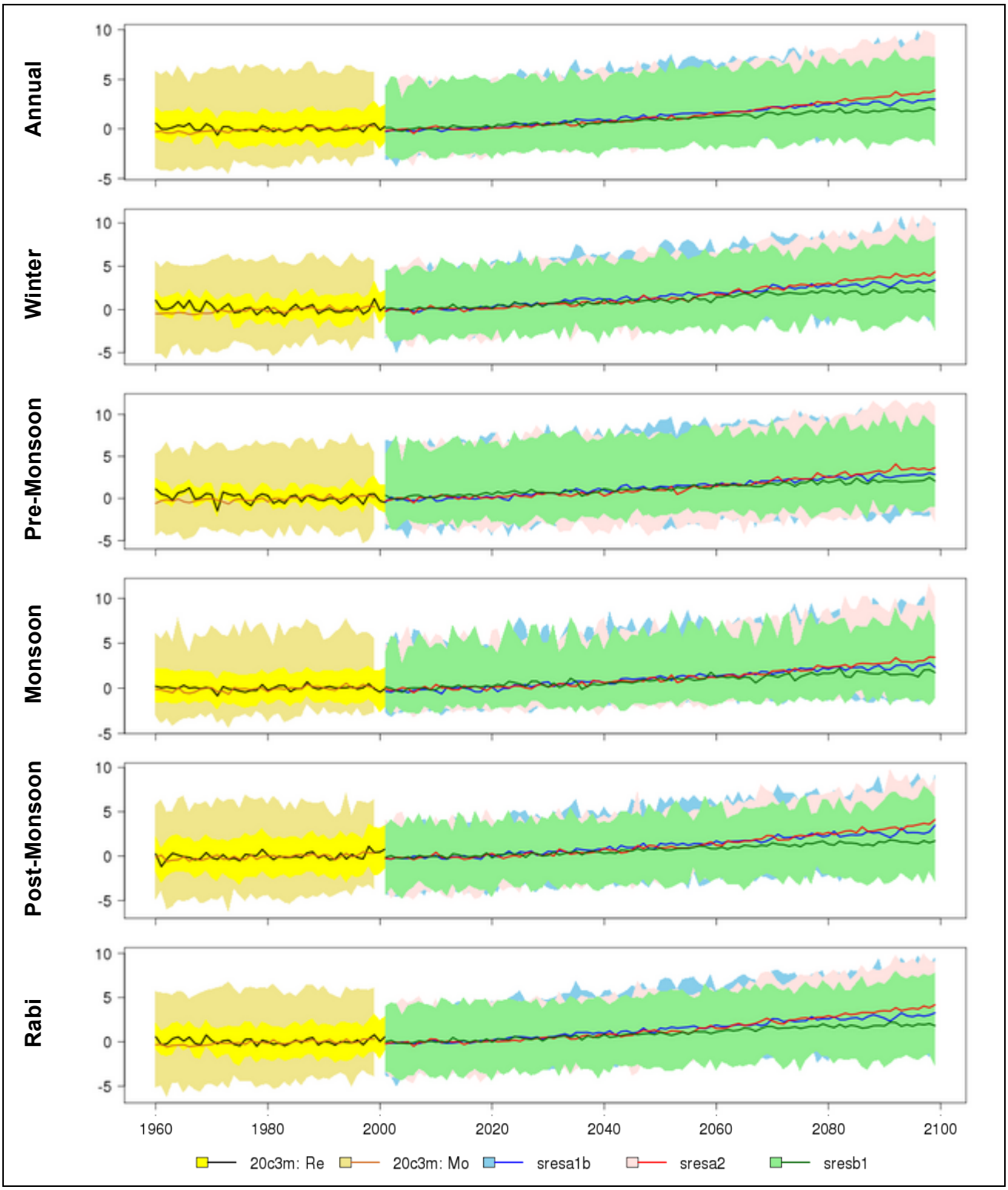

Figure F6: As Figure 4.2 but for Himalaya region

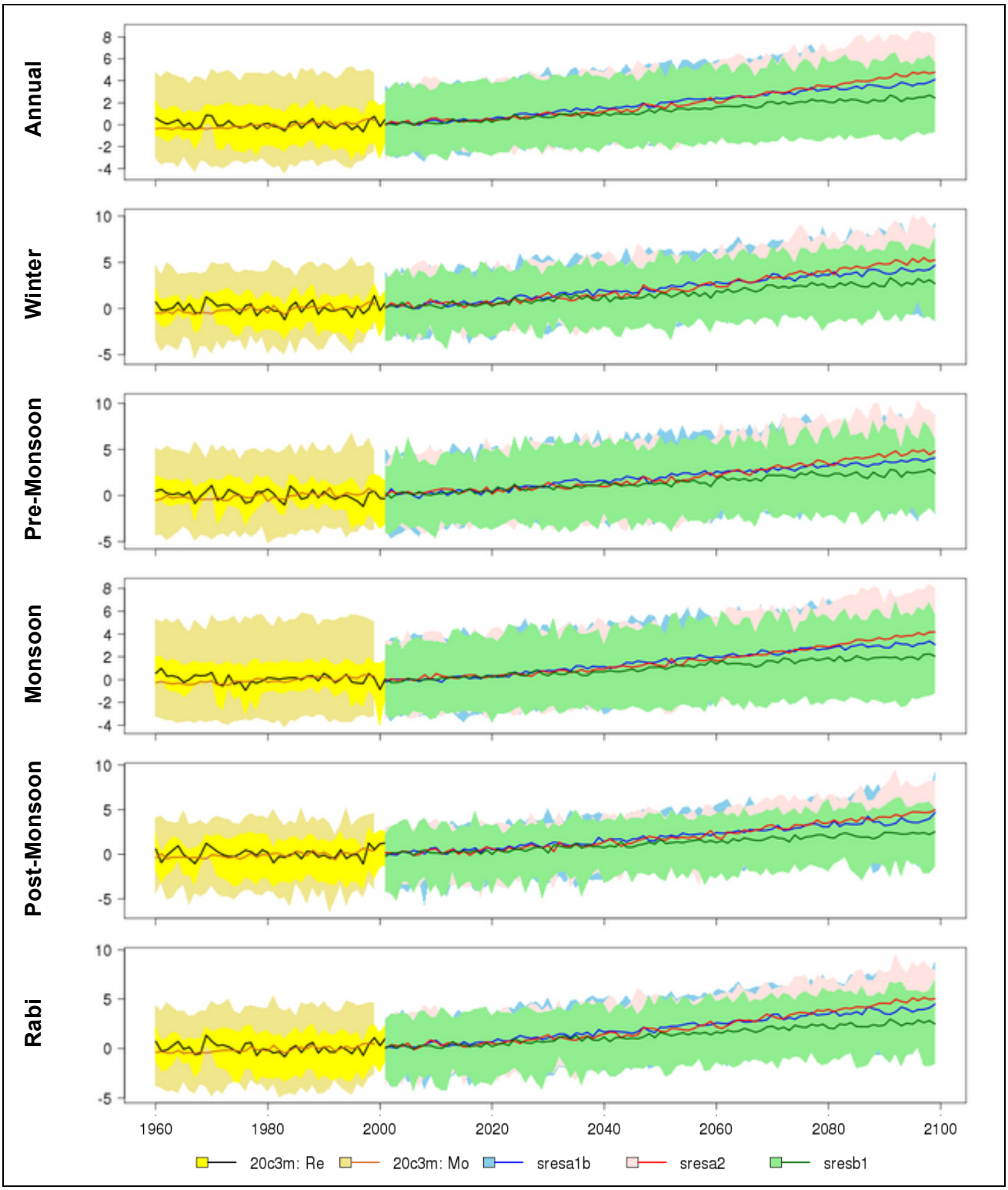

Appendix 7

Tables begin on next page.

Table G1: Ensemble minimum, mean and maximum annual precipitation changes (mm/day) for the Indo-Gangetic Plain, and the Indus, Ganges and Himalaya sub-regions under the three emission scenarios for 2030s, 2050s and 2090s. All values are anomalies, relative to the 1970–1999 mean climate.

		IGP	Indus	Ganges	Himalaya
2030s	SRESA1B				
	Min	-0.12	-0.23	-0.33	-0.22
	Mean	0.04	0.01	0.05	0.03
	Max	0.20	0.18	0.41	0.37
	SRESA2				
	Min	-0.19	-0.21	-0.36	-0.34
	Mean	0.02	0.02	0.02	0.02
	Max	0.17	0.15	0.20	0.34
	SRESB1				
	Min	-0.13	-0.24	-0.20	-0.08
	Mean	0.08	0.03	0.12	0.08
	Max	0.31	0.26	0.37	0.42
2050s	SRESA1B				
	Min	-0.13	-0.36	-0.23	-0.32
	Mean	0.12	0.04	0.19	0.14
	Max	0.46	0.32	0.58	0.61
	SRESA2				
	Min	-0.28	-0.29	-0.50	-0.45
	Mean	0.07	0.05	0.08	0.12
	Max	0.21	0.34	0.39	0.52
	SRESB1				
	Min	-0.24	-0.14	-0.37	-0.39
	Mean	0.11	0.03	0.17	0.16
	Max	0.26	0.13	0.53	0.49
2090s	SRESA1B				
	Min	-0.19	-0.31	-0.41	-0.42
	Mean	0.24	0.07	0.38	0.35
	Max	0.57	0.47	1.11	1.31
	SRESA2				
	Min	-0.11	-0.48	-0.33	-0.31
	Mean	0.26	0.10	0.38	0.35
	Max	0.61	0.41	1.02	1.60
	SRESB1				
	Min	-0.17	-0.28	-0.32	-0.40
	Mean	0.11	0.02	0.19	0.13
	Max	0.33	0.20	0.49	0.61

Table G2: As Table G1 but for winter season

		IGP	Indus	Ganges	Himalaya
2030s	SRESA1B				
	Min	-0.14	-0.18	-0.35	-0.32
	Mean	-0.06	-0.04	-0.08	-0.16
	Max	0.13	0.23	0.08	0.04
	SRESA2				
	Min	-0.16	-0.17	-0.36	-0.36
	Mean	-0.06	-0.04	-0.08	-0.13
	Max	0.06	0.08	0.18	0.10
	SRESB1				
	Min	-0.11	-0.22	-0.09	-0.38
	Mean	0.00	-0.01	0.01	-0.08
	Max	0.12	0.23	0.17	0.16
2050s	SRESA1B				
	Min	-0.21	-0.15	-0.38	-0.50
	Mean	-0.03	-0.02	-0.03	-0.15
	Max	0.20	0.21	0.18	0.11
	SRESA2				
	Min	-0.28	-0.10	-0.55	-0.40
	Mean	-0.03	-0.02	-0.05	-0.07
	Max	0.12	0.15	0.22	0.16
	SRESB1				
	Min	-0.34	-0.14	-0.52	-0.54
	Mean	0.00	-0.02	0.02	0.00
	Max	0.17	0.12	0.34	0.27
2090s	SRESA1B				
	Min	-0.16	-0.19	-0.43	-0.35
	Mean	-0.04	-0.02	-0.06	-0.15
	Max	0.10	0.27	0.09	0.04
	SRESA2				
	Min	-0.15	-0.36	-0.46	-0.33
	Mean	-0.06	-0.05	-0.07	-0.14
	Max	0.04	0.24	0.14	0.08
	SRESB1				
	Min	-0.28	-0.24	-0.62	-0.55
	Mean	-0.05	-0.04	-0.05	-0.14
	Max	0.09	0.11	0.15	0.17

Table G3: As Table G1 but for pre-monsoon season

		IGP	Indus	Ganges	Himalaya
2030s	SRESA1B				
	Min	-0.20	-0.14	-0.29	-0.40
	Mean	0.06	-0.01	0.11	0.05
	Max	0.50	0.22	0.90	0.61
	SRESA2				
	Min	-0.22	-0.11	-0.51	-0.25
	Mean	0.05	0.02	0.07	0.06
	Max	0.63	0.17	1.12	0.75
	SRESB1				
	Min	-0.15	-0.10	-0.32	-0.21
	Mean	0.10	0.04	0.15	0.12
	Max	0.44	0.38	0.71	0.63
2050s	SRESA1B				
	Min	-0.15	-0.16	-0.31	-0.46
	Mean	0.15	-0.01	0.28	0.14
	Max	0.61	0.17	1.26	0.72
	SRESA2				
	Min	-0.31	-0.21	-0.41	-0.48
	Mean	0.12	0.02	0.20	0.19
	Max	0.60	0.53	1.08	0.86
	SRESB1				
	Min	-0.18	-0.30	-0.25	-0.36
	Mean	0.08	-0.03	0.18	0.15
	Max	0.34	0.19	0.76	0.53
2090s	SRESA1B				
	Min	-0.15	-0.15	-0.23	-0.61
	Mean	0.30	0.03	0.54	0.42
	Max	0.94	0.51	1.88	1.13
	SRESA2				
	Min	-0.20	-0.12	-0.45	-0.69
	Mean	0.29	0.06	0.48	0.38
	Max	1.06	0.62	1.44	1.84
	SRESB1				
	Min	-0.17	-0.13	-0.28	-0.56
	Mean	0.11	0.00	0.20	0.18
	Max	0.62	0.31	0.88	1.12

Table G4: As Table G1 but for monsoon season

		IGP	Indus	Ganges	Himalaya
2030s	SRESA1B				
	Min	-0.18	-0.58	-0.26	-0.57
	Mean	0.14	0.07	0.19	0.24
	Max	0.56	0.34	0.99	1.30
	SRESA2				
	Min	-0.21	-0.44	-0.43	-0.38
	Mean	0.12	0.09	0.15	0.22
	Max	0.42	0.38	0.45	0.79
	SRESB1				
	Min	-0.44	-0.54	-0.65	-0.37
	Mean	0.15	0.10	0.18	0.27
	Max	0.61	0.59	0.89	1.07
2050s	SRESA1B				
	Min	-0.18	-0.89	-0.30	-0.23
	Mean	0.25	0.13	0.35	0.53
	Max	0.56	0.56	0.91	2.42
	SRESA2				
	Min	-0.30	-0.64	-0.63	-0.40
	Mean	0.18	0.16	0.18	0.43
	Max	0.52	1.00	0.96	1.85
	SRESB1				
	Min	-0.12	-0.23	-0.35	-0.17
	Mean	0.20	0.10	0.28	0.44
	Max	0.52	0.46	0.83	1.50
2090s	SRESA1B				
	Min	-0.15	-0.79	-0.38	-0.28
	Mean	0.59	0.23	0.89	1.06
	Max	1.41	1.34	2.72	3.86
	SRESA2				
	Min	-0.09	-1.16	-0.17	-0.28
	Mean	0.67	0.30	0.96	1.13
	Max	1.60	1.33	2.21	5.30
	SRESB1				
	Min	-0.08	-0.77	-0.20	-0.04
	Mean	0.31	0.09	0.49	0.53
	Max	0.91	0.85	0.94	2.07

Table G5: As Table G1 but for post-monsoon season

		IGP	Indus	Ganges	Himalaya
2030s	SRESA1B				
	Min	-0.18	-0.17	-0.47	-0.21
	Mean	0.02	-0.01	0.05	0.00
	Max	0.39	0.20	0.68	0.34
	SRESA2				
	Min	-0.29	-0.19	-0.49	-0.32
	Mean	-0.02	0.00	-0.04	0.01
	Max	0.25	0.17	0.45	0.22
	SRESB1				
	Min	-0.10	-0.10	-0.08	-0.43
	Mean	0.13	0.04	0.22	0.12
	Max	0.67	0.30	1.08	0.66
2050s	SRESA1B				
	Min	-0.19	-0.17	-0.21	-0.37
	Mean	0.13	0.05	0.19	0.06
	Max	0.82	0.35	1.27	0.66
	SRESA2				
	Min	-0.25	-0.18	-0.31	-0.31
	Mean	0.03	0.02	0.04	-0.04
	Max	0.31	0.21	0.46	0.43
	SRESB1				
	Min	-0.39	-0.27	-0.48	-0.48
	Mean	0.11	0.02	0.19	0.12
	Max	0.64	0.19	1.12	0.45
2090s	SRESA1B				
	Min	-0.43	-0.34	-0.52	-0.64
	Mean	0.13	0.03	0.22	0.04
	Max	0.39	0.20	0.69	0.41
	SRESA2				
	Min	-0.06	-0.13	-0.20	-0.27
	Mean	0.12	0.07	0.17	0.04
	Max	0.32	0.20	0.47	0.49
	SRESB1				
	Min	-0.38	-0.28	-0.46	-0.49
	Mean	0.07	0.02	0.14	0.00
	Max	0.42	0.20	0.72	0.32

Table G6: As Table G1 but for rabi season

		IGP	Indus	Ganges	Himalaya
2030s	SRESA1B				
	Min	-0.14	-0.10	-0.44	-0.31
	Mean	-0.03	-0.01	-0.03	-0.09
	Max	0.20	0.20	0.29	0.12
	SRESA2				
	Min	-0.19	-0.11	-0.34	-0.47
	Mean	-0.05	-0.02	-0.07	-0.10
	Max	0.12	0.09	0.23	0.05
	SRESB1				
	Min	-0.11	-0.13	-0.10	-0.31
	Mean	0.04	0.00	0.08	0.00
	Max	0.25	0.26	0.42	0.28
2050s	SRESA1B				
	Min	-0.14	-0.14	-0.25	-0.36
	Mean	0.03	0.00	0.05	-0.07
	Max	0.41	0.20	0.62	0.30
	SRESA2				
	Min	-0.30	-0.13	-0.51	-0.44
	Mean	-0.01	-0.01	-0.02	-0.07
	Max	0.14	0.13	0.28	0.29
	SRESB1				
	Min	-0.36	-0.17	-0.52	-0.55
	Mean	0.03	-0.01	0.07	0.02
	Max	0.30	0.12	0.57	0.44
2090s	SRESA1B				
	Min	-0.23	-0.09	-0.48	-0.41
	Mean	0.04	0.02	0.06	-0.04
	Max	0.15	0.22	0.27	0.17
	SRESA2				
	Min	-0.11	-0.22	-0.44	-0.29
	Mean	0.02	0.01	0.03	-0.05
	Max	0.17	0.24	0.31	0.25
	SRESB1				
	Min	-0.30	-0.24	-0.57	-0.52
	Mean	0.00	-0.01	0.03	-0.10
	Max	0.19	0.07	0.36	0.16

Table G7: Ensemble minimum, mean and maximum mean annual temperature (°C) changes for the Indo-Gangetic Plain, and the Indus, Ganges and Himalaya sub-regions under the three emission scenarios for 2030s, 2050s and 2090s. All values are anomalies, relative to the 1970-1999 mean climate.

		IGP	Indus	Ganges	Himalaya
2030s	SRESA1B				
	Min	0.82	0.87	0.67	0.90
	Mean	1.27	1.45	1.10	1.51
	Max	1.75	2.04	1.47	2.07
	SRESA2				
	Min	0.65	0.84	0.31	0.82
	Mean	1.10	1.26	0.95	1.29
	Max	1.66	1.91	1.53	1.87
	SRESB1				
	Min	0.72	0.65	0.50	0.63
	Mean	1.13	1.25	1.01	1.33
	Max	2.17	2.09	2.21	2.56
2050s	SRESA1B				
	Min	0.75	0.97	0.59	1.44
	Mean	2.08	2.30	1.86	2.39
	Max	3.11	3.39	2.81	3.21
	SRESA2				
	Min	0.87	0.93	0.55	1.19
	Mean	1.77	1.95	1.59	2.07
	Max	2.88	3.06	2.68	2.99
	SRESB1				
	Min	0.44	0.54	0.38	0.96
	Mean	1.49	1.65	1.32	1.70
	Max	2.11	2.32	2.03	2.45
2090s	SRESA1B				
	Min	2.07	2.45	1.74	2.65
	Mean	3.61	3.98	3.23	4.06
	Max	4.84	5.32	4.51	5.22
	SRESA2				
	Min	2.74	2.97	2.26	3.26
	Mean	4.13	4.52	3.74	4.62
	Max	5.42	6.01	5.02	5.96
	SRESB1				
	Min	1.05	1.33	0.84	1.59
	Mean	2.42	2.65	2.19	2.72
	Max	3.30	3.65	3.07	3.70

Table G8: As Table G7 but for winter season

		IGP	Indus	Ganges	Himalaya
2030s	SRESA1B				
	Min	0.93	0.94	0.74	0.94
	Mean	1.44	1.63	1.25	1.76
	Max	2.12	2.46	1.79	2.55
	SRESA2				
	Min	0.62	0.92	0.33	0.73
	Mean	1.28	1.44	1.11	1.51
	Max	2.10	2.20	2.07	2.27
	SRESB1				
	Min	0.68	0.64	0.65	0.81
	Mean	1.31	1.45	1.17	1.56
	Max	2.95	2.90	2.94	3.15
2050s	SRESA1B				
	Min	0.77	1.04	0.57	1.36
	Mean	2.20	2.41	1.98	2.56
	Max	3.17	3.10	3.20	3.39
	SRESA2				
	Min	0.76	1.10	0.50	1.23
	Mean	1.90	2.09	1.70	2.31
	Max	3.02	2.82	3.14	3.74
	SRESB1				
	Min	0.32	0.58	0.13	0.96
	Mean	1.52	1.67	1.35	1.80
	Max	2.29	2.72	2.11	2.96
2090s	SRESA1B				
	Min	2.03	2.34	1.77	2.74
	Mean	3.81	4.11	3.48	4.46
	Max	5.16	5.55	4.73	5.93
	SRESA2				
	Min	2.88	3.17	2.59	3.48
	Mean	4.49	4.78	4.16	5.17
	Max	5.68	6.18	5.47	6.44
	SRESB1				
	Min	0.97	1.14	0.87	1.61
	Mean	2.61	2.79	2.42	3.04
	Max	3.60	3.82	3.34	4.34

Table G9: As Table G7 but for pre-monsoon season

		IGP	Indus	Ganges	Himalaya
2030s	SRESA1B				
	Min	1.02	1.16	0.47	0.96
	Mean	1.39	1.60	1.17	1.66
	Max	2.12	2.55	1.69	2.73
	SRESA2				
	Min	0.72	0.71	0.20	0.78
	Mean	1.11	1.27	0.95	1.31
	Max	1.57	1.75	1.51	1.96
	SRESB1				
	Min	0.57	0.49	0.45	0.46
	Mean	1.21	1.38	1.04	1.40
	Max	2.01	2.35	1.69	2.34
2050s	SRESA1B				
	Min	0.77	0.71	0.81	1.50
	Mean	2.17	2.35	1.96	2.54
	Max	2.73	3.36	2.77	3.79
	SRESA2				
	Min	0.61	0.86	0.35	0.94
	Mean	1.80	2.12	1.50	2.05
	Max	2.84	3.04	2.67	3.34
	SRESB1				
	Min	0.20	0.07	0.33	0.63
	Mean	1.56	1.74	1.37	1.75
	Max	2.19	2.81	1.85	3.16
2090s	SRESA1B				
	Min	2.32	2.70	1.73	2.43
	Mean	3.70	4.09	3.29	4.13
	Max	5.12	5.49	4.68	6.07
	SRESA2				
	Min	2.59	3.00	1.84	2.82
	Mean	4.17	4.65	3.69	4.69
	Max	5.14	6.35	4.97	6.06
	SRESB1				
	Min	1.09	1.35	0.86	1.41
	Mean	2.49	2.72	2.25	2.78
	Max	3.42	3.63	3.18	4.83

Table G10: As Table G7 but for monsoon season

		IGP	Indus	Ganges	Himalaya
2030s	SRESA1B				
	Min	0.50	0.50	0.34	0.69
	Mean	1.09	1.21	0.99	1.24
	Max	1.71	2.24	1.63	1.80
	SRESA2				
	Min	0.25	0.20	0.30	0.46
	Mean	0.97	1.07	0.88	1.08
	Max	1.60	1.87	1.56	1.53
	SRESB1				
	Min	0.59	0.55	0.24	0.57
	Mean	0.95	1.00	0.90	1.09
	Max	1.70	2.12	1.57	1.77
2050s	SRESA1B				
	Min	0.55	0.60	0.51	1.40
	Mean	1.95	2.13	1.76	2.17
	Max	3.25	3.96	2.81	3.23
	SRESA2				
	Min	0.26	-0.18	0.43	0.73
	Mean	1.60	1.66	1.53	1.77
	Max	2.81	3.30	2.55	2.66
	SRESB1				
	Min	0.62	0.52	0.38	0.92
	Mean	1.41	1.53	1.29	1.53
	Max	1.96	2.32	2.19	2.04
2090s	SRESA1B				
	Min	2.10	2.44	1.68	2.51
	Mean	3.33	3.71	2.97	3.59
	Max	4.61	5.08	4.56	4.57
	SRESA2				
	Min	1.80	1.62	1.85	2.34
	Mean	3.69	4.02	3.36	4.01
	Max	5.27	6.33	4.89	5.59
	SRESB1				
	Min	1.16	1.45	0.90	1.49
	Mean	2.24	2.47	2.01	2.41
	Max	3.21	3.92	2.99	3.13

Table G11: As Table G7 but for post-monsoon season

		IGP	Indus	Ganges	Himalaya
2030s	SRESA1B				
	Min	0.49	0.61	0.27	0.76
	Mean	1.18	1.42	0.96	1.43
	Max	1.82	2.20	1.64	2.12
	SRESA2				
	Min	0.42	0.70	0.09	0.73
	Mean	1.03	1.27	0.81	1.22
	Max	1.83	2.25	1.43	1.97
	SRESB1				
	Min	0.55	0.61	0.35	0.47
	Mean	1.04	1.18	0.91	1.30
	Max	2.49	2.37	2.55	2.64
2050s	SRESA1B				
	Min	1.00	1.41	0.69	1.53
	Mean	1.99	2.25	1.73	2.32
	Max	3.10	3.54	2.68	3.34
	SRESA2				
	Min	0.79	1.08	0.53	1.57
	Mean	1.72	1.97	1.49	2.08
	Max	2.84	2.84	2.77	3.29
	SRESB1				
	Min	0.49	0.73	0.33	1.00
	Mean	1.46	1.67	1.27	1.70
	Max	2.45	2.89	2.03	2.62
2090s	SRESA1B				
	Min	1.90	2.40	1.49	2.44
	Mean	3.57	4.04	3.12	4.05
	Max	4.62	5.44	4.41	5.40
	SRESA2				
	Min	2.60	3.28	2.06	3.26
	Mean	4.00	4.52	3.51	4.49
	Max	5.08	6.02	4.92	5.98
	SRESB1				
	Min	1.04	1.45	0.73	1.45
	Mean	2.31	2.62	2.01	2.61
	Max	3.37	3.40	3.28	3.66

Table G12: As Table G7 but for rabi season

		IGP	Indus	Ganges	Himalaya
2030s	SRESA1B				
	Min	0.82	0.87	0.67	0.90
	Mean	1.27	1.45	1.10	1.51
	Max	1.75	2.04	1.47	2.07
	SRESA2				
	Min	0.65	0.84	0.31	0.82
	Mean	1.10	1.26	0.95	1.29
	Max	1.66	1.91	1.53	1.87
	SRESB1				
	Min	0.72	0.65	0.50	0.63
	Mean	1.13	1.25	1.01	1.33
	Max	2.17	2.09	2.21	2.56
2050s	SRESA1B				
	Min	0.75	0.97	0.59	1.44
	Mean	2.08	2.30	1.86	2.39
	Max	3.11	3.39	2.81	3.21
	SRESA2				
	Min	0.87	0.93	0.55	1.19
	Mean	1.77	1.95	1.59	2.07
	Max	2.88	3.06	2.68	2.99
	SRESB1				
	Min	0.44	0.54	0.38	0.96
	Mean	1.49	1.65	1.32	1.70
	Max	2.11	2.32	2.03	2.45
2090s	SRESA1B				
	Min	2.07	2.45	1.74	2.65
	Mean	3.61	3.98	3.23	4.06
	Max	4.84	5.32	4.51	5.22
	SRESA2				
	Min	2.74	2.97	2.26	3.26
	Mean	4.13	4.52	3.74	4.62
	Max	5.42	6.01	5.02	5.96
	SRESB1				
	Min	1.05	1.33	0.84	1.59
	Mean	2.42	2.65	2.19	2.72
	Max	3.30	3.65	3.07	3.70

Appendix 8

Figure H1: As Figure 4.3 but for winter season

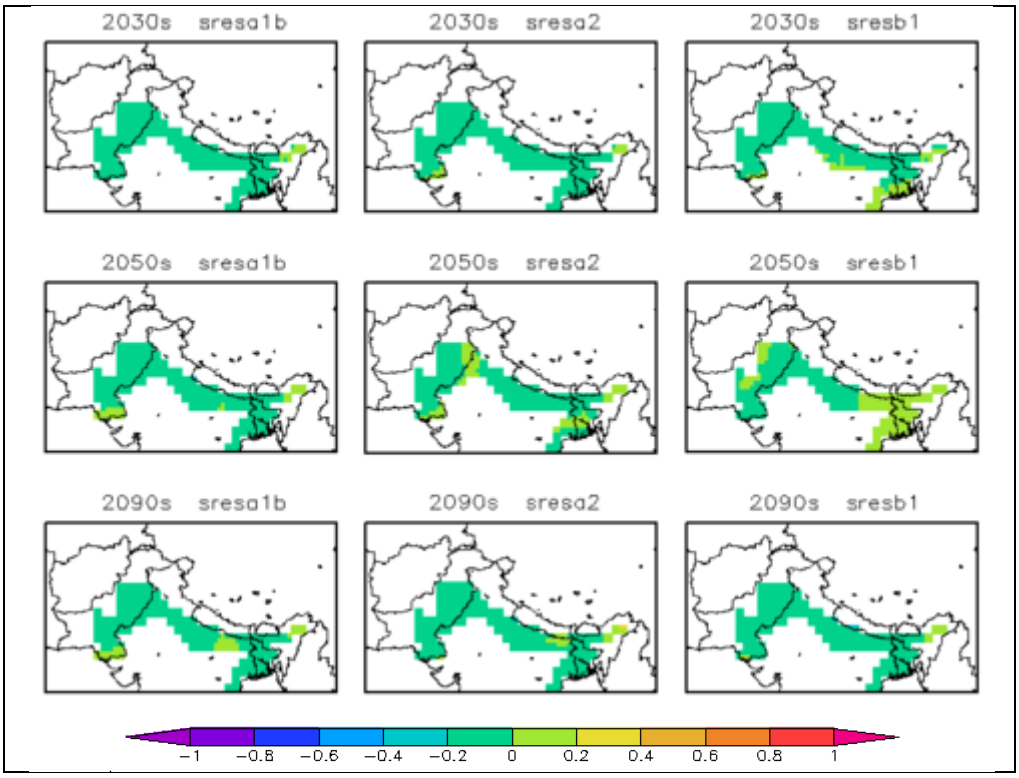

Figure H2: As Figure 4.3 but for pre-monsoon season

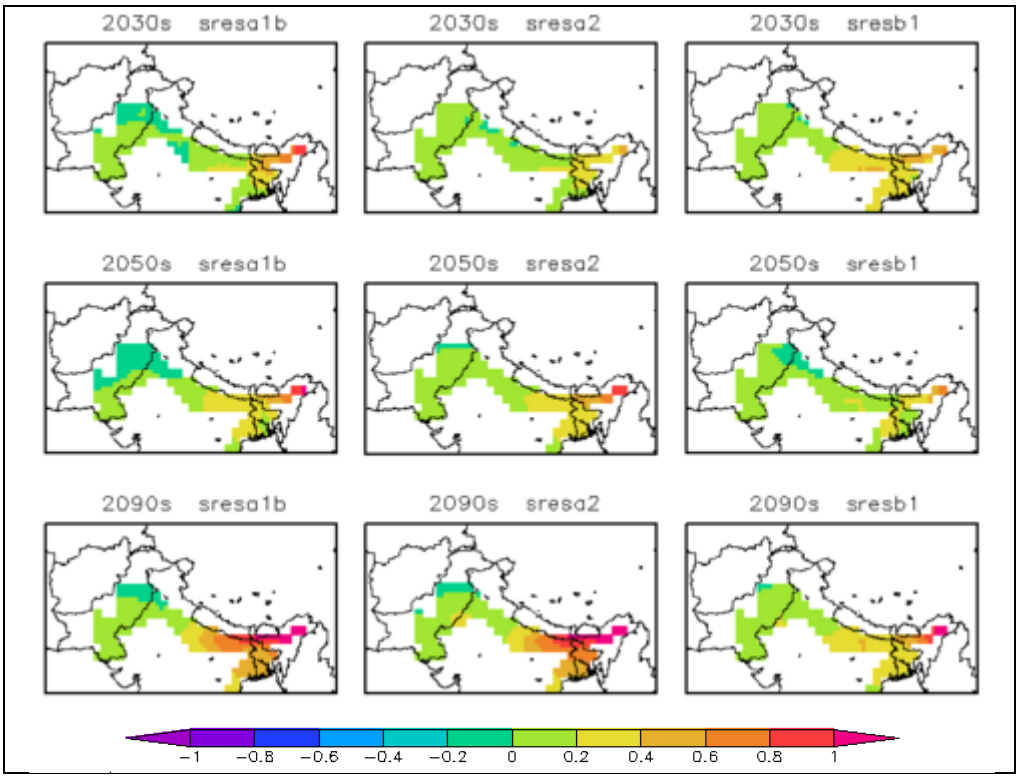

Figure H3: As Figure 4.3 but for monsoon season

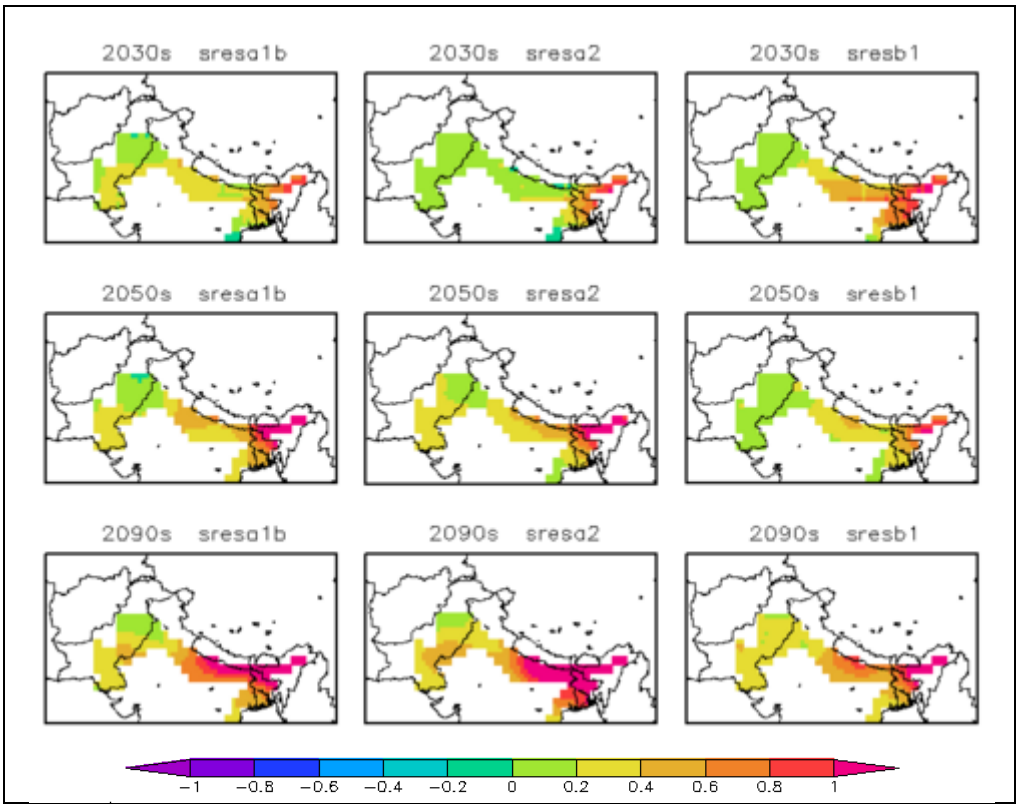

Figure H4: As Figure 4.3 but for post-monsoon season

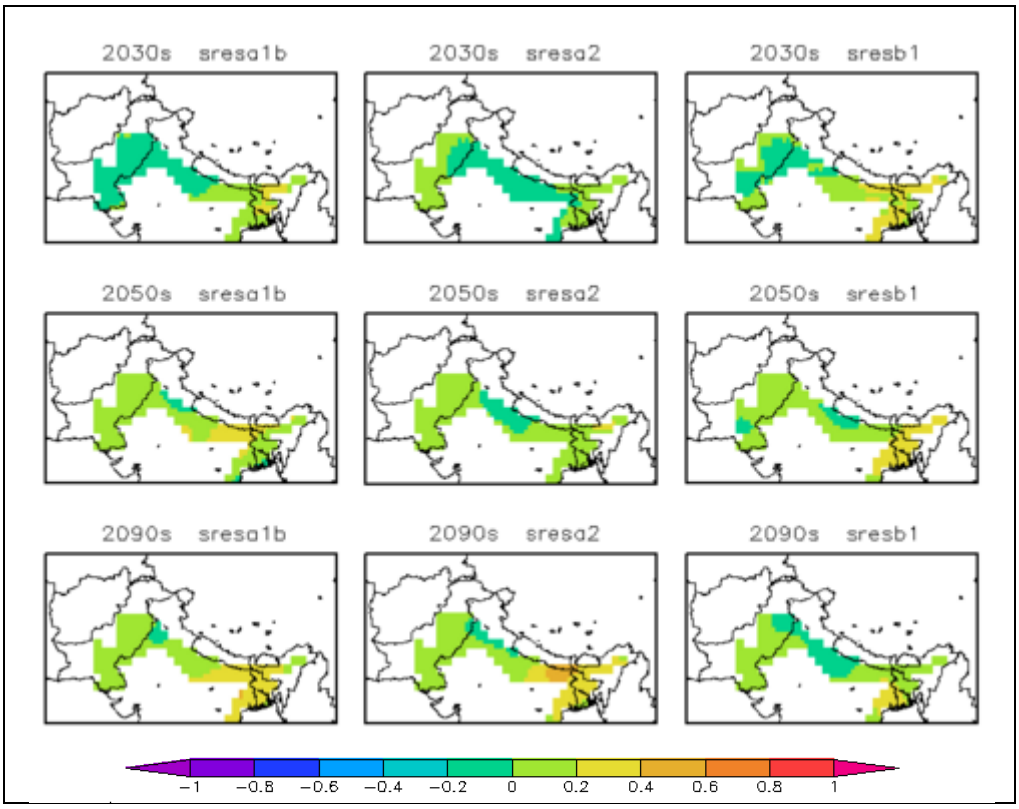

Figure H5: As Figure 4.3 but for rabi season

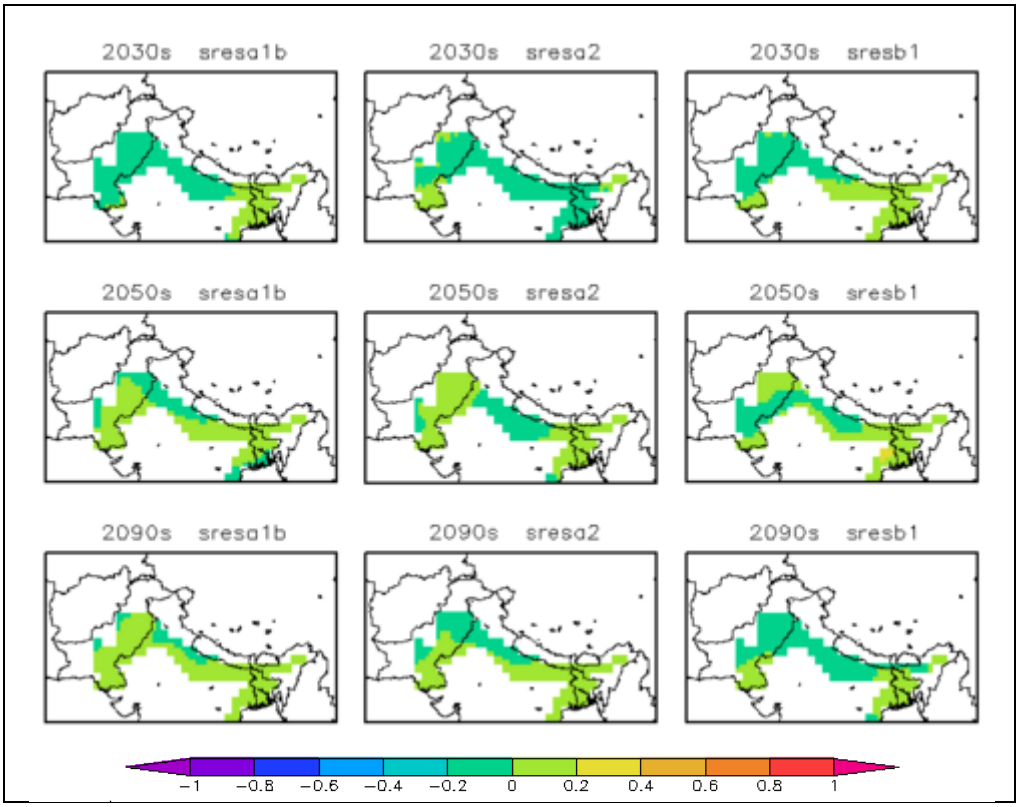

Figure H6: As Figure 4.4 but for winter season

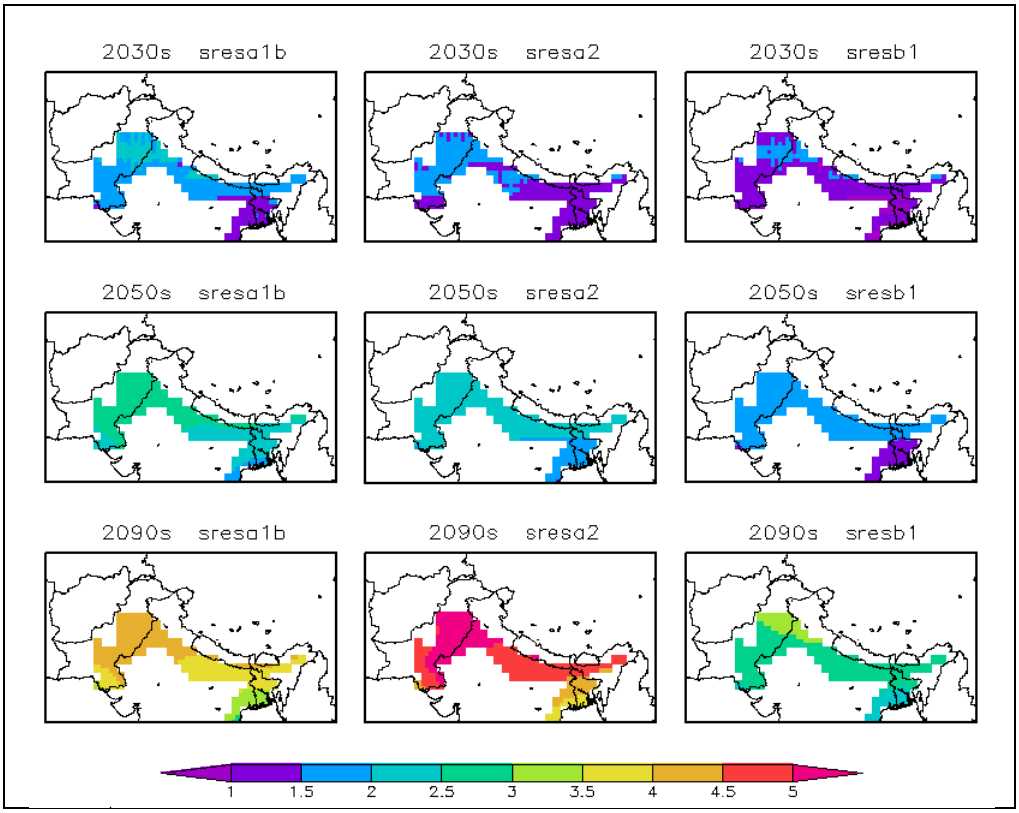

Figure H7: As Figure 4.4 but for pre-monsoon season

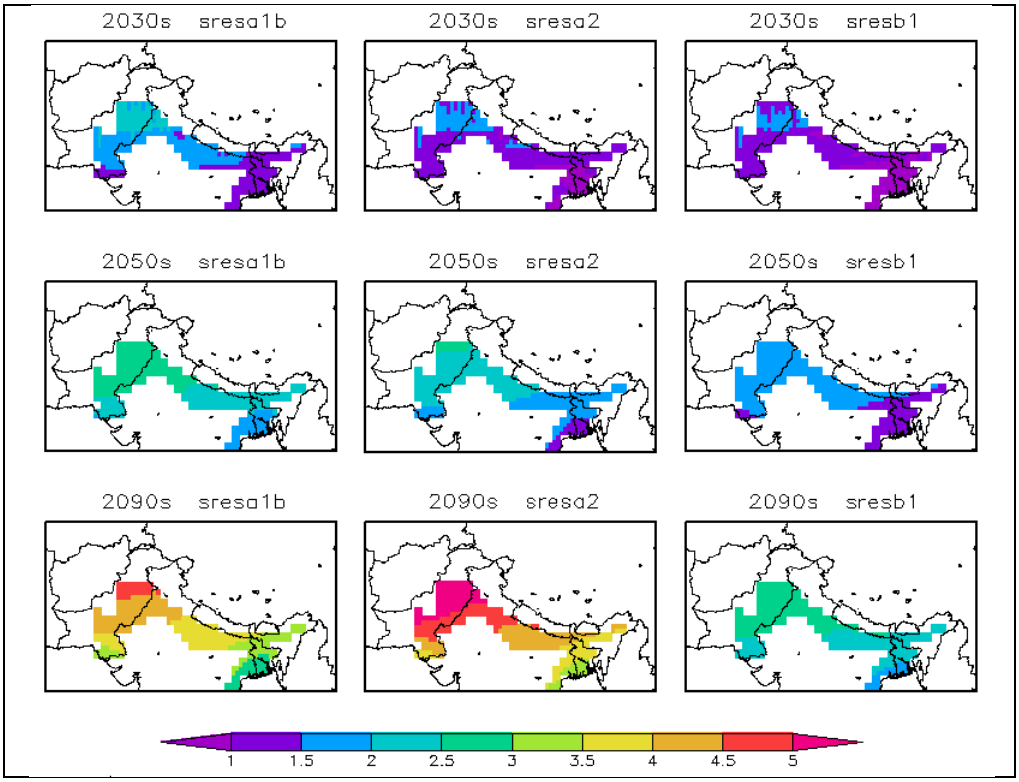

Figure H8: As Figure 4.4 but for monsoon season

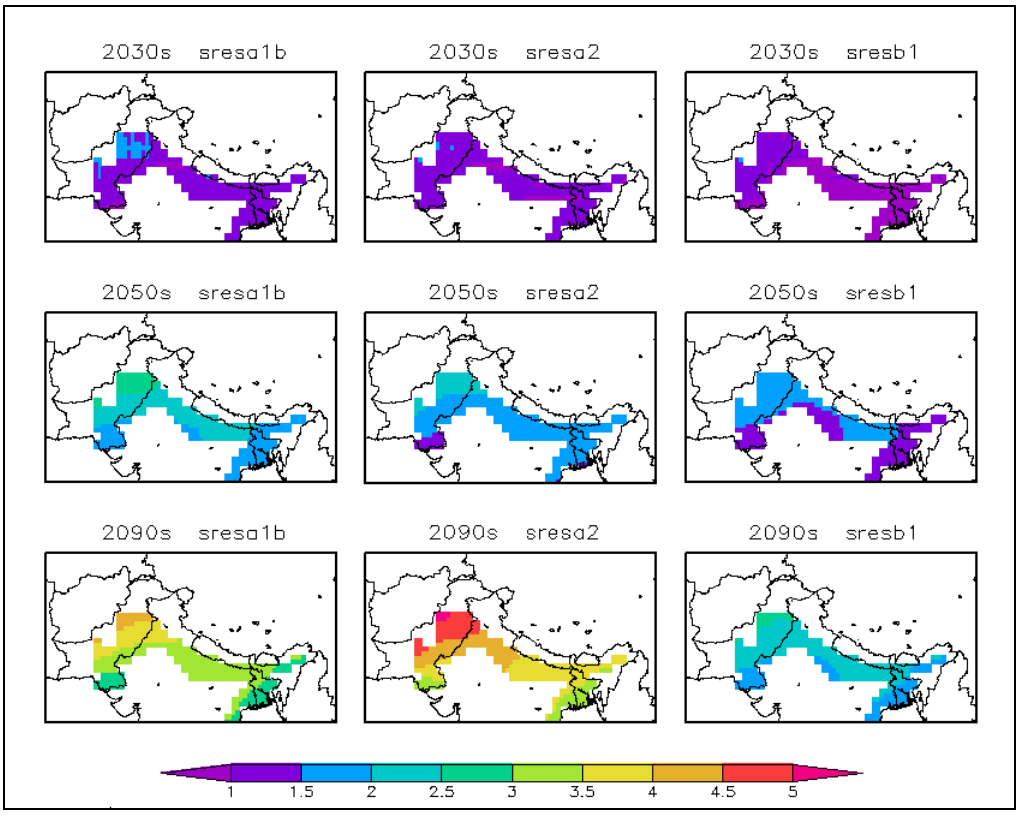

Figure H9: As Figure 4.4 but for post-monsoon season

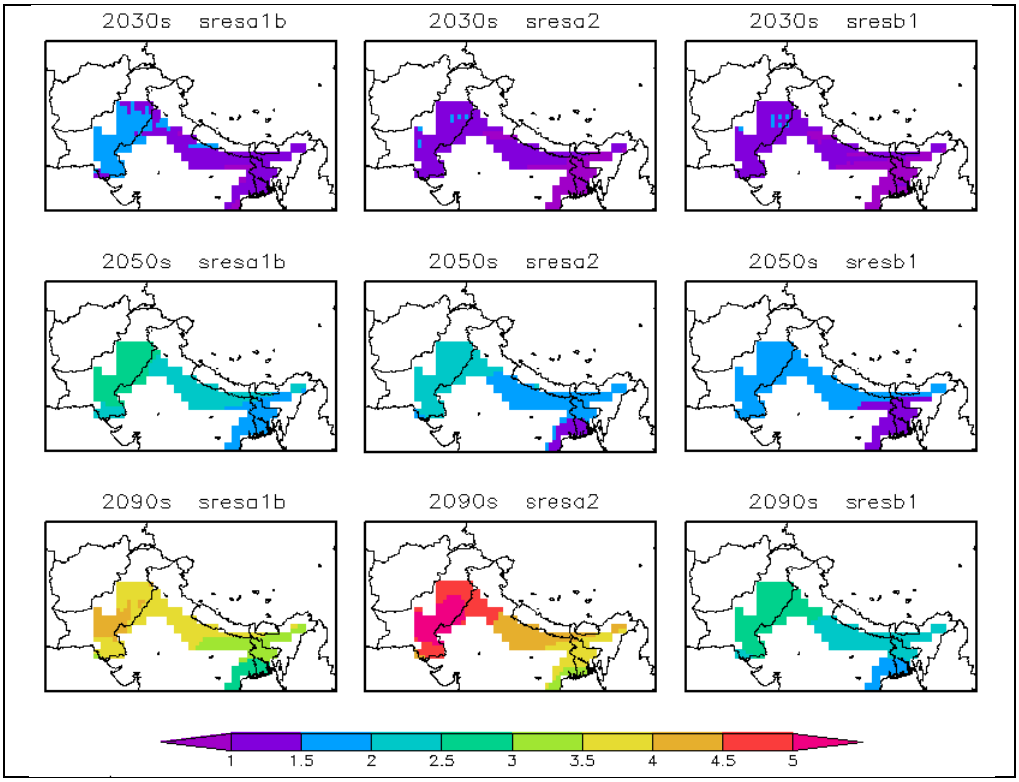

Figure H10: As Figure 4.4 but for rabi season

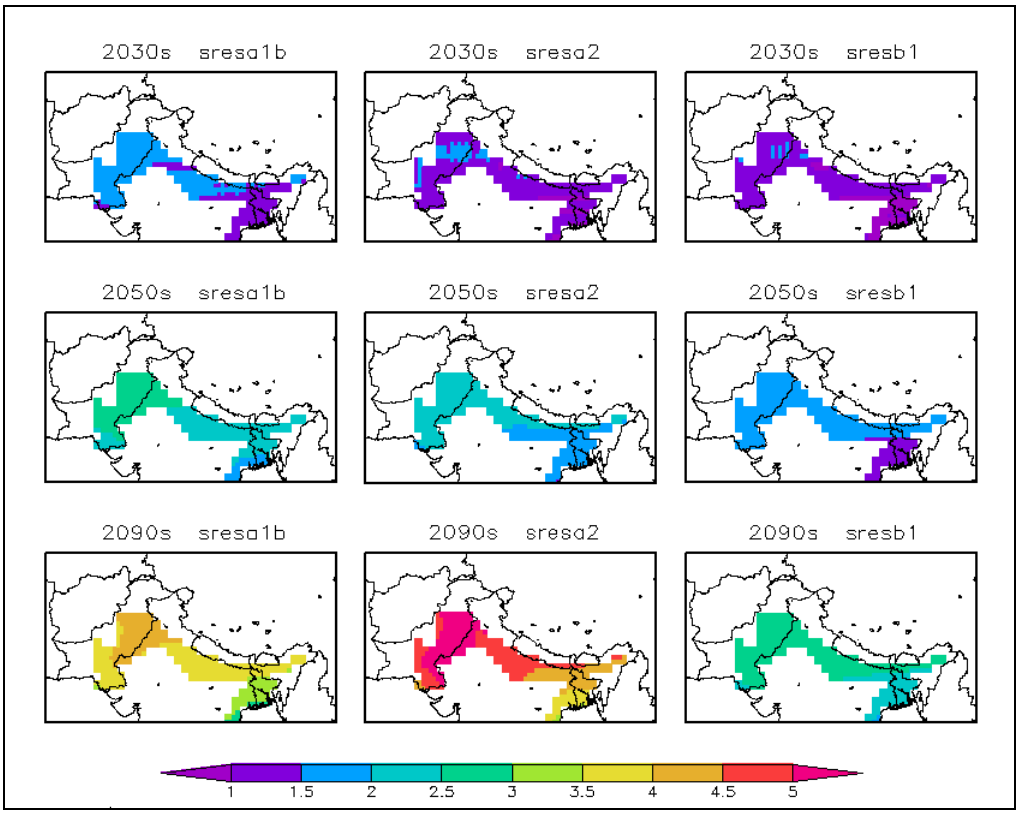

Appendix 9

Figure I1: Latitudinal mean precipitation (mm/day) for the 2050s and 2090s under the three SRES emission scenarios. Bold black line shows the present day conditions (20c3m). Vertical lines show the onset and end of the monsoon season, defined as the time of year where daily rainfall exceeds mean annual daily rainfall.

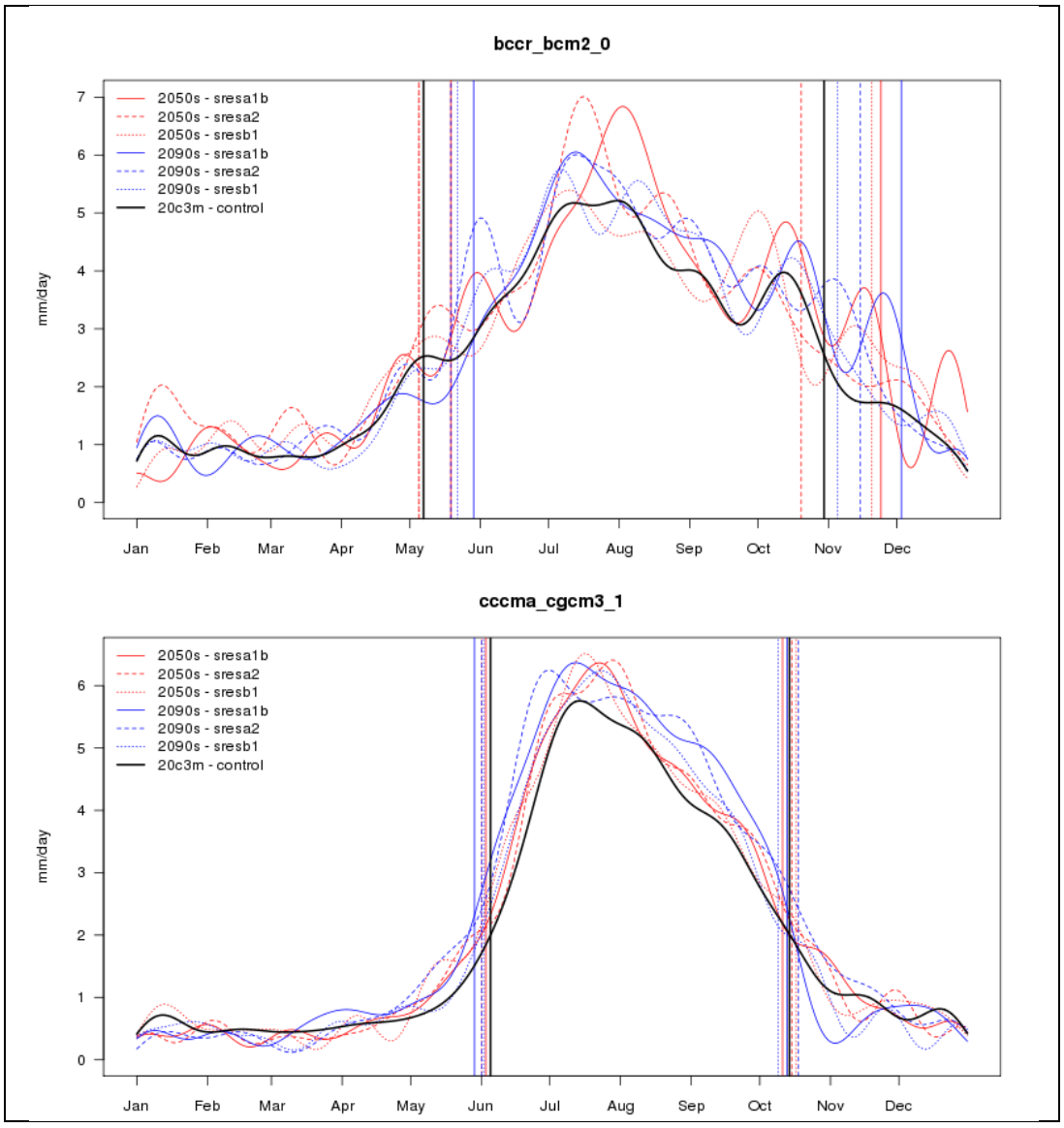

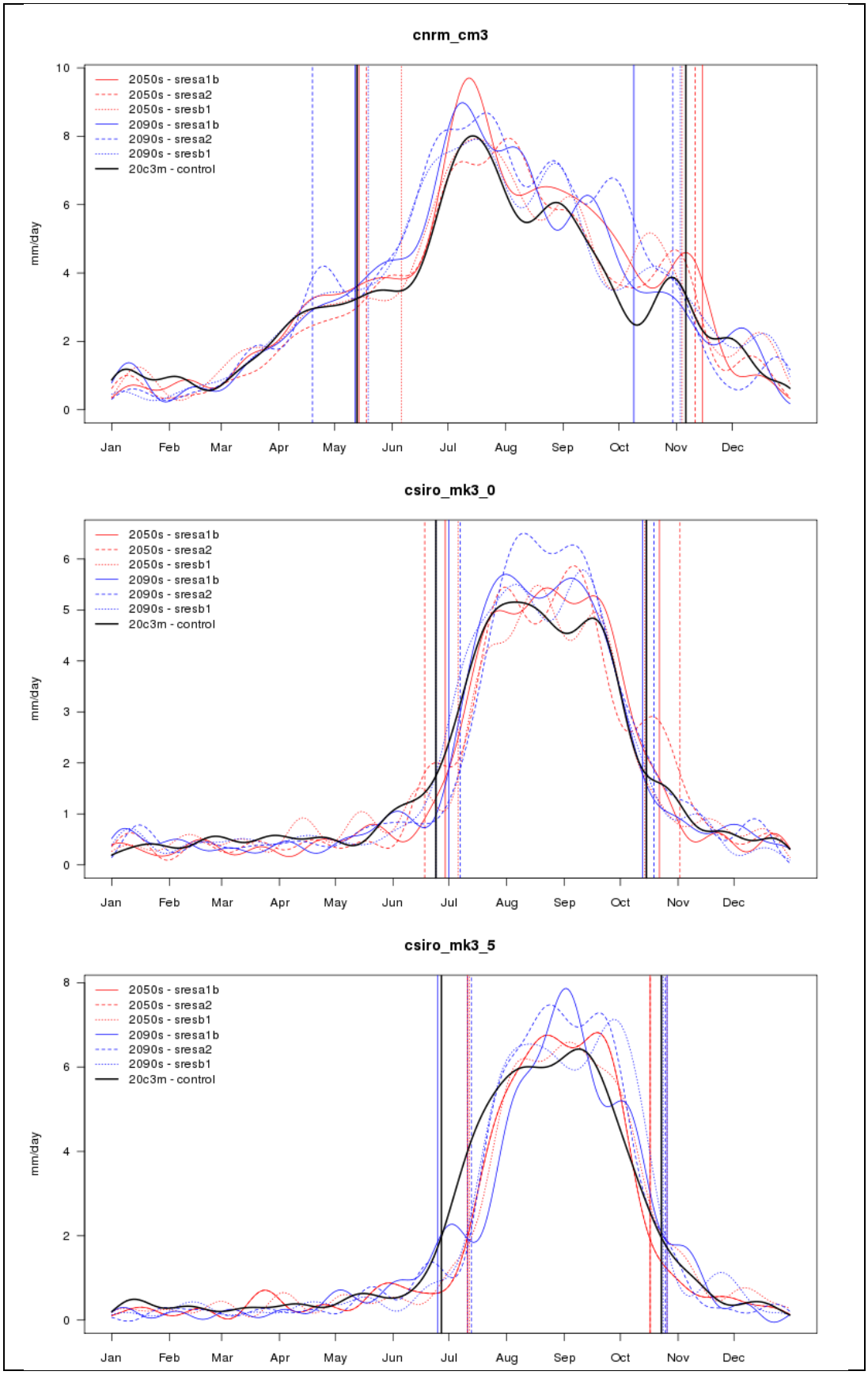
cnrm_cm3
2050s - sresa1b
2050s - sresa2
2050s - sresb1
2090s - sresa1b
2090s - sresa2
2090s - sresb1
20c3m - control
mm/day
0
2
4
6
8
10
Jan
Feb
Mar
Apr
May
Jun
Jul
Aug
Sep
Oct
Nov
Dec
csiro_mk3_0
2050s - sresa1b
2050s - sresa2
2050s - sresb1
2090s - sresa1b
2090s - sresa2
2090s - sresb1
20c3m - control
mm/day
0
1
2
3
4
5
6
Jan
Feb
Mar
Apr
May
Jun
Jul
Aug
Sep
Oct
Nov
Dec
csiro_mk3_5
2050s - sresa1b
2050s - sresa2
2050s - sresb1
2090s - sresa1b
2090s - sresa2
2090s - sresb1
20c3m - control
mm/day
0
2
4
6
8
Jan
Feb
Mar
Apr
May
Jun
Jul
Aug
Sep
Oct
Nov
Dec

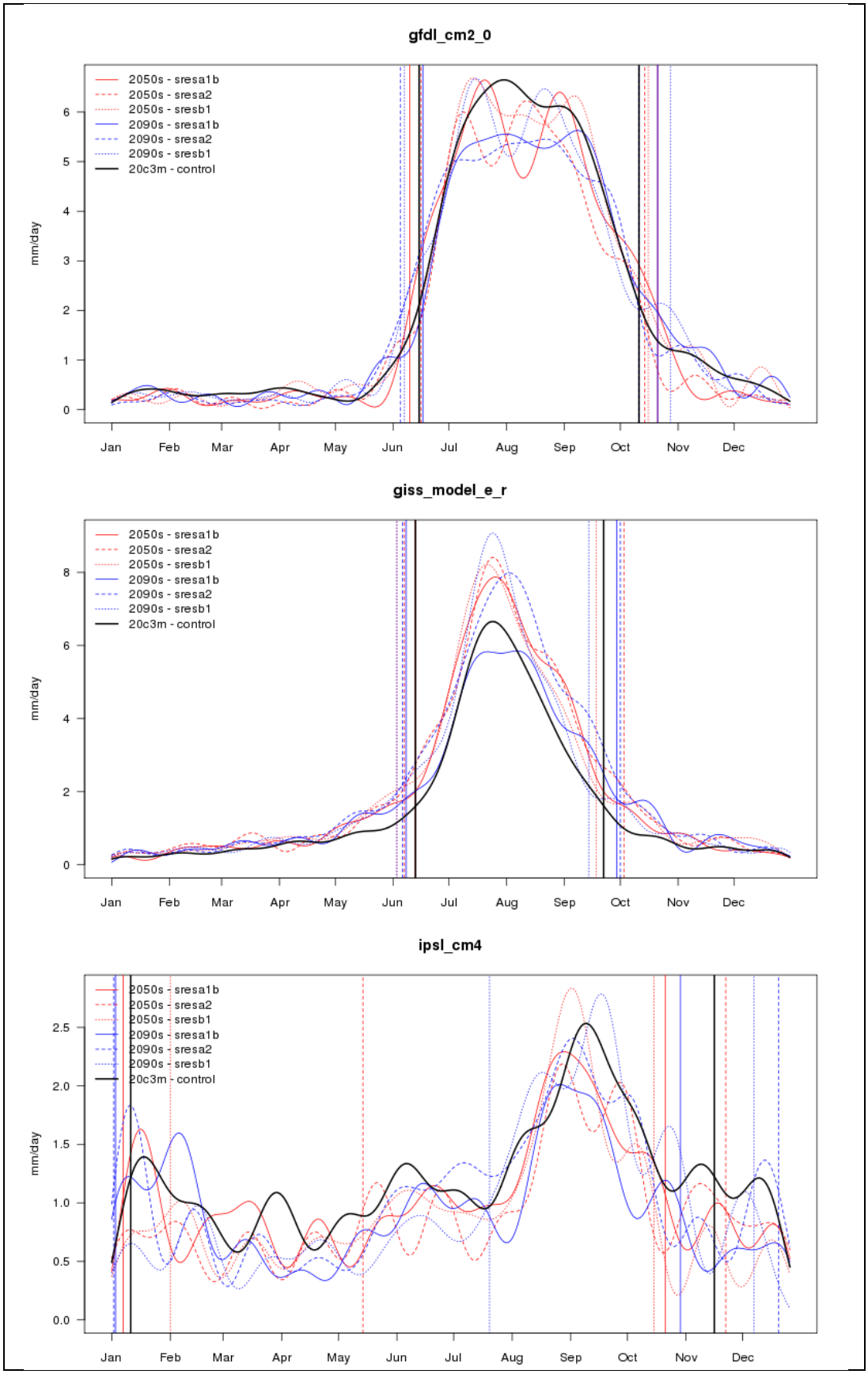
gfdl_cm2_0
2050s - sresa1b
2050s - sresa2
2050s - sresb1
2090s - sresa1b
2090s - sresa2
2090s - sresb1
20c3m - control
mm/day
0
1
2
3
4
5
6
Jan
Feb
Mar
Apr
May
Jun
Jul
Aug
Sep
Oct
Nov
Dec
giss_model_e_r
2050s - sresa1b
2050s - sresa2
2050s - sresb1
2090s - sresa1b
2090s - sresa2
2090s - sresb1
20c3m - control
mm/day
0
2
4
6
8
Jan
Feb
Mar
Apr
May
Jun
Jul
Aug
Sep
Oct
Nov
Dec
ipsl_cm4
2050s - sresa1b
2050s - sresa2
2050s - sresb1
2090s - sresa1b
2090s - sresa2
2090s - sresb1
20c3m - control
mm/day
0.0
0.5
1.0
1.5
2.0
2.5
Jan
Feb
Mar
Apr
May
Jun
Jul
Aug
Sep
Oct
Nov
Dec

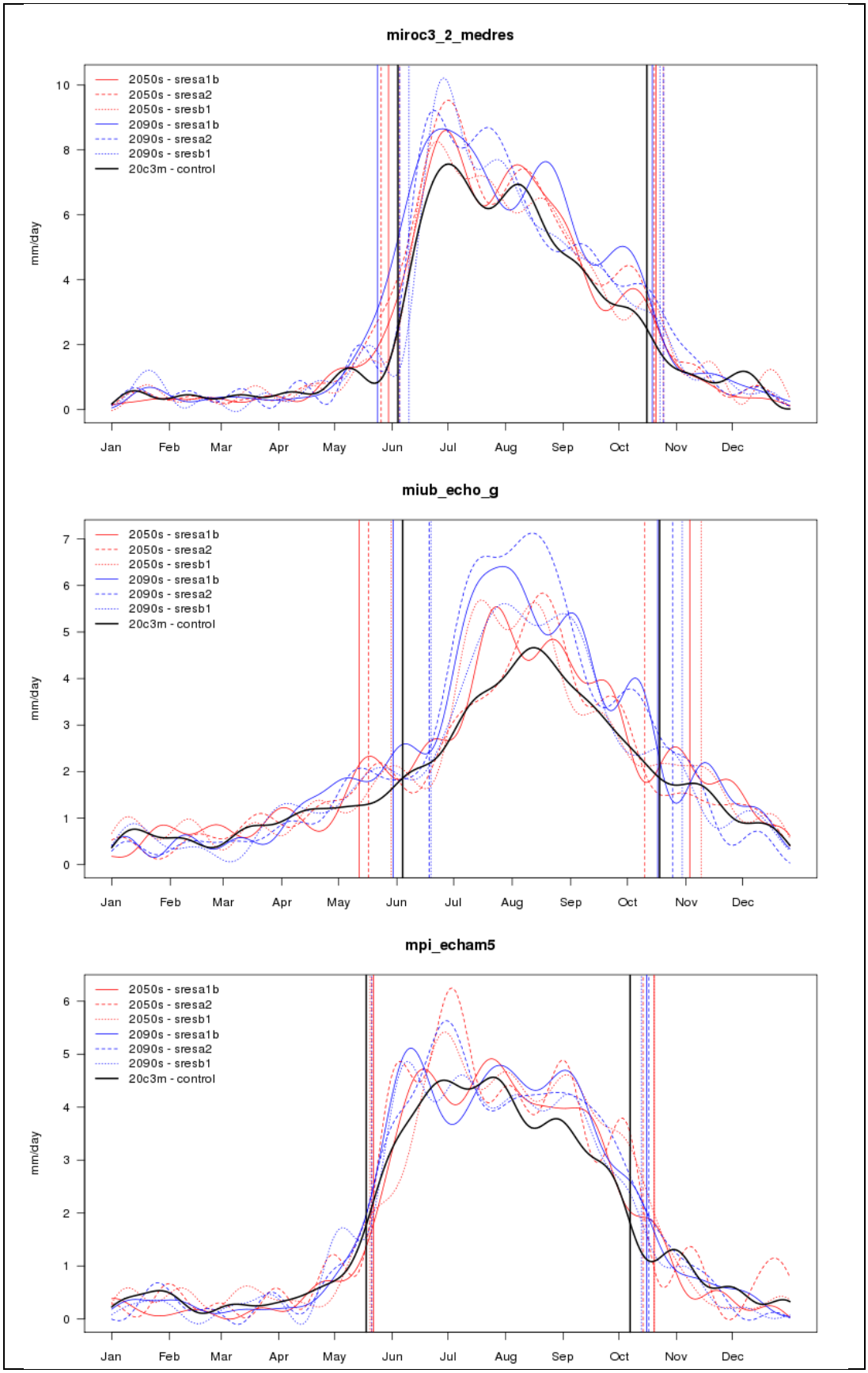
miroc3_2_medres
2050s - sresa1b
2050s - sresa2
2050s - sresb1
2090s - sresa1b
2090s - sresa2
2090s - sresb1
20c3m - control
mm/day
0
2
4
6
8
10
Jan
Feb
Mar
Apr
May
Jun
Jul
Aug
Sep
Oct
Nov
Dec
miub_echo_g
2050s - sresa1b
2050s - sresa2
2050s - sresb1
2090s - sresa1b
2090s - sresa2
2090s - sresb1
20c3m - control
mm/day
0
1
2
3
4
5
6
7
Jan
Feb
Mar
Apr
May
Jun
Jul
Aug
Sep
Oct
Nov
Dec
mpi_echam5
2050s - sresa1b
2050s - sresa2
2050s - sresb1
2090s - sresa1b
2090s - sresa2
2090s - sresb1
20c3m - control
mm/day
0
1
2
3
4
5
6
Jan
Feb
Mar
Apr
May
Jun
Jul
Aug
Sep
Oct
Nov
Dec

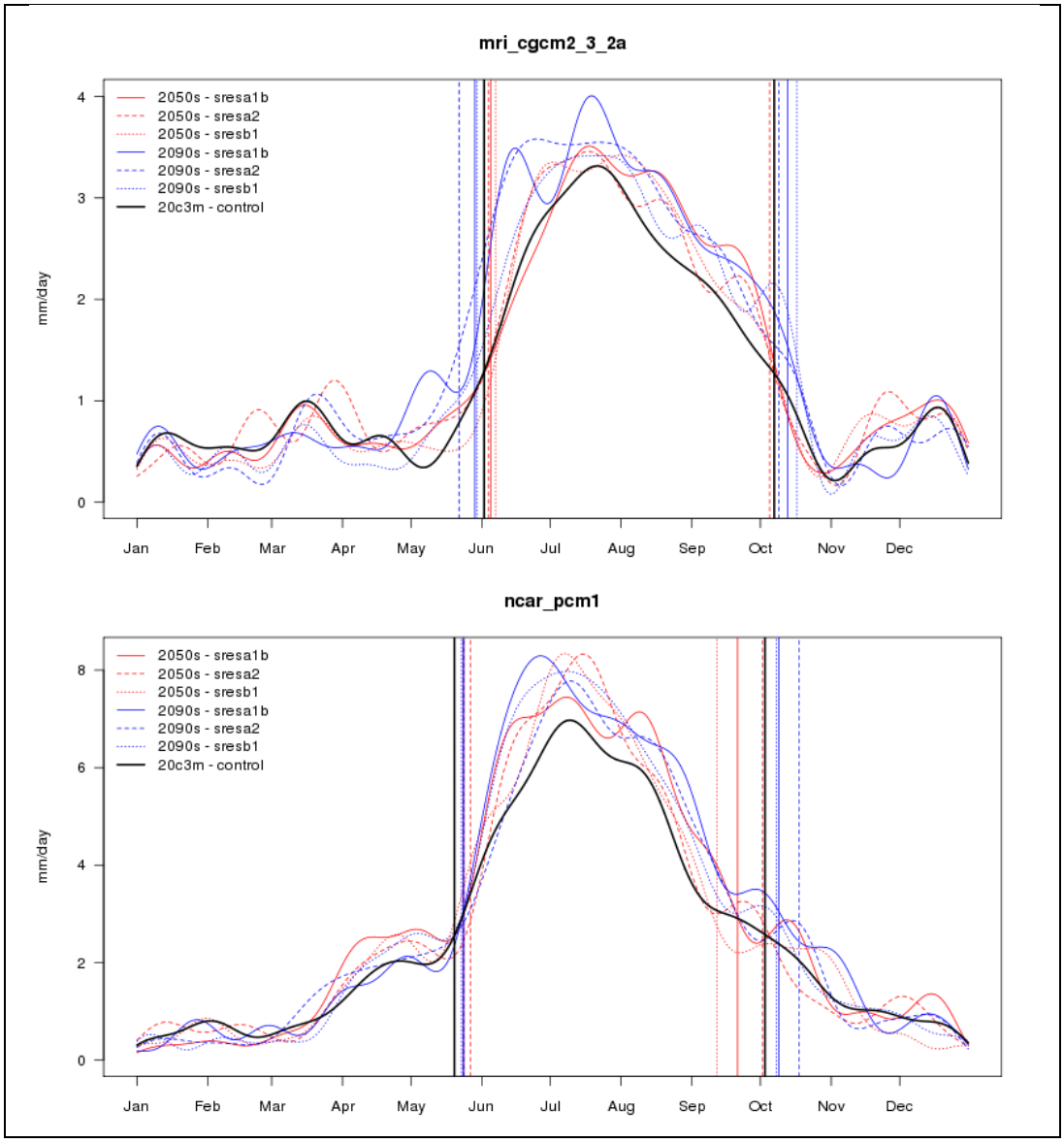
mri_cgcm2_3_2a
2050s - sresa1b
2050s - sresa2
2050s - sresb1
2090s - sresa1b
2090s - sresa2
2090s - sresb1
20c3m - control
mm/day
0
1
2
3
4
Jan
Feb
Mar
Apr
May
Jun
Jul
Aug
Sep
Oct
Nov
Dec
ncar_pcm1
2050s - sresa1b
2050s - sresa2
2050s - sresb1
2090s - sresa1b
2090s - sresa2
2090s - sresb1
20c3m - control
mm/day
0
2
4
6
8
Jan
Feb
Mar
Apr
May
Jun
Jul
Aug
Sep
Oct
Nov
Dec

Appendix 10

Figure J1: Spatial extent of **maize** for present-day conditions and projected future conditions under the multi-model ensemble mean climate change for the three SRES emission scenarios, using temperature and rainfall as limits. Colours represent the number of months a grid point is within the climatic thresholds; purple represents parts of the IGP that do not satisfy growing conditions in any single month

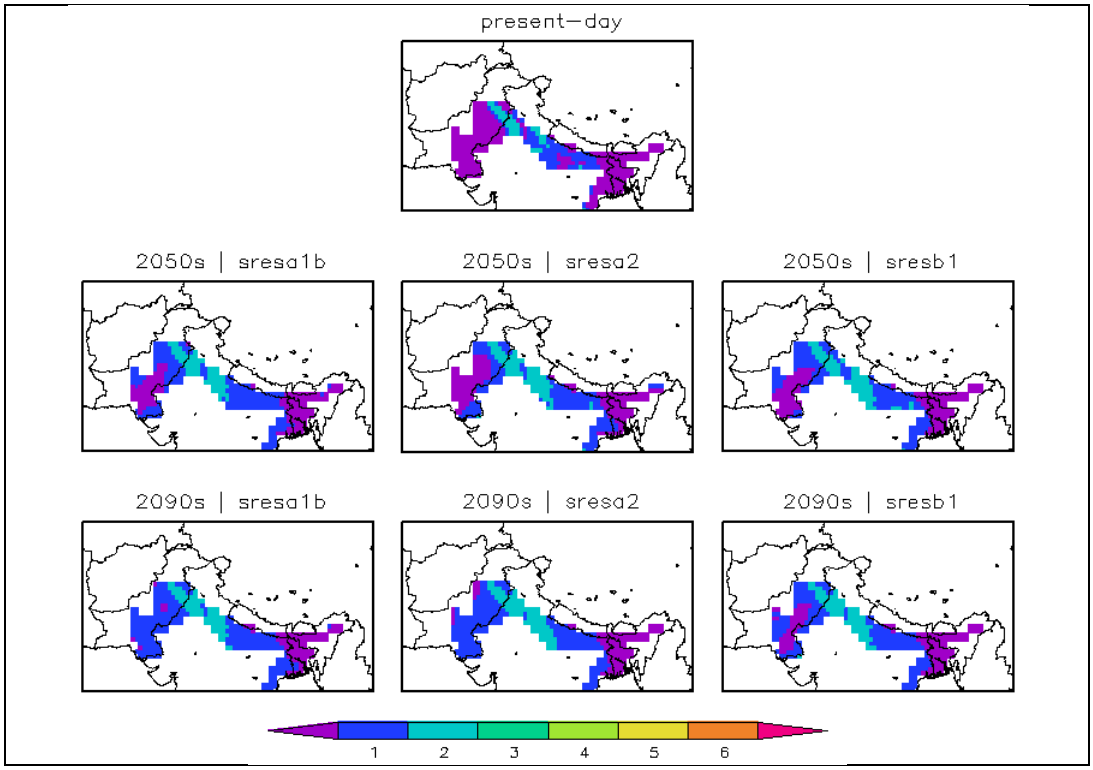

Figure J2: As for Figure J1, but assuming irrigation is available and therefore rainfall limitations are excluded.

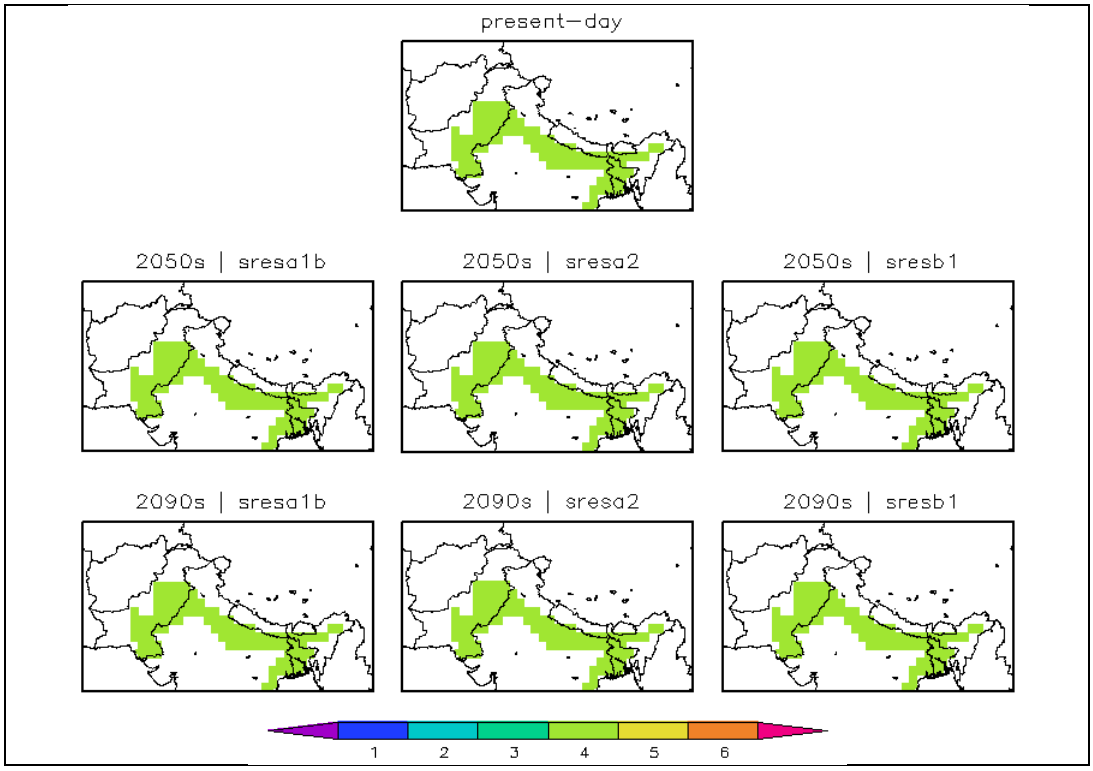

Figure J3: Spatial extent of **wheat** for present-day conditions and projected future conditions under the multi-model ensemble mean climate change for the three SRES emission scenarios, using temperature and rainfall as limits. Colours represent the number of months a grid point is within the climatic thresholds; purple represents parts of the IGP that do not satisfy growing conditions.

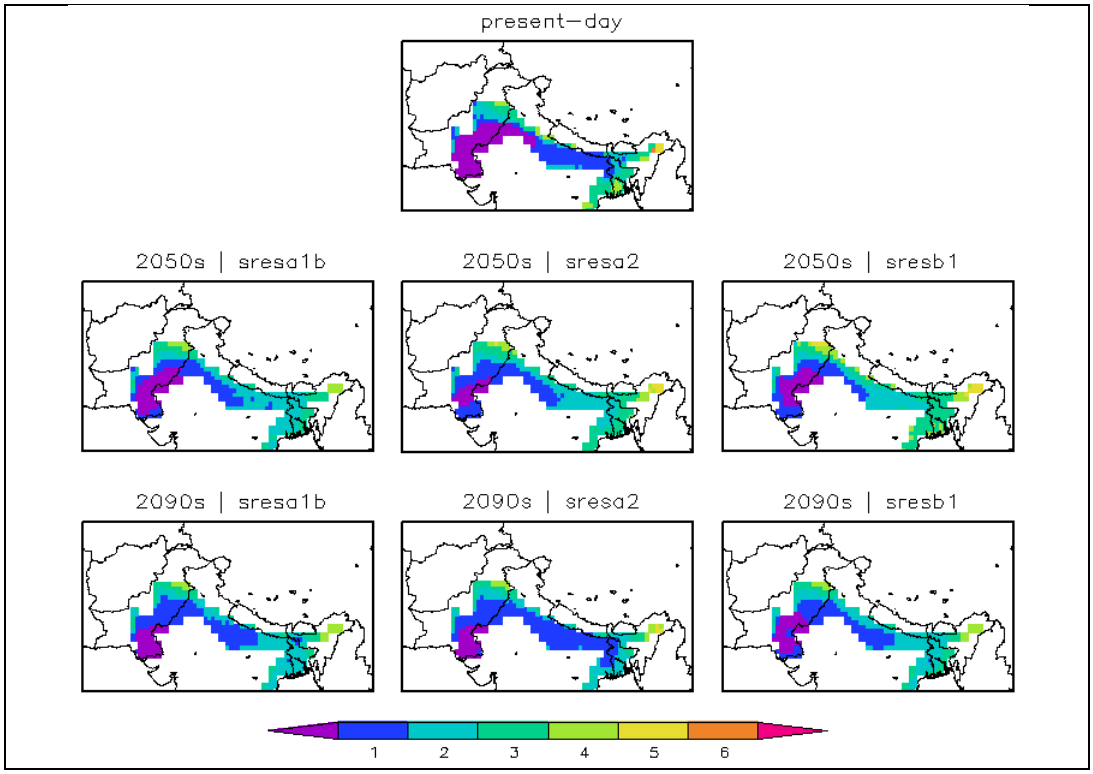

Figure J4: As for Figure J3, but assuming irrigation is available and therefore rainfall limitations are excluded.

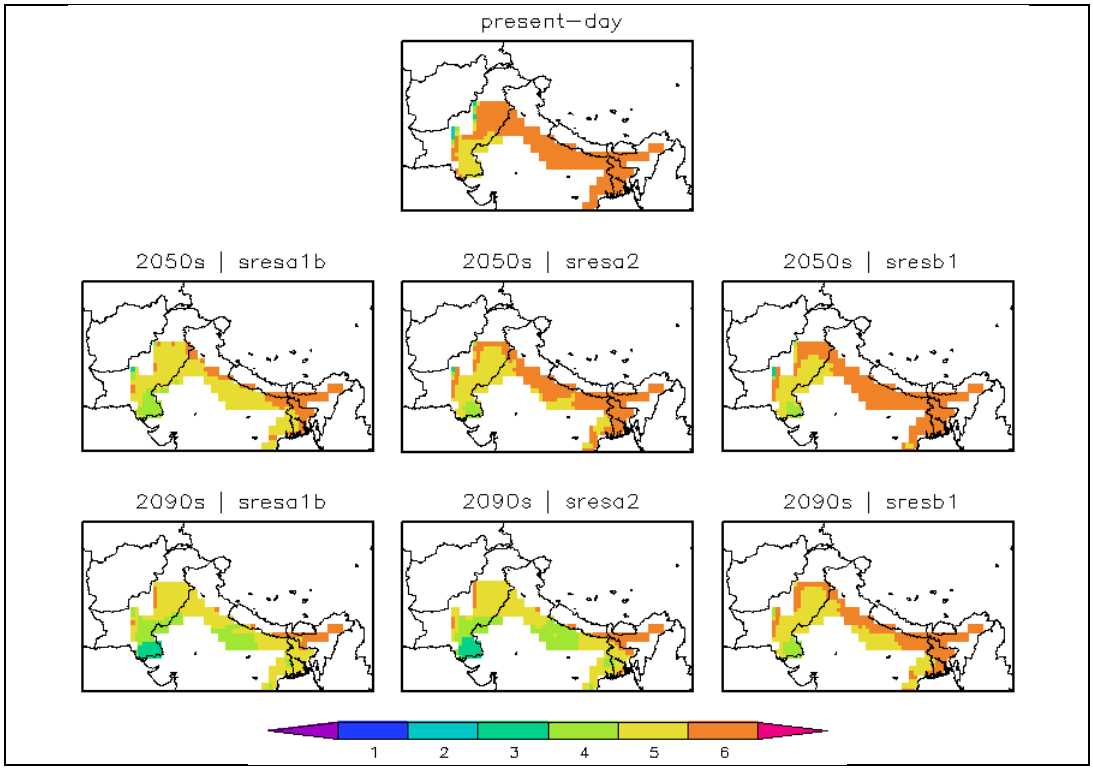

Figure J5: Spatial extent of **sugarcane** for present-day conditions and projected future conditions under the multi-model ensemble mean climate change for the three SRES emission scenarios, with temperature and rainfall as limits. Colours represent the number of months a grid point is within the climatic thresholds; purple represents parts of the IGP that do not satisfy growing conditions

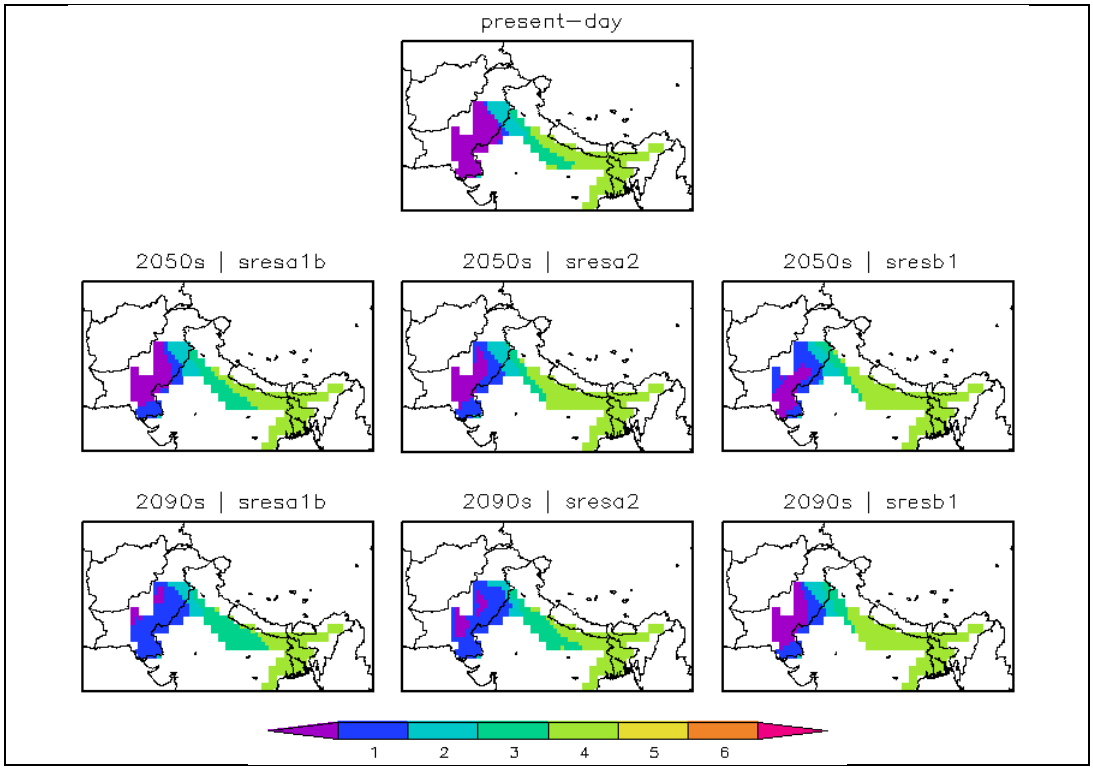

Figure J6: As for Figure J5, but assuming irrigation is available and therefore rainfall limitations are excluded.

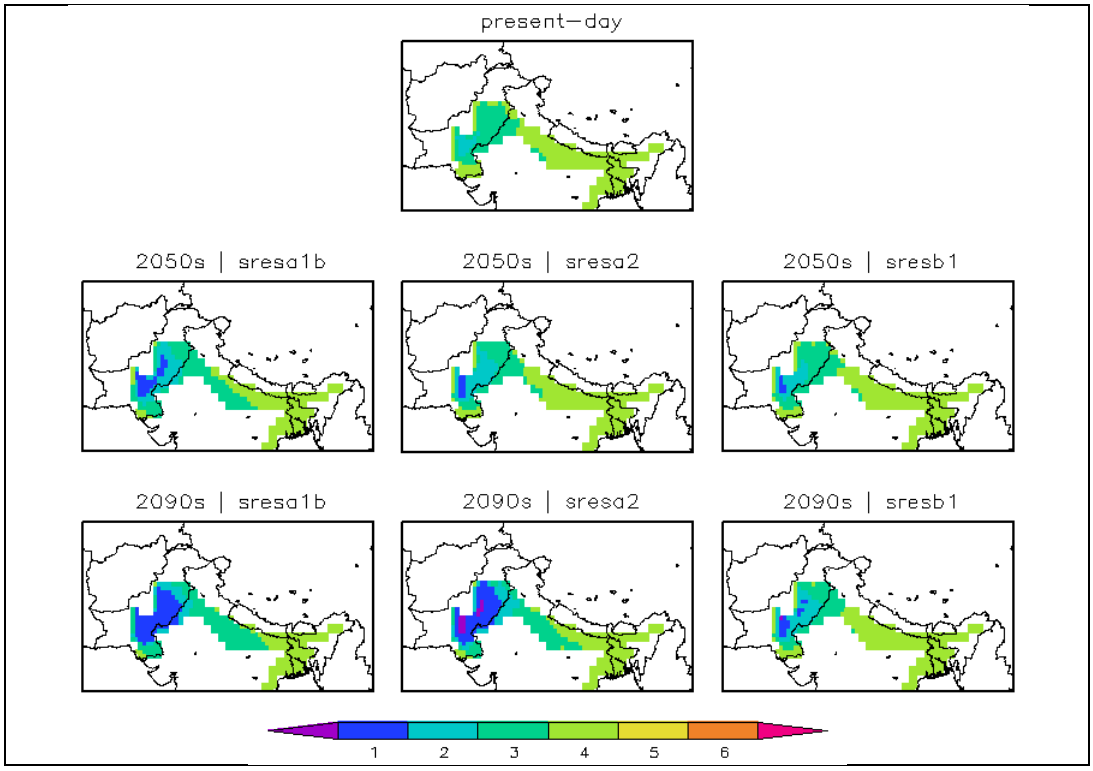

Figure J7: Spatial extent of **potatoes** for present-day conditions and projected future conditions under the multi-model ensemble mean climate change for the three SRES emission scenarios, with temperature and rainfall as limits. Colours represent the number of months a grid point is within the climatic thresholds; purple represents parts of the IGP that do not satisfy growing conditions

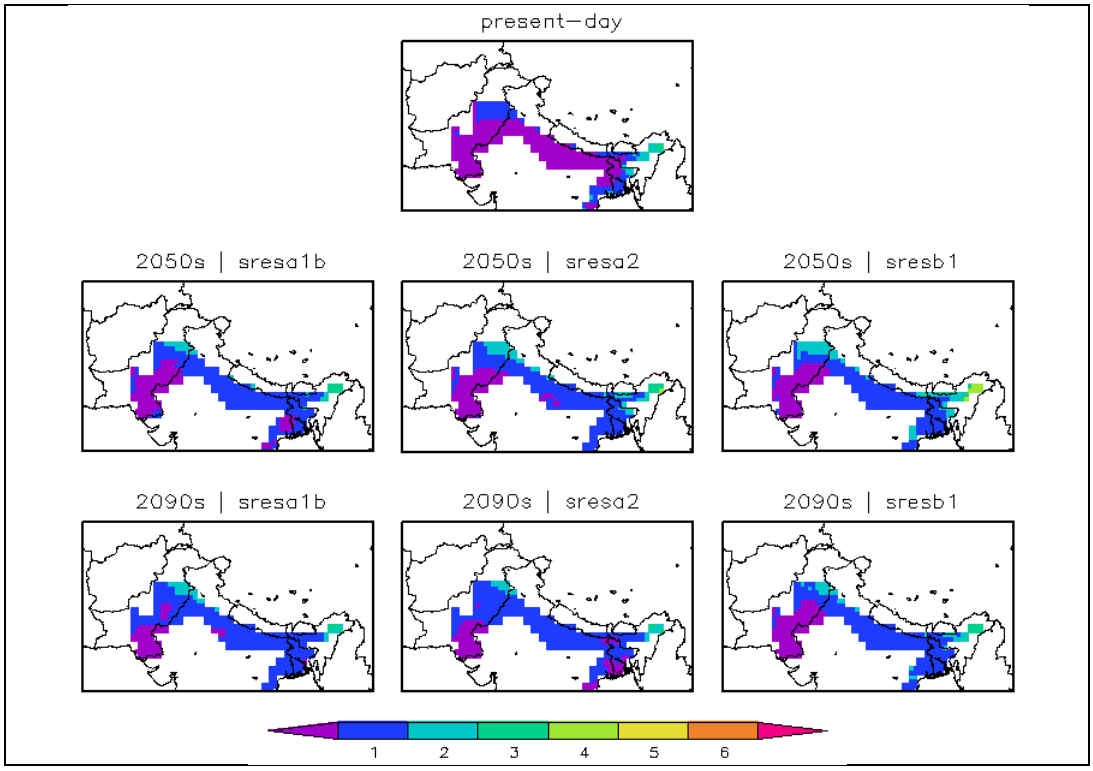

Figure J8: As for Figure J7, but assuming irrigation is available and therefore rainfall limitations are excluded.

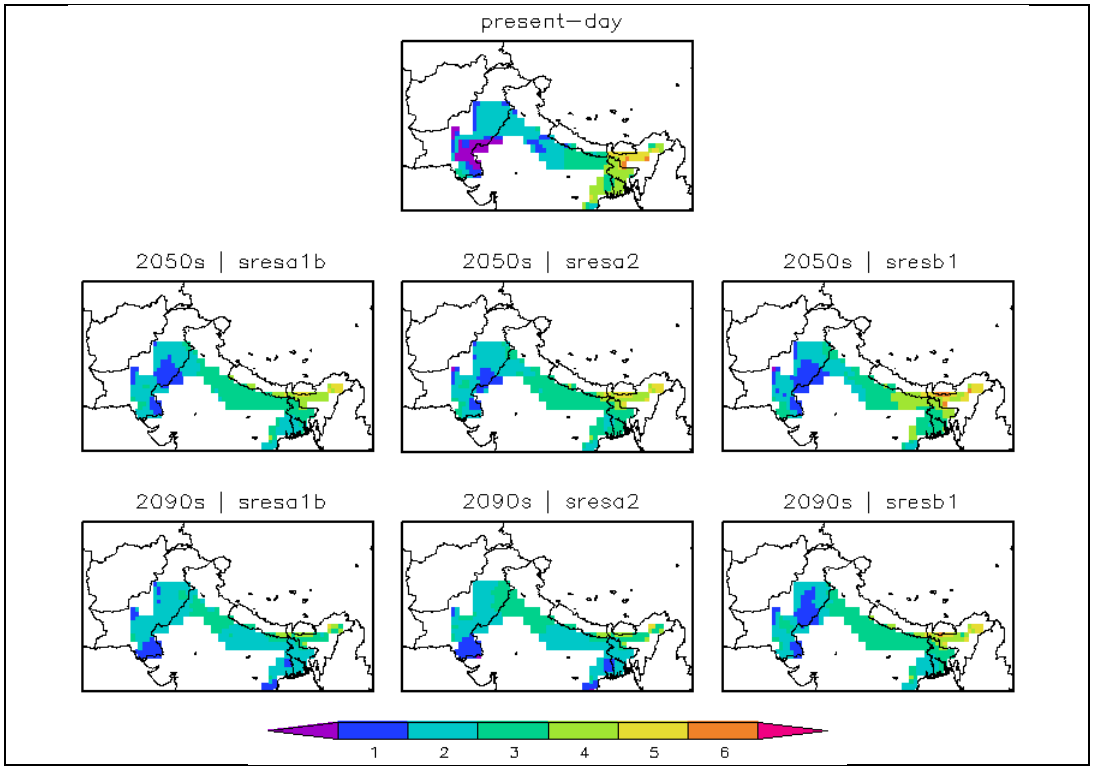

Figure J9: Spatial extent of **onions** for present-day conditions and projected future conditions under the multi-model ensemble mean climate change for the three SRES emission scenarios, using temperature and rainfall as limits. Colours represent the number of months a grid point is within the climatic thresholds; purple represents parts of the IGP that do not satisfy growing conditions

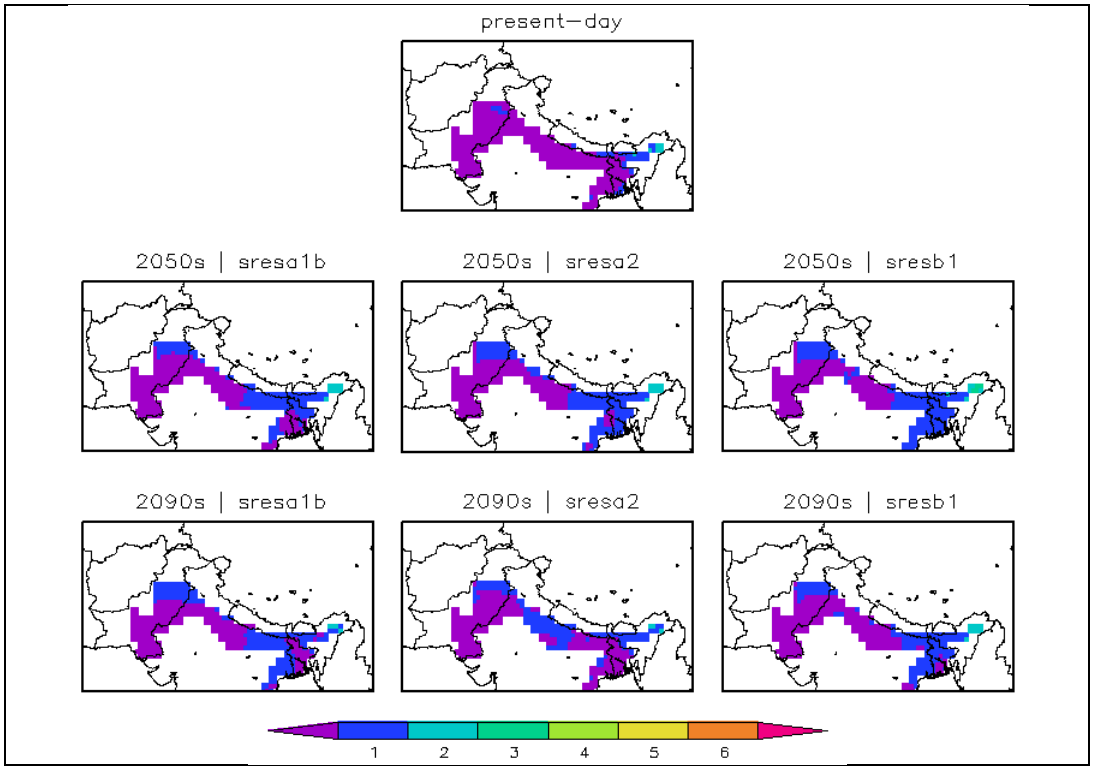

Figure J10: As for Figure J9, but assuming irrigation is available and therefore rainfall limitations are excluded.

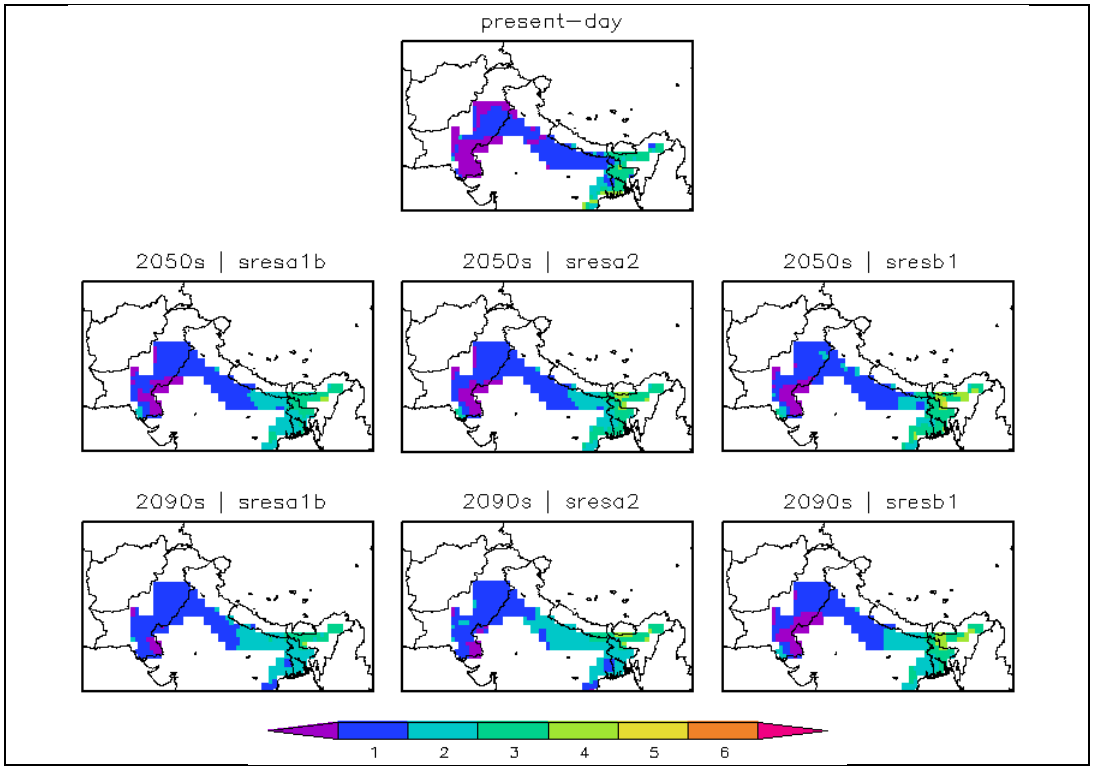

Figure J11: Spatial extent of **paddy rice** for present-day conditions and projected future conditions under the multi-model ensemble mean climate change for the three SRES emission scenarios, using temperature and rainfall as limits. Colours represent the number of months a grid point is within the climatic thresholds; purple represents parts of the IGP that do not satisfy growing conditions

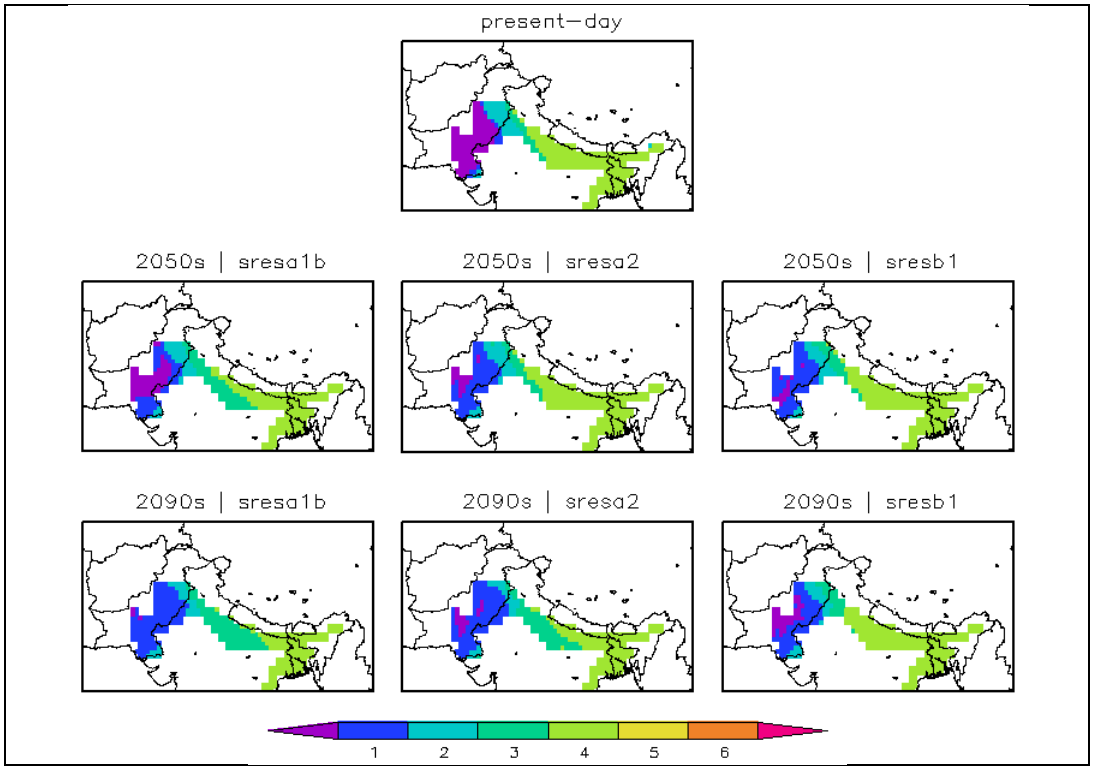

Figure J12: As for Figure J11, but assuming irrigation is available and therefore rainfall limitations are excluded.

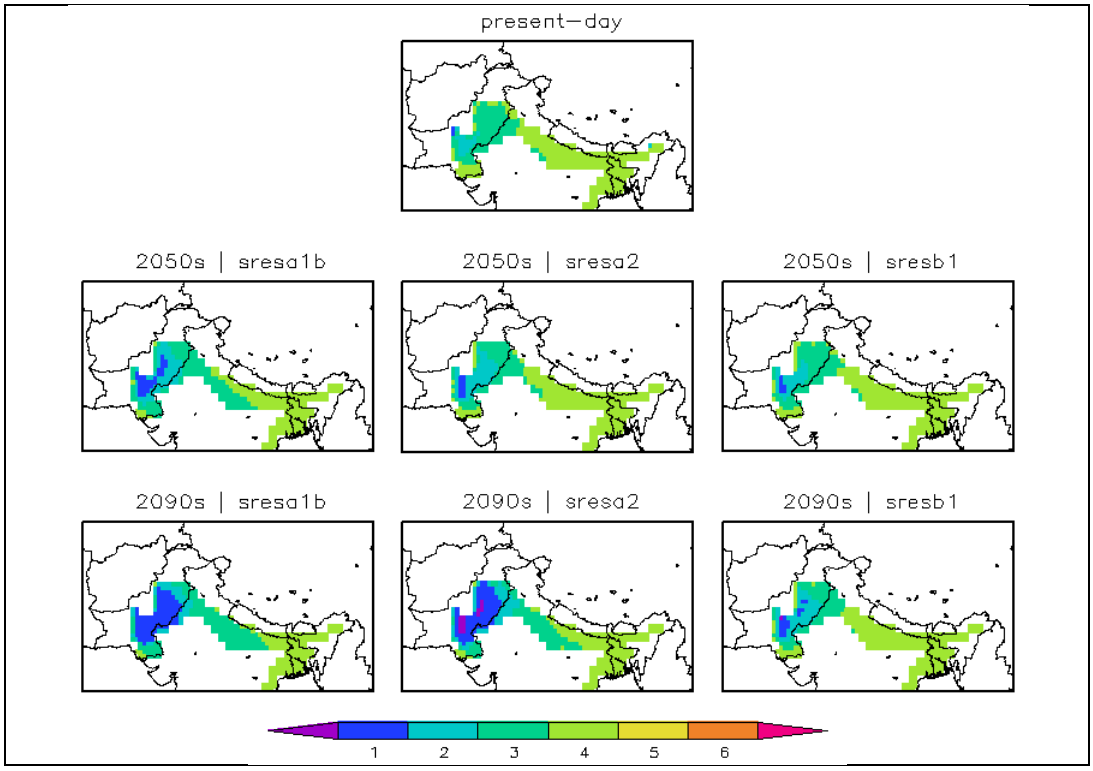

Table J1: Total area of crops grown in the IGP region for the present day and changes in area for future periods under the three emission scenarios using temperature and precipitation as control. Figures for future periods are expressed as percentage change relative to the present period. Values for present day are based on CRU gridded data and are expressed in terms of the number of grid points in the IGP domain, and the percentage of IGP region shown in parentheses. Values for 2050s and 2090s are based on ensemble mean of 13 GCMs. All values are expressed in terms of number of 0.5° x 0.5° grid points.

Crop	Present	2050s			2090s		
		SRESA1B	SRESA2	SRESB1	SRESA1B	SRESA2	SRESB1
Maize	129 (31)	112	96	102	153	144	115
Wheat	288 (69)	18	31	23	27	27	27
Sugarcane	277 (67)	16	24	27	42	38	19
Potato	114 (27)	154	169	167	197	176	165
Onion	43 (10)	256	328	347	291	221	263
Rice	297 (71)	16	31	33	37	32	26

Table J2: As Table J1 but using only temperature as control (assuming irrigation is possible).

Crop	Present	2050s			2090s		
		SRESA1B	SRESA2	SRESB1	SRESA1B	SRESA2	SRESB1
Maize	411 (99)	0	0	0	0	0	0
Wheat	411 (99)	0	0	0	0	0	0
Sugarcane	411 (99)	0	0	0	0	-3	0
Potato	367 (88)	12	12	12	12	11	12
Onion	302 (73)	20	21	21	32	30	16
Rice	411 (99)	0	0	0	0	-3	0

References

Aggarwal PK, et al. 2004. Adapting food systems of the Indo-Gangetic plains to global environmental change: Key information needs to improve policy formulation. *Environmental Science and Policy* 7(6): 487–498.

Aggarwal PK, Mall RK. 2002. Climate change and rice yields in diverse agro-environments of India. II. Effect of uncertainties in scenarios and crop models on impact assessment. *Climatic Change* 52(3): 331–343.

Annamalai H, et al. 1999. The mean evolution and variability of the Asian summer monsoon: Comparison of ECMWF and NCEP-NCAR reanalyses. *Monthly Weather Review* 127(6II): 1157–1186.

Annamalai H, et al. 2007a. The South Asian summer monsoon and its relationship with ENSO in the IPCC AR4 simulations. *Journal of Climate* 20(6): 1071–1092.

Annamalai H, et al. 2007b. Possible impact of the Indian Ocean SST on the northern hemisphere circulation during El Nino. *Journal of Climate* 20(13): 3164–3189.

Annamalai H, Slingo JM. 2001. Active/break cycles: diagnosis of the intraseasonal variability of the Asian Summer Monsoon. *Climate Dynamics* 18(1–2): 85–102.

Ashok K, et al. 2001. Impact of the Indian Ocean dipole on the relationship between the Indian monsoon rainfall and ENSO. *Geophysical Research Letters* 28(23): 4499–4502.

Ashrit RG, et al. 2001. ENSO-Monsoon relationship in a greenhouse warming scenario. *Geophysical Research Letters* 28(9): 1727–1730.

Ashrit RG, et al. 2003. Response of the Indian monsoon and ENSO-monsoon teleconnection to enhanced greenhouse effect in the CNRM coupled model. *Journal of the Meteorological Society of Japan* 81(4): 779–803.

Ashrit RG, et al. 2005. Transient response of ENSO-monsoon teleconnection in MRI-CGCM2.2 climate change simulations. *Journal of the Meteorological Society of Japan* 83(3): 273–291.

Bansal VK, Koshal AK. 2008. Pest detection in cropping systems of the Indo-Gangetic Plains through remote sensing.

Erenstein O, et al. 2007. *Livelihoods, poverty and targeting in the Indo-Gangetic Plains: A spatial mapping approach*. New Delhi: CIMMYT and the Rice-Wheat Consortium for the Indo-Gangetic Plains.

[FAO] Food and Agriculture Organization of the United Nations. 2008. *FAOSTAT-Agriculture*. (Available from http://faostat.fao.org/site/339/default.aspx) (Accessed on 7 February 2012).

Gadgil S. 1988. Recent advances in monsoon research with particular reference to the Indian monsoon. *Australian Meteorological Magazine* 36(3): 193–204.

Gadgil S. 2003. The Indian monsoon and its variability. *Annual Review of Earth and Planetary Science* 31: 429–467.

Hahn DG, Manabe S. 1975. Role of mountains in the South Asian monsoon circulation. *Journal of the Atmospheric Sciences* 32(8): 1515–1541.

Hawkins E, Sutton R. 2009. The potential to narrow uncertainty in regional climate predictions. *Bulletin of the American Meteorological Society* 90(8): 1095–+.

[IPCC] Intergovernmental Panel on Climate Change. 2007. Summary for Policymakers. In: Solomon, S et al., eds. *Climate Change 2007: The Physical Science Basis. Contribution of Working Group I to the Fourth Assessment Report of the Intergovernmental Panel on Climate Change.* Cambridge: Cambridge University Press.

Kothawale DR, et al. 2010. Recent trends in pre-monsoon daily temperature extremes over India. *Journal of Earth System Science* 119(1): 51–65.

Kripalani RH, et al. 1996. Empirical study on Nimbus-7 snow mass and Indian summer monsoon rainfall. *International Journal of Climatology* 16(1): 23–34.

Kripalani RH, et al. 2007. South Asian summer monsoon precipitation variability: Coupled climate model simulations and projections under IPCC AR4. *Theoretical and Applied Climatology* 90(3–4): 133–159.

Kumar KK, et al. 2005. Advancing dynamical prediction of Indian monsoon rainfall. *Geophysical Research Letters* 32(8): 1–4.

Kumar KK, et al. 2006. Unraveling the mystery of Indian monsoon failure during El Nino. *Science* 314(5796): 115–119.

Lau KM, et al. 2006. Asian summer monsoon anomalies induced by aerosol direct forcing: The role of the Tibetan Plateau. *Climate Dynamics* 26(7–8): 855–864.

Li C, Yanai M. 1996. The onset and interannual variability of the asian summer monsoon in relation to land-sea thermal contrast. *Journal of Climate* 9(2): 358–375.

Mandal AK, Sharma RC. 2006. Computerized database of salt affected soils for agro-climatic regions in the Indo-Gangetic Plain of India using GIS. *Geocarto International* 21(2): 47–57.

Meehl G. 2002. Indian monsoon GCM sensitivity experiments testing tropospheric biennial oscillation transition conditions. *Journal of Climate* 15(9): 923–944.

Meehl GA, Arblaster JM. 2003. Mechanisms for projected future changes in south Asian monsoon precipitation. *Climate Dynamics* 21(7–8): 659–675.

Meehl GA, et al. 2008. Effects of black carbon aerosols on the Indian monsoon. *Journal of Climate* 21(12): 2869–2882.

Moss RH, et al. 2010. The next generation of scenarios for climate change research and assessment. *Nature* 463(7282): 747–756.

[PACS] Poorest Areas Civil Society Programme. 2008. Drought in India: Challenges & Initiatives. New Delhi: PACS.

Pal DK, et al. 2009. "Soils of the Indo-Gangetic Plains: Their historical perspective and management. *Current Science* 96(9): 1193–1202.

Qian Y, et al. 2010. Sensitivity studies on the impacts of Tibetan Plateau snowpack pollution on the Asian hydrological cycle and monsoon climate. *Atmospheric Chemistry and Physics Discussions* 10(10): 22855–22903.

Rajeevan M, McPhaden MJ. 2004. Tropical Pacific upper ocean heat content variations and Indian summer monsoon rainfall. *Geophysical Research Letters* 31(18): 18201–18204.

Ramanathan V, et al. 2005. Atmospheric brown clouds: Impacts on South Asian climate and hydrological cycle. *Proceedings of the National Academy of Sciences of the United States of America* 102(15): 5326–5333.

Rasmusson EM, Carpenter TH. 1983. The relationship between eastern equatorial Pacific sea surface temperatures and rainfall over India and Sri Lanka. *Monthly Weather Review* 111(3): 517–528.

Saini HS. 2008. Climate change and its future impact on the Indo-Gangetic Plain (IGP). *Earth Science India* 1(3): 138–147.

Saji NH, et al. 1999. A dipole mode in the tropical Indian ocean. *Nature* 401(6751): 360–363.

Saseendran SA, et al. 2000. Effects of climate change on rice production in the tropical humid climate of Kerala, India. *Climatic Change* 44(4): 495–514.

Shukla J. 1987. Interannual variability of monsoons. In: Fein JS, Stephens PL, eds. *Monsoons*. New York: Wiley. p 399–464.

Sikka DR. 1980. Some aspects of the large scale fluctuations of summer monsoon rainfall over India in relation to fluctuations in the planetary and regional scale circulation parameters. *Proceedings of the Indian Academy of Sciences - Earth and Planetary Sciences* 89(2): 179–195.

Simpson GC. 1921. The origin of the south-west monsoon. *Nature* 107(2683): 154.

Stowasser M, et al. 2009. Response of the South Asian summer monsoon to global warming: Mean and synoptic systems. *Journal of Climate* 22(4): 1014–1036.

Taylor KE, et al. 2009. A summary of the CMIP5 experiment design (updated Jan 2011). (Available from http://cmip-pcmdi.llnl.gov/cmip5/docs/Taylor_CMIP5_design.pdf) (Accessed on 7 February 2012).

Turner AG, et al. 2007. The effect of doubled CO2 and model basic state biases on the monsoon-ENSO system. I: Mean response and interannual variability. *Quarterly Journal of the Royal Meteorological Society* 133(626 A): 1143–1157.

Webster PJ, et al. 1998. Monsoons: processes, predictability, and the prospects for prediction. *Journal of Geophysical Research–Oceans* 103(C7): 14451–14510.

Webster PJ, et al. 1999. Coupled ocean-atmosphere dynamics in the Indian Ocean during 1997–98. *Nature* 401(6751): 356–360.

Wu G, Zhang Y. 1998. Tibetan Plateau forcing and the timing of the monsoon onset over South Asia and the South China Sea. *Monthly Weather Review* 126(4): 913–927.

Yang S. 1996. Enso-snow-monsoon associations and seasonal-interannual predictions. *International Journal of Climatology* 16(2): 125–134.